Stabilization of carbon assimilation in a dynamic environment

Dissertation

Zur Erlangung des Doktorgrades

der Naturwissenschaften

(Dr. rer. nat.)

der Fakultät für Biologie

der Ludwig-Maximilians-Universität München

vorgelegt von

Jakob Sebastian Hernandez

München, 2024

Diese Dissertation wurde angefertigt

unter Leitung von Prof. Dr. Thomas Nägele im Bereich

Evolutionäre Zellbiologie der Pflanzen der Fakultät für Biologie

an der Ludwig-Maximilians-Universität München

Gutachter:

1. Prof. Dr. Thomas Nägele
2. Prof. Dr. Korbinian Schneeberger

Datum der Abgabe: 30.10.2024

Tag der mündlichen Prüfung: 06.02.2025

I Statutory declaration and statement

Eigenständigkeitserklärung

Hiermit versichere ich an Eides statt, dass die vorliegende schriftliche Dissertation / Masterarbeit / Bachelorarbeit / Zulassungsarbeit mit dem Titel

Stabilization of Carbon Assimilation in a dynamic Environment

von mir selbstständig verfasst wurde und dass keine anderen als die angegebenen Quellen und Hilfsmittel benutzt wurden. Die Stellen der Arbeit, die anderen Werken dem Wortlaut oder dem Sinne nach entnommen sind, wurden in jedem Fall unter Angabe der Quellen (einschließlich des World Wide Web und anderer elektronischer Text- und Datensammlungen) kenntlich gemacht. Weiterhin wurden alle Teile der Arbeit, die mit Hilfe von Werkzeugen der künstlichen Intelligenz de novo generiert wurden, durch Fußnote/Anmerkung an den entsprechenden Stellen kenntlich gemacht und die verwendeten Werkzeuge der künstlichen Intelligenz gelistet. Die genutzten Prompts befinden sich im Anhang. Diese Erklärung gilt für alle in der Arbeit enthaltenen Texte, Graphiken, Zeichnungen, Kartenskizzen und bildliche Darstellungen.

München, 21.08.2024

(Ort / Datum)

Jakob Sebastian Hernandez

(Vor und Nachname in Druckbuchstaben)   (Unterschrift)

Affidavit

Herewith I certify under oath that I wrote the accompanying Dissertation / MSc thesis / BSc thesis / Admission thesis myself.

Title: Stabilization of Carbon Assimilation in a dynamic Environment

In the thesis no other sources and aids have been used than those indicated. The passages of the thesis that are taken in wording or meaning from other sources have been marked with an indication of the sources (including the World Wide Web and other electronic text and data collections). Furthermore, all parts of the thesis that were de novo generated with the help of artificial intelligence tools were identified by footnotes/annotations at the appropriate places and the artificial intelligence tools used were listed. The prompts used were listed in the appendix. This statement applies to all text, graphics, drawings, sketch maps, and pictorial representations contained in the Work.

Munich, 21.08.2024

(Location/date)

Jakob Sebastian Hernandez

(First and last name in block letters)   (Signature)

II Content

III Abbreviations

Abbreviation	Meaning
1,3-BPG	1,3-bisphosphoglycerate
2-OG	2-oxoglutarate
2OGDH	2-oxoglutarate dehydrogenase
2-PG	2-phosphoglycolate
3-PGA	3-phospho-D-glycerate
aCO2	Ambient CO2
ALD	Aldolase
BASS6	Bile acid sodium symporter 6
BCKDC	Branched-chain α-ketoacid dehydrogenase complex
BnB	Branch-and-Bound
BOU	A bout de souffle
CAT2	Catalase 2
CBBC	Calvin-Benson-Bassham cycle
DES1	L-cysteine desulfhydrase 1
DHAP	Dihydroxyacetone phosphate
eCO2	Elevated CO2
Ery4P	Erythrose-4-phosphate
ETR	Electron transport rate
F6P	Fructose-6-phosphate
FBP	Fructose-1,6-bisphosphate
FBPase	Fructose-1,6-bisphosphatase
G6P	Glucose-6-phosphate
GAP	Glyceraldehyde 3-phosphate
GAPDH	Glyceraldehyde 3-phosphate dehydrogenase
GDC	Glycine decarboxylase
GGAT	Glutamate-glyoxylate aminotransferase
GLYK	Glycerate kinase
GO	Glycolate oxidase
GPT2	Glucose-6-phosphate/phosphate transporter 2
HPR	Hydroxypyruvate reductase
HXK	Hexokinase
J	Jacobian matrix
JA	Jasmonic acid
NAF	Non-aqueous fractionation
ODE	Ordinary differential equation
PAM	Pulse amplitude modulation
PAR	Photosynthetically active radiation
PCA	Principle component analysis
PDH	Pyruvate dehydrogenase
PEP	Phosphoenolpyruvate
PFK	Phosphofructokinase
PGK	Phosphoglycerate kinase
PGP	Phosphoglycolate phosphatase

Abbreviation	Meaning
PLGG1	Plastidal glycolate/glycerate translocator
PLS	Partial least squares regression
PMF	Proton motive force
PQ	Plastoquinone
PQH2	Plastoquinol
PSI	Photosystem I
PSII	Photosystem II
PSO	Particle swarm optimization
pSuT	Plastidic sugar transporter
PUFA	Polyunsaturated fatty acid
Rbo5P	Ribose-5-phosphate
Rbu5P	Ribulose-5-phosphate
RPE	Ribulose-phosphate epimerase
RPI	Ribose-5-phosphate isomerase
Rubisco	Ribulose-1,5-bisphosphate carboxylase/oxygenase
RuBP	Ribulose-1,5-bisphosphate
S6P	Sucrose-6-phosphate
SBP	Sedoheptulose-1,7-bisphosphate
SBPase	Sedoheptulose-1,7-bisphosphatase
Sed7P	Sedoheptulose-7-phosphate
SGAT	Serine-glyoxylate aminotransferase
SHMT	Serine hydroxymethyltransferase
SKM	Structural kinetic modeling
SPP	Sucrose-phosphate phosphatase
SPS	Sucrose-phosphate synthase
TP	Triosephosphate
TPI	Triose-phosphate isomerase
Xyl5P	Xylulose-5-phosphate
Y(II)	Yield of effective photochemical quantum of PS II
Y(NO)	Yield of unregulated heat dissipation and fluorescence emission
Y(NPQ)	Yield of light-induced non-photochemical quenching

IV List of Publications

IV.I Publication I:

Natural variation of temperature acclimation of *Arabidopsis thaliana*

Jakob Sebastian Hernandez, Dejan Dziubek, Laura Schröder, Charlotte Seydel, Anastasia Kitashova, Vladimir Brodsky, Thomas Nägele *

IV.II Publication II:

The trade-off function of photorespiration in a changing environment

Jakob Sebastian Hernandez, Thomas Nägele *

IV.III Manuscript I:

Regulation of plant metabolism under elevated CO$_2$

Danial Shokouhi [§], Jakob Sebastian Hernandez [§], Dirk Walther, Gabriele Kepp, Serena Schwenkert, Dario Leister, Jürgen Gremmels, Ellen Zuther, Jessica Alpers, Thomas Nägele *, Arnd G. Heyer *

Corresponding Author: *

Authors contributed equally: §

V Declaration of contribution as a co-author

Manuscript I:

Danial Shokouhi grew and harvested the plant samples, performed non-aqueous fractionation and measured metabolite concentrations. In addition, Danial Shokouhi characterized and wrote the chapter regarding the effects observed in the *h-bou* mutant.

Jakob Sebastian Hernandez prepared proteomics samples and integrated all omics data. In addition, Jakob Sebastian Hernandez conceptualized and wrote the code for the OmicsDB tech stack and performed statistical analysis. Furthermore, Jakob Sebastian Hernandez characterized and wrote the chapter regarding the effects observed in the *hpr1-1* mutant.

Danial Shokouhi

Location and Date: __Stuttgart , 22/08/2024__   Signature:

Jakob Sebastian Hernandez

Location and Date: __Munich, 22/08/2024__   Signature:

VI Summary

In the context of increasing climate variability, understanding how plants respond to environmental fluctuations is critical for enhancing crop resilience and maintaining ecosystem stability. This dissertation aims to contribute to this field by investigating regulatory principles of plant metabolism and photosynthetic carbon assimilation. By employing a combination of experimental and computational approaches, the research offers insights that may help mitigate the adverse effects of climate change and ensure food security for a rapidly expanding global population. When a plant is exposed to a dynamic environment, there are substantial consequences to its metabolism, development and propagation. For example, a change in temperature regimes affects the thermodynamics of enzymes, which severely impacts the metabolic state. If these changes cannot be stabilized, they may result in the accelerated formation of reactive oxygen species, leading to oxidation of proteins and lipids, ultimately causing cell death. As such, plant cells undergo acclimation, a process involving significant reprogramming of the transcriptome, proteome, and metabolome.

In a first project, the acclimation response of 18 natural accessions of *Arabidopsis thaliana* to temperature changes was experimentally quantified. By analyzing photosynthetic efficiency and carbohydrate metabolism both at the acclimated temperature and after subsequent fluctuation, this work revealed that subcellular carbohydrate distributions, especially within plastids, play a key role in stabilizing photosynthesis under variable growth conditions. These findings highlight the importance of subcellular metabolic regulation in natural temperature acclimation. A second study investigated the photorespiratory pathway, a key metabolic process that returns carbon from the oxygenation reaction of Rubisco back to the Calvin–Benson–Bassham Cycle (CBBC). Using structural kinetic modeling, this research demonstrated that Rubisco's oxygenation function enhances metabolic plasticity, allowing plants to better cope with environmental perturbations. Thus, photorespiration was suggested to represent a trade-off that stabilizes the CBBC despite reducing carbon assimilation rates. The analysis also underscored the stabilizing effect of carbon flux towards sucrose biosynthesis, suggesting a complex trade-off between carbon loss and metabolic resilience. Building on this, the physiological function of photorespiration was examined closer in a third study, which utilized a multi-omics approach to explore the transcriptomic, proteomic, and metabolomic responses of photorespiratory mutants to elevated CO_2 concentrations. By including such mutants, the research uncovered novel interactions between metabolic pathways across cellular compartments, revealing previously unknown roles for enzymes in pyruvate and lipoic acid metabolism. These insights underscore the complexity of plant metabolic networks in acclimating to changing environments. Together, these three projects enhance the current understanding of how plants respond to a dynamic environment. Finally, this dissertation presents new insights into how the stability of carbon assimilation can be maintained in the face of perturbations, thus offering potential strategies for enhancing plant resilience in a dynamic environment.

1. Introduction

Inorganic carbon in the form of CO_2 can be converted into organic compounds via the process of carbon fixation. Organisms capable of such, which include most plants, are known as autotrophs (ancient Greek: "auto" – self, "trophic" – of or relating to nutrition). This process has wide reaching impacts besides supplying autotrophic organisms with organic matter, as it allows carbon to enter the biosphere. Thus, it strongly influences ecosystem dynamics and forms the basis for global food production either directly through the biomass of crops, or indirectly by supplying nourishment to livestock. The by far biggest portion of carbon in the biosphere is found in terrestrial plants, emphasizing their substantial contribution to global carbon fixation (Bar-On et al., 2018). In addition, the reduction of atmospheric CO_2 has a direct impact on global climate, as CO_2 acts as a greenhouse gas (Masson-Delmotte et al., 2021). It thus becomes evident, that to achieve sustainability of life on earth, a firm grasp of biological carbon fixation, in particular of land plants, is of utmost importance.

The rate of carbon fixation in plants, as well as the physiological homeostasis, is largely dependent on a host of biotic and abiotic factors (Suzuki et al., 2014). If changes in these environmental conditions are not stabilized, plants may suffer adverse effects on development and growth or even irreversible tissue damage (Athanasiou et al., 2010; Herrmann et al., 2019; Strand et al., 1997). For example, a change in temperature directly alters the underlying thermodynamics of biochemical reactions and the fluidity of membranes, therefore resulting in a substantial shift in transmembrane concentration gradients and metabolic fluxes (Cano-Ramirez et al., 2021; Elias et al., 2014). If plant's stress response and acclimation capacity is unable to keep metabolic deflections below a certain threshold, its tissue is damaged via the rise of reactive oxygen species (ROS) due to a disbalanced homeostasis between energy availability and consumption (Choudhury et al., 2017). This might result in a substantial reduction of cell performance or even cell death.

1.1 Carbon assimilation in C_3 plants

Plants perform photosynthesis in the chloroplast in a two-step process. First, light energy is converted to chemical energy in the form of NADPH and ATP via a series of transmembrane proteins in the thylakoid membrane. Following this, carbon is fixed with the now available chemical energy in one of three pathways, those being C_3, C_4, or CAM, depending on the plant species (Kadereit et al., 2014). Of these, C_3 carbon fixation is the most common pathway while C_4 and CAM carbon fixation particularly occur under arid and high temperature conditions (Dodd et al., 2002; Sage, 2004).

1.1.1 Primary reactions of photosynthesis

In order to convert the electromagnetic energy of light into photochemical energy used to drive carbon fixation and other metabolic pathways, protons first excite chlorophyll associated with the antenna

complexes of Photosystem I (PSI) and Photosystem II (PSII). The absorbed energy is then transferred down the antenna complex to chlorophylls with increasingly higher absorption wavelengths, and finally to the reaction centers of PSI and PSII (Mirkovic et al., 2017). The reaction center is composed of a chlorophyll a dimer (Chla$_2$) which, upon excitation, separates its charge to form a positive chlorophyll radical and one electron (e$^-$) which is transferred to an electron acceptor (Vinyard et al., 2013). In PSII, plastoquinone (PQ) acts as the electron acceptor in order to produce plastoquinol (PQH$_2$), while the necessary H$^+$ protons are supplied from the stroma of the chloroplast. The chlorophyll radical is reduced to its ground state via electrons obtained by splitting water, releasing oxygen and protons in the thylakoid lumen. This reaction is catalyzed by the water-oxidizing complex of PSII. The resulting PQH$_2$ is ultimately used to reduce plastocyanin (PC) in the cytochrome b$_6$f complex, releasing additional H+ protons to the lumen. The reduced PC is then used to return the chlorophyll radical, produced in the PSI reaction center, to its ground state. The electron generated via the charge separation in PSI uses Ferredoxin as an electron acceptor which then reduces NADP$^+$, and in conjunction with H$^+$ from the stroma, finally generates NADPH (Kadereit et al., 2014). This ultimately results in the following reaction stoichiometry:

$$2\, H_2O + 8\, H^+_{(stroma)} + 2\, NADP^+ \rightarrow 2\, O_2 + 8\, H^+_{(lumen)} + 2\, NADPH + 2\, H^+_{(stroma)} \tag{1}$$
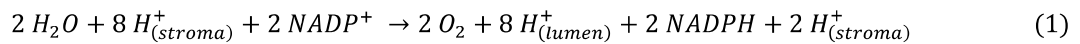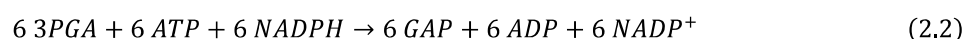
The resulting proton gradient between the stroma and the thylakoid lumen forms a proton motive force (PMF) composed of a chemical contribution (ΔpH) and an electrical contribution in the form of the membrane potential ($\Delta\Psi$). The PMF is then used to shuttle protons through the ATP synthase complex, providing the driving force to generate ATP in the stroma (Hahn et al., 2018). A simplified overview of the conversion of light energy into chemical energy is visible in the top of Fig. 1 (black arrows).

1.1.2. Carbon fixation and Calvin-Benson-Bassham cycle

Plants fixate carbon via the enzyme ribulose-1,5-bisphosphate carboxylase/oxygenase (Rubisco) which catalyzes the carboxylation of ribulose-1,5-bisphosphate (RuBP), yielding two molecules of 3-phospho-D-glycerate (3-PGA; Erb & Zarzycki, 2018). This reaction is considered the rate limiting step in carbon assimilation, when RuBP regeneration is not constrained by energy availability, as is the case at ambient conditions (Busch 2020). Owing to this, Rubisco represents 30 to 50% of soluble proteins found in plant leaves, making it one of the most abundant proteins in the biosphere (Erb & Zarzycki, 2018).

The chemical energy, available from the primary reactions, is used to reduce 3-PGA into triosephosphates (TPs). TPs represent critical metabolites in the assimilation of carbon as they can either be used to regenerate the CO$_2$ acceptor RuBP or to synthesize starch and sucrose. These molecules are needed to drive biomass accumulation and to supply the plant with energy when photosynthesis is not possible, e.g., in the night or in non-photosynthetic tissue (Kadereit et al., 2014). The vital process of generating TPs is catalyzed via the Calvin-Benson-Bassham cycle (CBBC) which is presented in (Fig. 1; Bassham et al., 1954). TPs are generated by first phosphorylating 3-PGA to 1,3-bisphosphoglyceric acid (1,3-BPG) via the enzyme phosphoglycerate kinase (PGK), which consumes

one molecule of ATP in the process (Lavergne et al., 1974). Following this, the enzyme glyceraldehyde 3-phosphate dehydrogenase (GAPDH) catalyzes the reduction of 1,3-BPG to the TP glyceraldehyde 3-phosphate (GAP), utilizing NADPH as the reducing agent (Schulman & Gibbs, 1968). GAP exist in an equilibrium with the TP dihydroxyacetone phosphate (DHAP), the conversion of which is catalyzed by triose-phosphate isomerase (TPI; Pichersky & Gottlieb, 1984). The pool of TPs is substrate for diverse pathways, depending on the metabolic needs of the plants. One central pathway is the regeneration of RuBP, as depletion of this metabolite would result in an arrest of carbon fixation (Bassham et al., 1954). During this process, five molecules of TPs are converted into three molecules of RuBP, for which three molecules of ATP are required. These three RuBP molecules then act as CO_2 acceptors for three carboxylation reactions, resulting in the generation of six TPs. This process allows one TP to be used in pathways unrelated to the regeneration of RuBP, for every three carbons fixated:

$$3\,RuBP + 3\,CO_2 \rightarrow 6\,3PGA \tag{2.1}$$

$$6\,3PGA + 6\,ATP + 6\,NADPH \rightarrow 6\,GAP + 6\,ADP + 6\,NADP^+ \tag{2.2}$$

$$5\,GAP + 3\,ATP \rightarrow 3\,RuBP + 3\,ADP \tag{2.3}$$

$$1\,GAP \rightarrow other\ pathway \tag{2.4}$$

It thus becomes evident that for every TP used outside of the CBBC, energy in the form of 9 ATP and 6 NADPH is needed.

The process of RuBP regeneration is initiated by the aldol addition of GAP and DHAP to form fructose 1,6-bisphosphate (FBP), which is catalyzed by the enzyme aldolase (ALD; Bassham et al., 1954). This is followed by the dephosphorylation of FBP by fructose 1,6-bisphosphatase (FBPase), giving rise to fructose 6-phosphate (F6P). The enzyme transketolase (TK) removes two carbons from F6P, generating erythrose 4-phosphate (Ery4P), and adds them to a previously generated GAP, leading to the formation of xylulose 5-phosphate (Xyl5P; Murphy & Walker, 1982). The now available Ery4P is utilized in an aldol addition with a previously generated DHAP, to form sedoheptulose-1,7-bisphosphate (SBP), which is again catalyzed by ALD (Carrera et al., 2021). SBP now undergoes a similar sequence as FBP, first being dephosphorylated by sedoheptulose-1,7-bisphosphatase (SBPase), to form sedoheptulose-7-phosphate (Sed7P; Breazeale et al., 1978). The enzyme TK removes two carbons from Sed7P, forming ribose-5-phosphate (Rbo5P), and again adds them to GAP to generate Xyl5P (Murphy & Walker, 1982). The phosphorylated pentoses Rbo5P and Xyl5P can now be isomerized to ribulose 5-phosphate (Rbu5P) via the enzymes ribose-5-phosphate isomerase (RPI) and ribulose-phosphate epimerase (RPE), respectively (Kadereit et al., 2014). In a final step, the three molecules of Rbu5P (one from Rbo5P and two from Xyl5P) are phosphorylated by phosphoribulokinase (PRK) to regenerate RuBP,

consuming ATP in the process (Surek et al., 1985). This completes the steps of the CBBC, with the now available RuBP acting as new CO_2 acceptors, thus closing the cycle.
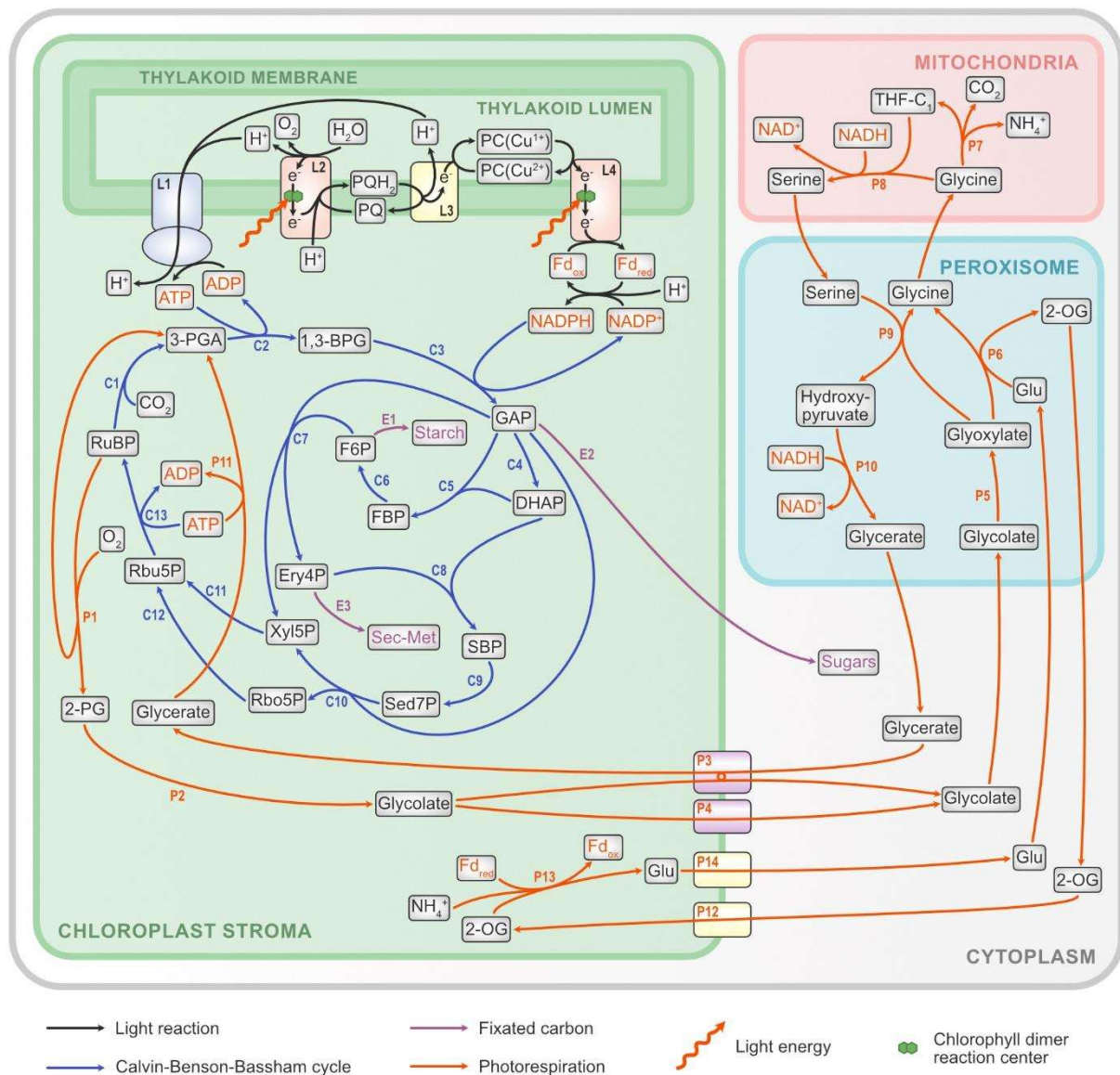

Fig. 1: Schematic overview of carbon fixation in C₃-Plants. Enzymes/ Proteins: L1: ATP synthase, L2: PSII - Photosystem II, L3: Cytochrome b6f complex, L4: PSI - Photosystem I, C1: Rubisco (carboxylase reaction), C2: PGK - phosphoglycerate kinase, C3: GAPDH - glyceraldehyde 3-phosphate dehydrogenase, C4: TPI - triose-phosphate isomerase, C5: ALD – aldolase, C6: FBPase - fructose 1,6-bisphosphatase, C7: TK - transketolase, C8: ALD - aldolase, C9: SBPase - sedoheptulose-1,7-bisphosphatase, C10: TK - transketolase, C11: RPE - ribulose-phosphate epimerase, C12: RPI - ribose-5-phosphate isomerase, C13: PRK - phosphoribulokinase, E1: fixed carbon used for Starch synthesis, E2: fixed carbon exported for sugar (mainly sucrose) synthesis. E3: fixed carbon used for secondary metabolism, P1: Rubisco (oxygenase activity), P2: PGP - phosphoglycolate phosphatase, P3: PLGG1 - plastidal glycolate/glycerate translocator 1, P4: BASS6 – bile acid sodium symporter 6, P5: GO - glycolate oxidase, P6: GGAT - glutamate-glyoxylate aminotransferase, P7: GDC - glycine decarboxylase, P8: SHMT - serine hydroxymethyltransferase, P9: SGAT - serine-glyoxylate aminotransferase, P10: HPR1 - hydroxypyruvate reductase 1, P11: GLYK - glycerate kinase, P12: DiT1 - dicarboxylate translocator 1, P13: FdGOGAT - ferredoxin-dependent glutamate synthase, P14: DiT2.1 - dicarboxylate translocator 2.1. Metabolites: PQ: plastoquinone, PQH₂: plastoquinol, PC: plastocyanin,

4

RuBP: ribulose-1,5-bisphosphate, 3-PGA: 3-phospho-D-glycerate, 1,3-BPG: 1,3-bisphosphoglyceric acid, GAP: glyceraldehyde 3-phosphate, DHAP: dihydroxyacetone phosphate, FBP: fructose 1,6-bisphosphate, F6P: fructose 6-phosphate, Ery4P: erythrose 4-phosphate, Xyl5P: xylulose 5-phosphate, SBP: sedoheptulose-1,7-bisphosphate, Sed7P: sedoheptulose-7-phosphate, Rbu5P: ribulose 5-phosphate, Rbo5P: ribose-5-phosphate, 2-PG: 2-phosphoglycolate, Glu: glutamate, 2-OG: 2-oxoglutarate, THF-C1: C-1-tetrahydrofolate.

1.1.3 Photorespiration

The rate of carbon assimilation is, however, not only tied to the concentration of CO_2 and the resulting carboxylation reaction rate, but also to the concentration of O_2 (Foyer et al., 2009; Warburg, 1920). This is a consequence of the dual catalytic function of Rubisco, which in addition to catalyzing the carboxylation reaction of RuBP, catalyzes its oxygenation. The oxygenation of RuBP generates one molecule of 3-PGA and one molecule of 2-phosphoglycolate (2-PG; Bowes et al., 1971; Foyer et al., 2009). While 3-PGA can enter the CBBC as described previously, 2-PG is metabolized in a process termed photorespiration (Fig. 1, orange arrows). As the photorespiratory pathway releases previously fixated carbon, it directly reduces the carbon assimilation rate, thus representing a substantial cost to the cell (Foyer et al., 2009). Owing to this, and to the fact that 2-PG is a strong inhibitor of several enzymes of the CBBC and chloroplast metabolism, it becomes evident that photorespiration is an integral part of the carbon assimilation process (Anderson, 1971; Flügel et al., 2017; Kelly & Latzko, 1976).

Enzymes that are known to be inhibited by 2-PG are TPI (Anderson, 1971), SBPase (Flügel et al., 2017), and phosphofructokinase (PFK; Kelly & Latzko, 1976). Both TPI and SBPase are involved in the CBBC. In addition to its function in the CBBC, TPI is also involved in starch biosynthesis. The enzyme PFK, on the other hand, is proposed to be involved in the generation of TPs from starch in the night (Kelly & Latzko, 1976).

Due to its role as an enzyme inhibitor, the metabolism of 2-PG plays a central role in the regulation of photosynthesis. Dephosphorylation of 2-PG to glycolate is catalyzed by the enzyme phosphoglycolate phosphatase (PGP; Somerville & Ogren, 1979). Glycolate is then exported from the chloroplast to the cytosol either via the plastidal glycolate/glycerate translocator (PLGG1) or the bile acid sodium symporter 6 (BASS6; Kuhnert et al., 2021). After transport into the peroxisome, glycolate is oxidized into glyoxylate via glycolate oxidase (GO), in a reaction that produces H_2O_2 (Foyer et al., 2009). The subsequent conversion of glyoxylate to glycine can either be catalyzed by glutamate-glyoxylate aminotransferase (GGAT) or by serine-glyoxylate aminotransferase (SGAT; Foyer et al., 2009). The reaction catalyzed by GGAT transfers the amino group from glutamate to glyoxylate, producing 2-oxoglutarate (2-OG) and glycine (Foyer et al., 2009). In order to maintain photorespiration, 2-OG produced by GGAT has to be regenerated into glutamate via the GOGAT cycle in the chloroplast (Kadereit et al. 2014). The glycine produced in the peroxisome by GGAT/SGAT is then transported into the mitochondria, where the two enzyme complexes glycine decarboxylase (GDC) and serine hydroxymethyltransferase (SHMT) subsequently catalyze the NADPH dependent conversion of two

molecules of glycine into one molecule of serine resulting in the generation of NH_4^+ and the release of CO_2 (Kadereit et al., 2014; Somerville & Ogren, 1982). Once serine is transported back into the peroxisome, its amino group can be transferred to glyoxylate via SGAT to produce hydroxypyruvate and glycine (Foyer et al., 2009). The flux partitioning between the two aminotransferases GGAT and SGAT hence depends on the fraction of glycine and serine that leaves the photorespiratory pathway (Busch, 2020). If photorespiration operates as a closed cycle, the ratio is 1:1 as one glycine generated via GGAT and one generated by SGAT are needed to generate one molecule of serine, thus balancing the stoichiometry (Busch, 2020). If amino acids are used in a diverging pathway, this ratio increases, as a higher flux through GGAT is needed (Busch, 2020). The hydroxypyruvate generated by SGAT in the peroxisome is next reduced to glycerate in a reaction catalyzed by hydroxypyruvate reductase (HPR). After glycerate is exported form the peroxisome into the cytosol, it is imported into the chloroplast via PLGG1 (Kuhnert et al., 2021). Finally, glycerate is phosphorylated by glycerate kinase (GLYK) to produce 3-PGA which then enters the CBBC (Foyer et al., 2009). If the pathways operate as a closed cycle, 75% of carbon from 2-PG is recovered as two molecules of 2-PG produce one molecule of 3-PGA and release one molecule of CO_2:

$$2 \, 2PG \; \rightarrow 3PGA + CO_2 \tag{3}$$

In conclusion, the photorespiratory pathway comprises enzymatic reactions across the chloroplast, cytosol, peroxisome, and the mitochondria. Since two oxygenation reactions of RuBP result in the release of one molecule of CO_2 in a closed photorespiratory cycle (Eq. 3), this leads to a final carbon assimilation rate of:

$$A = \; V_c - 0.5V_o - \; R_d \tag{4}$$

with V_c representing the rate of RuBP carboxylation, V_o the rate of RuBP oxygenation, and R_d the rate of CO_2 release, which is not associated with photorespiration (Farquhar et al., 1980).

1.1.4 Metabolism of assimilated carbon

The pool of TPs available in the chloroplast, which are not utilized for the regeneration of RuBP, represent the direct output of carbon fixation. A portion of this fixated carbon is exported from the plastid into the cytosol, where it is utilized in the synthesis of F6P, which in turn serve as a substrate for the generation of sucrose (Koch, 2004). The generation of F6P in the cytosol follows similar steps as in the plastid, with cytosolic isoforms of ALD and FBPase catalyzing the aldol addition of TPs and subsequent dephosphorylation of FBP. Sucrose is a disaccharide composed of glycolytically linked glucose and fructose. Owing to this, half of the F6P used for the synthesis of sucrose is converted into UDP-glucose in three enzymatic steps (Kadereit et al., 2014). The hexosyl group is subsequently transferred to the remaining F6P, forming sucrose-6-phosphate (S6P) in a reaction catalyzed by sucrose-phosphate synthase (SPS; Lunn, 2016). Finally, S6P is dephosphorylated by sucrose-phosphate phosphatase

(SPP), yielding sucrose (Lunn, 2016). Sucrose serves as the main transport carbohydrate in plants, reaching sink tissues via the phloem, thus suppling non-photosynthetic tissue with energy and carbon (Wind et al., 2010). The breakdown of sucrose occurs either via invertase, yielding fructose and glucose, or via the reversed sucrose synthase reactions, yielding fructose and UDP-glucose (Koch, 2004). The precise mechanism and subcellular location of sucrose breakdown depends on a host of factors, such as the developmental stage or the occurrence of plant stress (Koch, 2004).

Fixated carbon, that is not exported form the chloroplast, is mainly used for the synthesis of transitory starch which typically represents a carbon partition of approximately 30% (Kölling et al., 2015; Stitt & Zeeman, 2012). The first steps of starch synthesis follow the same pattern as the CBBC, first being converted into F6P via an aldol addition and dephosphorylation of FBP (Pfister & Zeeman, 2016). In succeeding steps, F6P is converted into ADP-glucose, which is then added to the starch polymer via a glycolic bond (Stitt & Zeeman, 2012). Starch consists of α-1,4 and α-1,6-linked glucose polymers and serves as the main storage molecule of carbohydrates during the day, being degraded in the night to support metabolism and growth (Pfister & Zeeman, 2016). Starch is predominantly broken down into maltose, which is then exported from the chloroplast into the cytosol (Niittylä et al., 2004; Stitt & Zeeman, 2012). In the cytosol, maltose is cleaved to release glucose which is substrate for phosphorylation, catalysed by hexokinase (HXK). The product, glucose-6-phosphate (G6P), can then be used again to generate sucrose or act as a substrate for other metabolic pathways, e.g., glycolysis (Kadereit et al., 2014).

The generation of sucrose and starch represent the primary outputs of carbon fixation. However, due to changing environmental conditions or stress exposure, a substantial portion of fixated carbon is used to synthesize specialized metabolites with protective functions, e.g., flavonoids via the shikimate pathway (Tzin et al., 2012). In this pathway, Ery4P and phosphoenolpyruvate (PEP) are used to generate chorismate, the major precursor of benzene containing compounds (Weaver & Herrmann, 1997).

Taken together, in many plant species, pathways of sucrose and starch biosynthesis represent central fluxes of assimilated carbon. Under stress conditions, additional carbon fluxes are allocated towards specialized metabolites. Photosynthesis and carbon partitioning between these pathways need to be tightly regulated to stabilize metabolism and prevent irreversible tissue damage (Stitt et al., 2010).

1.2 Regulation and stability of plant carbon metabolism

1.2.1 Carbon assimilation in a changing environment

Environmental factors like temperature or light directly affect metabolic fluxes, e.g., by constraining enzymatic reaction rates or by affecting membrane fluidity (Busch, 2020; Cano-Ramirez et al., 2021; Elias et al., 2014; Seydel et al., 2022). Both the reaction rates as well as the membrane fluidity are increased in elevated temperature and are reduced in low temperature, resulting in shifted concentration

gradients. Further, light intensity not only governs the amount of energy available for photosynthesis, but also affects the concentration of CO_2 within the chloroplast, and thus, the RuBP carboxylation rate (Busch, 2020; Kadereit et al., 2014). The plastidial CO_2 concentration is dependent on the state of the stomata as well as chloroplast positioning in the cell, both of which are affected, among other factors, by the intensity and quality of light (Busch, 2020; Wada, 2013). It thus becomes evident that a host of environmental factors are integrated to form the state of the carbon assimilation process at any given moment. Within the constraints of the current environmental condition, the cells transcriptome, proteome, and metabolome are adjusted to optimize this state towards optimal growth and development (Herrmann et al., 2019). Once this adjustment is complete, the cell forms a quasi-steady state in which input and output reactions of metabolites are balanced forming a homeostasis. Exceptions to this are metabolites which exhibit the diurnal dynamics such as starch (Herrmann et al., 2019; Stitt & Zeeman, 2012).

Environmental conditions are, however, reflective of a dynamic ever-changing system, resulting in perturbations of the aforementioned homeostasis. Following these perturbations, the metabolic state has to be stabilized, as otherwise the balance between energy production and consumption is lost, thus shifting the redox potential (via NADPH) and proton gradient (via H+ in the thylakoid lumen) of subcellular compartments (Gan et al., 2019; Järvi et al., 2013). Although such shifts are vital to adjust and balance metabolic fluxes via redox mediated signaling cascades and activation of the xanthophyll cycle, they can lead to the accumulation of ROS once metabolic deviations surpass a certain threshold (Kadereit et al., 2014; Michelet et al., 2013). An over-reduction of the plastidial electron transport chain involved in the light reaction may result in electrons not being transferred to NADP but O_2 instead, resulting in the formation of superoxide (O_2^-; Wang et al., 2018). In addition, excess light energy results in the formation of triplet chlorophyll ($^3Chl^*$) in the reaction center of PSII which in turn leads to the formation of singlet oxygen ($^1O_2$; Tripathy & Oelmüller, 2012). The formation of some degree of ROS is an unavoidable byproduct of aerobic metabolism, with ROS acting as important signaling molecules within the cell (Choudhury et al., 2017). If, however, ROS generation significantly exceeds scavenging capacities, cellular structures and molecules, such as lipids and membranes, DNA, and proteins, may be irreversibly affected in their function which results in reduced performance or, ultimately, in cell death (Tripathy & Oelmüller, 2012).

1.2.2 Mathematical modeling as a tool to understand regulatory and stabilizing effects

In order to quantitatively describe a metabolic state of a cell, mathematical modeling presents itself as a suitable tool (Islam et al., 2021). Simulations of a model allow for the behavior of a metabolic system to be examined following a perturbation. This allows for stabilizing or destabilizing effects on the metabolism to be quantified, and to draw conclusions on how alterations in metabolic fluxes, pathways, and regulation effect the stability (Klipp et al., 2016; Steuer et al., 2006). In order to understand the plant's stress response and acclimation capacity, a solid understanding of the underlying mathematics governing dynamic systems is thus vital.

Dynamics of metabolism over time (t) can be described via a system of ordinary differential equations (ODEs; Klipp et al., 2016). In such a dynamic system, the change of each metabolite is described via one ODE and is made up of reactions that produce and consume a metabolite. For example, an aldolase (ALD) reaction can be described by (Eq. 5):

$$\xrightarrow[Inp]{} 2\ TP \xrightarrow[ALD]{} FBP \xrightarrow[Exp]{} \tag{5}$$

This example system consists of the two metabolites TP and FBP. The two metabolites are linked via ALD, which catalyzes the aldol addition of two TPs to generate one FBP. An unspecific input reaction supplies the system with TPs, while an unspecific efflux exports FBP out of the system, e.g., for RuBP regeneration. The dynamics of these metabolites can then be described via the following ODEs (Eqs. 6.1 and 6.2):

$$(d/dt)TP = INP - 2 * ALD \tag{6.1}$$

$$(d/dt)FBP = ALD - EXP \tag{6.2}$$

In this example, it is assumed that the input is a constant rate. The reaction rates of ALD and EXP can be described by kinetic equations, such as mass action or michaelis-menten kinetics. This example will use mass action kinetics, resulting in the following dynamic system:

$$\dot{x} = \frac{d}{dt}x = \begin{pmatrix} INP - 2 * k_{ALD} * TP^2 \\ k_{ALD} * TP^2 - k_{EXP} * FBP \end{pmatrix} \tag{7.1}$$

$$with\ x = \begin{pmatrix} TP \\ FBP \end{pmatrix} \tag{7.2}$$

Here, the vector $\dot{x}$ describes the temporal change of the state x, which represents a vector containing the concentrations of the metabolites. With the starting concentrations x_0 the system can then be solved numerically (Fig 2).
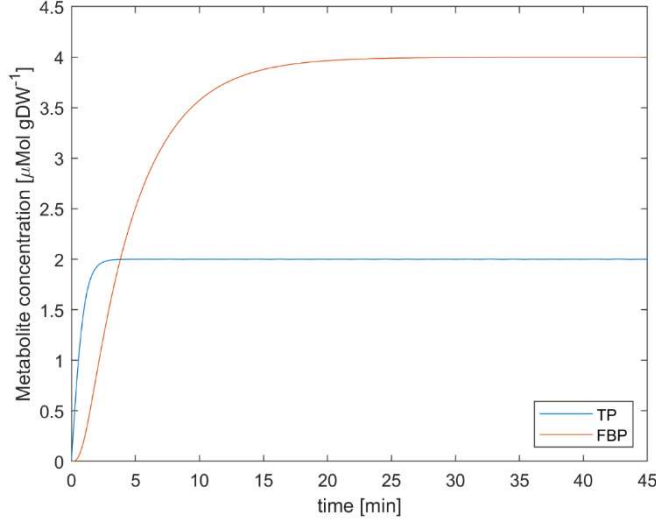
Parameter	Value
TP_0	0
FBP_0	0
INP	2
k_ALD	0.25
k_EXP	0.25

Fig. 2: Simulation of the example system of Eq. 7.1. The parameters used in the simulation are shown on the right-hand side. The model was simulated for the time span between 0 and 45 min. A homeostasis is formed after approximately 30 min. Here, the input reaction and output reactions of the metabolites are balanced.

A state x of this system is considered a steady state $\overline{x}$ if no change in metabolite concentration occurs, thus fulfilling $\dot{x} = 0 \; for \; x = \overline{x}$. Without any external perturbations, the system will remain in its current state. This can be seen in the homeostasis that is formed in fig. 2 after 30 min. If the system x is perturbated from the steady state $\overline{x}$, it can either return to its original state (the steady state is stable), exponentially diverge from $\overline{x}$ (the steady state is unstable) or be indifferent i.e., metastable.

A change in environmental conditions can be reflected in such a perturbation of the steady state, resulting in one of the behaviors mentioned above. Thus, in order to analyze the stability of the metabolism in the face of environmental fluctuations, the stability of the quasi steady state that is formed when metabolism exists in homeostasis needs to be considered. For this, the behavior of a dynamic system close to its steady state can be described via a Taylor approximation developed until the first derivative, resulting in a linearization of the system (Klipp et al., 2016). The approximation of the example system would thus be given by (Eq. 8):

$$\dot{x} \approx \begin{pmatrix} \frac{\partial f(TP)}{\partial TP} * (TP - \overline{TP}) + \frac{\partial f(TP)}{\partial FBP} * (FBP - \overline{FBP}) \\ \frac{\partial f(FBP)}{\partial TP} * (TP - \overline{TP}) + \frac{\partial f(FBP)}{\partial FBP} * (FBP - \overline{FBP}) \end{pmatrix} \tag{8}$$

This linearized system can be decomposed into a matrix containing all partial differentials, known as the Jacobian matrix J, and a vector $\hat{x} = x - \overline{x}$ which quantifies the deviations, i.e., fluctuations, from the steady state (Eqs. 9.1, 9.2)

$$\dot{x} \approx J\hat{x} = \begin{bmatrix} \dfrac{\partial f(TP)}{\partial TP} & \dfrac{\partial f(TP)}{\partial FBP} \\ \dfrac{\partial f(FBP)}{\partial TP} & \dfrac{\partial f(FBP)}{\partial FBP} \end{bmatrix} * \begin{pmatrix} \widehat{TP} \\ \widehat{FBP} \end{pmatrix} \tag{9.1}$$

$$\dot{x} \approx J\hat{x} = \begin{bmatrix} -4 * k_{ALD} * \overline{TP} & 0 \\ 2 * k_{ALD} * \overline{TP} & -k_{EXP} \end{bmatrix} * \begin{pmatrix} \widehat{TP} \\ \widehat{FBP} \end{pmatrix} \tag{9.2}$$

It thus becomes evident that the changes around the steady state can be approximated via the linear transformation of the fluctuation $\hat{x}$ with the Jacobian matrix J. As such, the resulting vector field points towards the origin if all eigenvalues λ of J possess a negative real part (Fig. 3 A). As the origin represents the state $\hat{x}$ with no further changes to the system state, this results in the stable original steady state as $x = \hat{x} + \overline{x}$ and $x = \overline{x}\ for\ \hat{x} = 0$, as can be seen in an example simulation with a randomly perturbated state (Fig. 3 C). If, however, one of the eigenvalues has a positive real part, the vector field points away from the origin (Fig. 3 B). This is illustrated in the example simulation shown in Fig. 3 D. Note, the dynamics shown in Fig. 3 B and C are not from the ALD example system, as this system is inherently stable.

The same can be seen when solving the linearized homogeneous system after the coordinate transformation $\hat{x} = x - \overline{x}$, which yields the general solution (Eq. 10):

$$\hat{x}(t) = \sum_{i=1}^{n} c_i b_i e^{\lambda_i t} \tag{10}$$

Here, λ are again the eigenvalues of J, while b represent the corresponding eigenvectors (Klipp et al., 2016). The coefficients c_i can be obtained by solving for $\hat{x}(0)$. This again shows that the stability of the steady state is entirely dependent on the real values of the eigenvectors of J, as $e^{\lambda t} = e^{(a+ib)t} = e^{at}(\cos bt + i \sin bt)$. Thus, if a is negative, then $\hat{x}$ converges to 0, again resulting in $x = \overline{x}\ for\ \hat{x} = 0$, making the steady state stable.

As such, the stability analyses of dynamic systems presents itself as excellent method to analyze the consequences of environmental fluctuations on a given metabolic homeostasis. This allows for stabilizing and destabilizing effects of metabolic fluxes, pathways and regulatory patterns to be examined (Klipp et al., 2016; Nägele, 2022; Steuer et al., 2006).
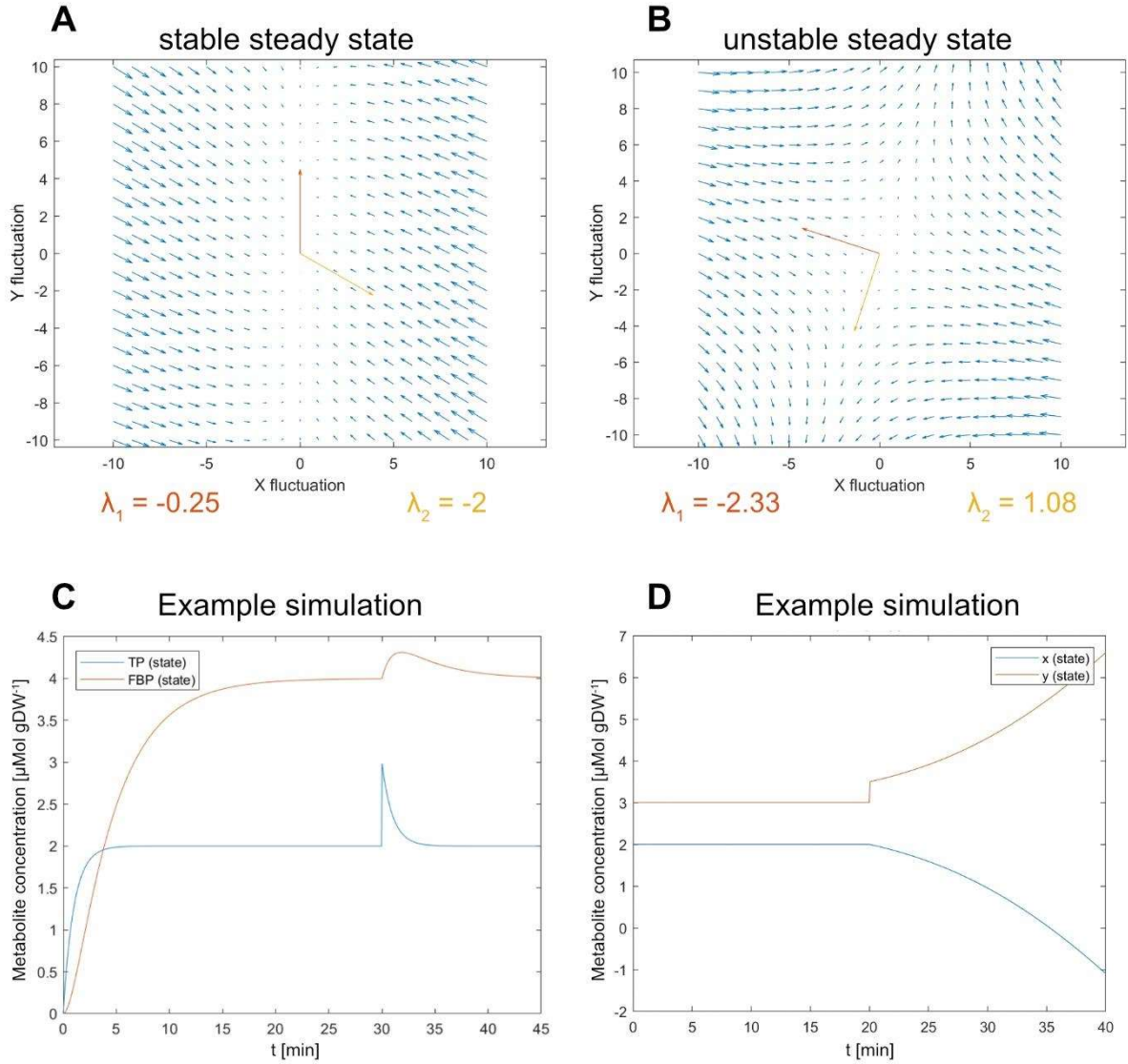
Fig. 3: Vector field of a stable and unstable steady state with corresponding example simulations. A) Vector field obtained through the linear transformation $J\hat{x}$, with $\hat{x}$ representing the perturbation from the *steady state* (origin). J was calculated as shown in Eq. 9.2 using the same parameters as in the simulation in Fig. 2. In addition, the eigenvectors are shown in red and orange. B) Vector field of an unspecific unstable steady state. The ALD example system is inherently stable and cannot be used for this demonstration. C) Example simulation of the ALD system with perturbation in both directions of the steady state. D) Example simulation of an unspecific unstable steady state.

1.2.3 Stabilization of metabolic homeostasis in a changing environment

The metabolism of plants possesses a wide range of structures, which ensure, that a given homeostasis can be stabilized against environmental fluctuations (Kadereit et al., 2014; Reznik & Segrè, 2010). To this extent, a plethora of enzymatic reactions are allosterically regulated, ensuring a constant feedback between the current metabolic state of a plant and its associated metabolic fluxes. Furthermore, key pathways involved in metabolism possess non-autocatalytic cyclic structures which are inherently stable, further contributing to the stability of a given homeostasis (Reznik & Segrè, 2010). In addition,

some pathways exist, which are capable of safely dispersing excesses in energy, thus maintaining the balance between energy generation and consumption (Kadereit et al., 2014). A well-known example of this is the xanthophyll cycle, capable of converting excess excitation energy into heat (Niyogi et al., 1998). These systems combine to make the plants metabolic homeostasis stable against a certain amount of environmental fluctuation, thus the plant is not faced with having to invest into reprogramming the transcriptome and proteome whenever a perturbation occurs.
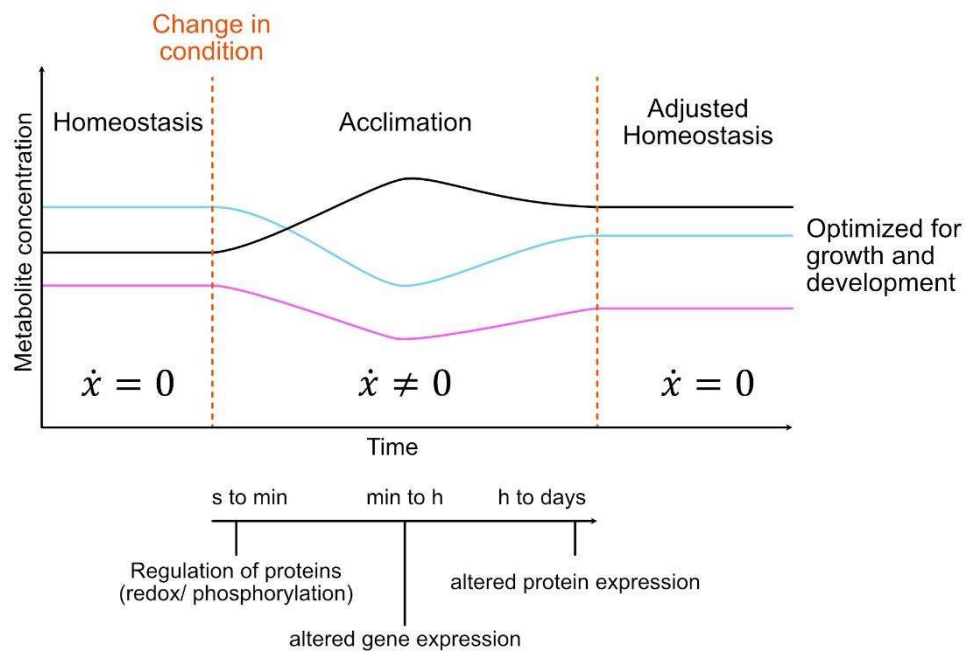

Fig. 4: Schematic representation of metabolic homeostasis acclimation. Once the hemostasis $\dot{x} = 0$ cannot be maintained in the face of a substantial and persistent environmental change, the acclimation process begins. After substantial reprograming of the transcriptome and proteome, a new adjusted homeostasis is formed which is optimized for the new environmental condition.

If, however, the perturbation is severe and persists in time, the plant has to acclimate to this new environmental condition, as the current homeostasis is no longer optimal or maintainable (Herrmann et al., 2019). Acclimation represents a multigenic trait in which significant reprogramming of the transcriptome and proteome occurs (Gilmour et al., 1988; Hannah et al., 2005). This in turn alters the capacity of enzymes involved in metabolism, resulting in a reprogramed metabolome. The acclimation process thus results in the formation of a new homeostasis, which stabilizes growth and development in a new environment (Fig. 4).

The high degree of compartmentalization of plant cells complicates the quantitative analysis of metabolism and its regulation. The subcellular concentrations of metabolites greatly differ between compartments resulting in complex non-intuitive behavior and regulation (Hoermiller et al., 2017; Nägele, 2022; Weiszmann et al., 2018). For example, the large volume of the vacuole causes a dilution of metabolites compared to their concentration in the cytosol. This dilution may lead to significantly

different regulatory interactions between a metabolite and the vacuolar versus cytosolic isoforms of an enzyme (Nägele, 2022). In addition, obtaining subcellular metabolite data remains a difficult and laborious process with only recent improvements allowing for a high throughput (Fürtauer et al., 2019). In a process of non-aqueous fractionation, subcellular metabolite distributions can be estimated based on their density distribution and correlation to a set of marker enzymes.

Owing to these challenges, the importance of such data has only recently come into focus, opening up a host of questions on the impact of subcellular metabolite dynamics on stability and performance of the photosynthetic output (Hurry, 2017; Nägele, 2022). Therefore, it becomes evident, that not only the absolute metabolite concentration, but also the subcellular distribution is needed to fully understand the stability of a given homeostasis and consequences of an acclimated metabolome.

1.3 Quantitative analysis of carbon assimilation in a dynamic environment

Although a substantial effort has been made to analyze stability and regulation of carbon assimilation, both experimental and theoretical limitations currently prevent the curation of a predictive mathematical model. Predicting subcellular metabolite concentrations in plants from genomic and transcriptomic data is highly challenging, if not impossible, as this data does not directly reflect the actual metabolite levels or their regulatory dynamics. Metabolite concentrations are influenced by post-transcriptional processes, enzyme activities, and environmental factors, which are not captured by genetic and transcriptomic information alone. Without accurate metabolite data, it becomes nearly impossible to fully understand how a plant acclimates to environmental changes. This challenge is reflected in the fact that a plant's geographic origin does not reliably predict its capacity for acclimation. This suggests that, beyond identifying the specific traits of an acclimated state, it is essential to account for the plasticity of the plant's metabolic homeostasis, which helps buffer against further environmental fluctuations. Acclimated homeostasis may play a critical role in stabilizing key cellular processes, such as carbon assimilation, under changing conditions. Based on these considerations, the first project presented in this dissertation (see chapter 2.1) analyzed the role of the subcellular sugar compartmentation of acclimated plants, in stabilizing photosynthetic efficiency against strong environmental perturbations. In this project, natural accessions of the model organism *Arabidopsis thaliana,* from a wide geographic range of Europe and the Cape Verde Islands, were subjugated to both low and high temperature regimes. The photosynthetic efficiency was then measured both under the acclimated temperature regime as well as under strong temperature fluctuations. The photosynthetic performance was finally correlated to the geographic origin and the subcellular sugar concentration. In order to effectively calculate the subcellular distributions of metabolites, a new tool was created and published as an R shiny app.

Besides the impact of subcellular metabolism on the stability and performance of photosynthesis, another aspect of the carbon assimilation process that is not well studied is the role of photorespiration,

besides in its function of degrading 2-PG. In the past, photorespiration was viewed as a costly detoxification pathway (Lorimer & Andrews, 1973). It was thought that the production of 2-PG is an inevitable side effect of an oxygen rich atmosphere, with an increase in specificity leading to a decreased enzymic turnover rate (Erb & Zarzycki, 2018; Lorimer & Andrews, 1973). However, some forms of Rubisco appear to have evolved variable oxygenation kinetics (Tcherkez, 2016). Based on this, Rubisco has become a major target for bioengineering to boost both substrate specificity and catalytic conversion rates (Poudel et al., 2020). This, however, leads to the question of why the occurrence of the oxygenation reaction persists and was not eliminated by natural selection (Tcherkez, 2016). Besides possible biochemical constraints (Tcherkez, 2016), there is an increasing body of evidence which suggests that photorespiration is not merely a detoxification pathway, but serves important physiological functions (Hodges et al., 2016; Shi et al., 2022; Takahashi et al., 2007).

The photorespiratory pathway is well connected with the plants' primary metabolism and serves as an important source of a wide range of metabolites feeding into amino acid and C1 metabolism (Hodges et al., 2016). In addition, it has been suggested that photorespiration is involved in protecting the plant against photoinhibition (Shi et al., 2022; Takahashi et al., 2007). This effect was particularly evident under fluctuating light, where it was hypothesized, that an increased photorespiratory flux increases consumption of reducing power thus decreasing electron leakage (Shi et al., 2022). This observation raises the question of possible stabilizing effects of photorespiration on carbon assimilation against environmental fluctuations, in addition to decreasing acceptor side limitations on the consumption of reducing power.

Based on these considerations, the second project (see chapter 2.2) analyzed whether the photorespiratory pathway is capable of stabilizing carbon assimilation and what role regulation by 2-PG possesses in increasing or decreasing the stability of a given metabolic homeostasis. A mathematical model representing the CBBC and photorespiration was derived and analyzed as described (chapter 1.2.2). Following the approach of structural kinetic modeling (SKM), the model consisted of saturation kinetics (i.e. Michaelis-Menten kinetics) without explicit knowledge of enzymatic parameters such as the V_{max} and K_m which are often laborious and difficult to obtain (Steuer et al., 2006; Wittig et al., 2014). In addition, such parameters are dependent on numerous factors *in vivo*, further impairing the physiological interpretation of *in vitro* data (Bisswanger, 2017). As a result, the SKM approach has been proven very useful in analyzing metabolic stability and regulatory effects (Fürtauer & Nägele, 2016; Grimbs et al., 2007; Reznik & Segrè, 2010). Furthermore, the regulatory interactions by 2-PG where analyzed using a modified Brach-and-Bound algorithm for discrete parameter optimization (Land & Doig, 1960).

With the goal of understanding the interplay between photorespiration and primary metabolism, the effects of disrupting the photorespiratory pathway were analyzed in a third project (see chapter 2.3). For this, the *A. thaliana* wild type plants (Col-0) were compared to the T-DNA insertions lines *hpr1-1*, *h-bou*, and *hxk1*. The enzyme HPR1 is the main isoform of Hydroxypyruvate reductase (see chapter 1.1.3) and is located in the peroxisome (Foyer et al., 2009). The knock out mutant *hpr1-1* only shows a mild

photorespiratory phenotype, as a cytosolic bypass via HPR2 is proposed to maintain a high photorespiratory flux (Timm et al., 2008). BOU (A BOUT DE SOUFFLE) is hypothesized to be a mitochondrial glutamate transporter which is involved in the synthesis of THF, thus impacting the photorespiratory serine synthesis (Eisenhut et al., 2013). The absence of BOU shows a strong photorespiratory phenotype with substantially impaired growth at ambient CO_2 conditions (aCO_2; approx. 400 ppm; Eisenhut et al., 2013). When grown at a CO_2 concentration of 3000 ppm, these effects can be mostly compensated (Eisenhut et al., 2013). Finally, HXK1 (Hexokinase 1) is both involved in phosphorylating hexoses and in sugar sensing and signaling (Aguilera-Alvarado & Sánchez-Nieto, 2017). Although not showing a photorespiratory phenotype, it was reported that HXK1 is involved in regulating photorespiration under high light conditions (Küstner et al., 2019). For this project, plants were grown under aCO_2 before being transferred to elevated CO_2 conditions (eCO_2; 1000 ppm). The flux through the photorespiratory pathway is greatly reduced at eCO_2, thus allowing to distinguish between general effects and alterations resulting from disrupted photorespiration. Proteomics, transcriptomics, and subcellular metabolomics data was obtained at aCO_2 (0 days) and at e$CO2$ after 1, 3, 5 and 7 days. An exception to this, being for metabolomics after 5 days of eCO_2, where no data was obtained. In order to integrate this vast dataset, an SQLite database was created in conjunction with a Python toolbox, to allow for rapid data exploration. The combination of these omics-datasets provides detailed information on the effects of the mutant lines, allowing for new insides to be gained on the metabolic connections between photorespiration and primary metabolism, further hinting towards possible regulatory interactions within the carbon assimilation process.

2. Publications and Manuscripts

2.1 Natural variation of temperature acclimation of *Arabidopsis thaliana*

Jakob Sebastian Hernandez, Dejan Dziubek, Laura Schröder, Charlotte Seydel, Anastasia Kitashova, Vladimir Brodsky, Thomas Nägele *

Acclimation is a multigenic trait by which plants adjust photosynthesis and metabolism to cope with a changing environment. Here, natural variations of photosynthetic efficiency and acclimation of the central carbohydrate metabolism were analyzed in response to low and elevated temperatures. For this, 18 natural accessions of *Arabidopsis thaliana*, originating from Cape Verde Islands and Europe, were grown at 22°C before being exposed to 4°C and 34°C for cold and heat acclimation, respectively. Absolute amounts of carbohydrates were quantified together with their subcellular distribution across plastids, cytosol and vacuole. Linear electron transport rates (ETRs) were determined together with the maximum quantum efficiency of photosystem II (Fv/Fm) for all growth conditions and under temperature fluctuation. Under elevated temperature, ETR residuals under increasing photosynthetic photon flux densities significantly correlated with the degree of temperature fluctuation at the original habitat of accessions, indicating a geographical east/west gradient of photosynthetic acclimation capacities. Plastidial sucrose concentrations positively correlated with maximal ETRs under fluctuating temperature, indicating a stabilizing role within the chloroplast. Our findings revealed specific subcellular carbohydrate distributions that contribute differentially to the photosynthetic efficiency of natural *Arabidopsis thaliana* accessions across a longitudinal gradient. This sheds light on the relevance of subcellular metabolic regulation for photosynthetic performance in a fluctuating environment and supports the physiological interpretation of naturally occurring genetic variation of temperature tolerance and acclimation.

Corresponding Author: *

ORIGINAL RESEARCH

Physiologia Plantarum

Natural variation of temperature acclimation of *Arabidopsis thaliana*

Jakob Sebastian Hernandez[1] | Dejan Dziubek[1] | Laura Schröder[1] | Charlotte Seydel[1,2] | Anastasia Kitashova[1] | Vladimir Brodsky[1] | Thomas Nägele[1]

[1]Faculty of Biology, Plant Evolutionary Cell Biology, Ludwig-Maximilians-Universität München, Planegg

[2]Faculty of Biology, Plant Development, Ludwig-Maximilians-Universität München, Planegg

Correspondence
Thomas Nägele,
Email: thomas.naegele@lmu.de

Abstract

Acclimation is a multigenic trait by which plants adjust photosynthesis and metabolism to cope with a changing environment. Here, natural variations of photosynthetic efficiency and acclimation of the central carbohydrate metabolism were analyzed in response to low and elevated temperatures. For this, 18 natural accessions of *Arabidopsis thaliana*, originating from Cape Verde Islands and Europe, were grown at 22°C before being exposed to 4°C and 34°C for cold and heat acclimation, respectively. Absolute amounts of carbohydrates were quantified together with their subcellular distribution across plastids, cytosol and vacuole. Linear electron transport rates (ETRs) were determined together with the maximum quantum efficiency of photosystem II (Fv/Fm) for all growth conditions and under temperature fluctuation. Under elevated temperature, ETR residuals under increasing photosynthetic photon flux densities significantly correlated with the degree of temperature fluctuation at the original habitat of accessions, indicating a geographical east/west gradient of photosynthetic acclimation capacities. Plastidial sucrose concentrations positively correlated with maximal ETRs under fluctuating temperature, indicating a stabilizing role within the chloroplast. Our findings revealed specific subcellular carbohydrate distributions that contribute differentially to the photosynthetic efficiency of natural *Arabidopsis thaliana* accessions across a longitudinal gradient. This sheds light on the relevance of subcellular metabolic regulation for photosynthetic performance in a fluctuating environment and supports the physiological interpretation of naturally occurring genetic variation of temperature tolerance and acclimation.

1 | INTRODUCTION

Environmental dynamics have direct effects on plant metabolism and performance. Plant stress response and acclimation to environmental changes stabilize physiological homeostasis and prevent irreversible tissue damage or adverse effects on development and growth. Both stress response and acclimation are multigenic traits and typically comprise many physiological and molecular changes, including significant reprogramming of photosynthesis, primary and secondary metabolisms (Hannah et al., 2006; Garcia-Molina et al., 2020; Schwenkert et al., 2022; Seydel et al., 2022). For example, a changing temperature regime affects the properties of membrane systems and enzyme

kinetics, resulting in shifts in membrane fluidity, transmembrane concentration gradients and reaction rates (Elias et al., 2014; Cano-Ramirez et al., 2021). Metabolic pathways and signaling cascades need to be reprogrammed in order to sustain and stabilize metabolism (Herrmann et al., 2019). If environmentally driven deflection from a metabolic state exceeds a certain threshold, this might lead to the formation of reactive oxygen species (ROS) and irreversible tissue damage (Choudhury et al., 2017). Below this threshold, plants are able to prevent irreversible damage by adjusting metabolism, membrane structure and the composition of the photosynthetic apparatus. For example, low temperatures result in an increase of cytochrome b6f complex, ATP synthase, Rubisco and other Calvin-Benson-Bassham cycle (CBBC) enzymes, whereas heat leads to increased proportions of light-harvesting complex II (LHCII) and photosystem I (PSI), while CBBC activity is downregulated (Gjindali and Johnson, 2023). This shows that changes in environmental temperature regimes adjust various processes on a molecular and physiological scale, which challenges our understanding and experimental analysis of pathways involved in temperature stress response and acclimation. Further complication of experimental and theoretical analysis is added by the interaction effects of different environmental stimuli, e.g., effects different light intensities have on temperature response (Huner et al., 1998). Although light has been found to be essential for full acclimation to low temperatures (Wanner and Junttila, 1999), too high intensities result in photoinhibition and photooxidative damage (Gray et al., 2003).

When exposed to low temperatures, sucrose metabolism was observed to play a key role in stabilizing photosynthetic efficiency, CO_2 fixation and carbon allocation (Kitashova et al., 2023). It was previously shown that carbon uptake in a low-temperature regime is limited by the capacity to synthesize sucrose (Strand et al., 2003). Cold-sensitive natural accessions of *Arabidopsis thaliana* were restricted in their maximal sucrose phosphate synthase (SPS) activity, which might result in ROS generation (Nägele et al., 2012). Furthermore, photosynthesis was found to be stabilized by vacuolar sucrose cleavage as metabolic control is preserved under cold stress (Weiszmann et al., 2018; Nägele, 2022). These findings suggest a central role of subcellular sucrose metabolism in temperature stress response and acclimation. Previously, it has been suggested that carbon partitioning plays a crucial role in enhancing photosynthesis at low temperatures. Specifically, a higher flux of carbon directed towards sucrose, rather than starch, can result in this improvement (Lundmark et al., 2006). A theoretical model has demonstrated that a shift in carbon partitioning towards sucrose can stabilize metabolism in the face of fluctuating environmental conditions (Hernandez and Nägele, 2022). Sucrose, together with galactinol, is a substrate for raffinose biosynthesis, which has previously been found to stabilize photosystem II during freeze–thaw cycles (Knaupp et al., 2011). Hence, carbon partitioning into sucrose might also stabilize downstream biosynthetic pathways, which play a central role for temperature acclimation.

Increased starch degradation results in a drop of starch amount during the first 24 h of cold exposure. This was suggested to serve as carbon resource for hexose biosynthesis, which has the capacity to act as cryoprotectants and as a source for rapid energy supply (Sicher, 2011). Further, soluble sugars were discussed to effectively scavenge ROS (Morelli et al., 2003) and simultaneously represent substrates for sugar alcohol biosynthesis, which supplies, e.g., raffinose family oligosaccharide (RFO) biosynthesis (Peterbauer and Richter, 2001). Following the initial decrease in starch amount, plants then accumulate starch to higher levels than before cold exposure (Guy et al., 2008). It was reported earlier that natural variation of starch accumulation during cold acclimation might be explained by a differential regulation of the starch degradation pathway resulting in higher starch amount in the freezing sensitive accession Cvi-0 (Cape Verde Islands), originating from Africa, than in the freezing tolerant accession Rsch (Rschew), originating from Russia (Nagler et al., 2015). Comparing Rsch under elevated temperature to the Sicilian accession Ct-1 (Catania) revealed that, similar to cold, Rsch accumulated a lower starch amount than Ct-1 (Atanasov et al., 2020). However, in contrast to cold, the total starch amount decreased under heat compared to control conditions, and the decrease was stronger in Rsch than in Ct-1. Further, decreased starch amount under heat is rather due to inhibition of ADP-glucose pyrophosphorylase and starch synthesis than increased capacities of starch degradation (Geigenberger et al., 1998; Awasthi et al., 2014).

Recently, the availability of sugars has been shown to be essential for plant survival under heat (Olas et al., 2021). While this demonstrates the crucial role of carbohydrate metabolism, its regulation under such conditions is less well understood. It has become evident that, to comprehensively address questions about metabolic regulation, subcellular and compartment-specific data is required (Nägele and Heyer, 2013; Hoermiller et al., 2017; Fürtauer et al., 2019; Höhner et al., 2021). A suitable method for addressing such questions is non-aqueous fractionation, which allows metabolites to be proportionally attributed to the plastid, cytosol, vacuole, and mitochondria (Gerhardt and Heldt, 1984; Fürtauer et al., 2019).Using such an approach, it was, for example, found that substantial reorganization of soluble sugar concentrations occurs at low temperatures (Hoermiller et al., 2017; Weiszmann et al., 2018; Patzke et al., 2019). This subcellular reorganization is hypothesized to be both necessary to distribute cryoprotective sugars to key cellular structures, e.g., raffinose to thylakoid membranes, and to stabilize the cellular metabolic homeostasis (Knaupp et al., 2011; Nägele and Heyer, 2013). Also, under elevated temperature, subcellular compartmentation and reprogramming of metabolism plays an important role, e.g., for the regulation of signaling cascades and ROS production (Kohli et al., 2019). Changes in subcellular signaling might explain the previously observed downregulation of transcripts of photosynthesis and carbohydrate metabolism under heat stress (Prasch and Sonnewald, 2013). While transcripts are downregulated, sugar amounts were found to either stabilize or increase during heat acclimation (Atanasov et al., 2020; Garcia-Molina et al., 2020). Simultaneously, a heat-induced increase of neutral and cell wall-associated invertase activities may explain an observed hexose accumulation, which was more pronounced in a natural *Arabidopsis* accession originating from southern Europe than in a northern accession (Atanasov et al., 2020).

In summary, these findings indicate that it is necessary to study carbohydrate metabolism on a subcellular level, which is hardly

predictable from the genome or transcriptome. With such an approach, regulatory patterns that stabilize photosynthesis in a changing temperature regime might be identified. Comparing natural accessions of *Arabidopsis thaliana* has been shown before to be a promising strategy to unravel conserved and specialized stress response and acclimation mechanisms (Maloof et al., 2001; Hannah et al., 2006; Weiszmann et al., 2023). Here, we analyzed the role of subcellular sugar compartmentation in stabilizing photosynthetic efficiency by comparing the natural variations of metabolic acclimation in *Arabidopsis* to both a high- and a low-temperature regime. Natural *Arabidopsis* accessions, originating from a wide geographical range, were acclimated to low and high temperatures before being exposed to a fluctuating temperature regime. Carbohydrates were quantified on a cellular and subcellular level. Finally, we developed an app to estimate subcellular compound distribution from experimental data using Monte Carlo simulations.

2 | MATERIALS AND METHODS

2.1 | Growth conditions and plant material

Plants of 18 natural accessions of *Arabidopsis thaliana* were grown for 5 weeks in a climate chamber under short-day conditions (8 h/16 h light/dark; photosynthetically active radiation (PAR): 100 μmol photons m^{-2} s^{-1}; 22°C/16°C; 60% relative humidity; see Table S1 for a full list of natural accessions). Then, with same daylength, PAR and relative humidity, plants were transferred to 4°C, 34°C, or left at 22°C for 4 days. Plant material was sampled after 4 hours in the light, i.e., at the middle of the diurnal light period. Leaf rosettes were cut with a scalpel at the hypocotyl and immediately transferred to liquid nitrogen to quench metabolism. Under constant supply of liquid nitrogen, plant material was ground to a fine powder and subsequently lyophilized.

2.2 | Chlorophyll fluorescence measurements

Light response curves were recorded using a pulse-amplitude-modulation (PAM) protocol on single leaves using a WALZ JUNIOR-PAM® (www.walz.com) in which photosynthetic photon flux density (PPFD, μmol photons m^{-2} s^{-1}) was stepwise increased every 20 sec after 15 min of dark incubation at 4°C, 22°C or 34°C for all acclimation conditions (PPFD list: 0, 40, 72, 104, 144, 200, 304, 456, 672, 1000, 1312, 1840, 2400 μmol photons m^{-2} s^{-1}). This achieved quantifying photochemical energy conversion efficiency in acclimated plants (growth temperature = measurement temperature) and under temperature stress (growth temperature ≠ measurement temperature). The linear electron transport rate (ETR) was calculated as follows (Equation 1):

$$ETR = Y(II) \cdot E \cdot A \cdot 0.5, \qquad (Eq.1)$$

with $Y(II)$ being the effective photochemical quantum yield of PS II, E the incident irradiance, and A the absorptance.

2.3 | Quantification of carbohydrates

Starch and soluble sugars were extracted and determined as described before (Kitashova et al., 2023). In brief, approx. 3 mg of lyophilized leaf material was incubated twice with 80% ethanol at 80°C for 30 min to extract soluble sugars. The pellet contained leaf starch granules, which were hydrolyzed, digested with amyloglucosidase, and quantified in a photometric assay using a coupled reaction of glucose oxidase, peroxidase and o-dianisidine. Extracted supernatants were pooled, dried in a desiccator and sugars in the pellet were dissolved in H_2O_{dd}. Amounts of the soluble carbohydrates sucrose, glucose and fructose were determined photometrically. Sucrose was determined after incubation with 30% KOH at 95°C using an anthrone reagent composed of 14.6 M H_2SO_4 and 0.14% (w/v) anthrone, yielding a complex with a specific absorbance maximum at 620 nm. Glucose and fructose amounts were determined within a coupled hexokinase/glucose 6-phosphate dehydrogenase assay, which yielded NADPH + H$^+$ detectable at 340 nm.

2.4 | Non-aqueous fractionation (NAF)

Subcellular fractionation followed a NAF protocol described earlier (Fürtauer et al., 2016). After the fractionation of lyophilized leaf material in mixtures of tetrachlorethylene and n-heptane with differential densities, marker enzyme activities were determined for plastids (alkaline pyrophosphatase activity), cytosol (UDP-glucose pyrophosphorylase activity) and vacuole (acidic phosphatase activity). Subcellular amounts of sucrose, glucose and fructose were determined as described in the previous paragraph.

To calculate the relative distributions of metabolites present in each subcellular compartment, an approach based on linear regression and a Monte Carlo simulation was used. This approach is based on the fact that metabolite distributions are made from a linear combination of the compartment-specific gradients (Equation 2):

$$Ax = b \qquad (Eq.2)$$

With A being the matrix containing relative values of the marker metabolites or enzymes. Each row m represents a density fraction and each column n a subcellular compartment. The vector x consists of the relative distribution of our target metabolite present in each compartment n and is the unknown vector of interest. Finally, the vector b consists of the relative values of target metabolites in each fraction m.

Thus, to obtain the relative distribution of a target metabolite across the subcellular compartments, (Equation 2) needs to be solved for x. For this, linear least-squares fitting constrained to the interval [0, 1] was applied, as a relative distribution within a compartment cannot be negative or greater than 1.

However, experimental data has shown that a technical error of approx. 10% cannot be excluded when performing NAF (Fürtauer et al., 2016). To account for this, random noise was added to each measurement following a normal distribution with a standard deviation of 5%. This resulted in more robust results and negates infeasible relative distributions such as $x = (0,0,1)^T$.

This method has been converted into an R Shiny App for ease of use and can be found in a GitHub repository (https://github.com/cellbiomaths/NAFalyzer). The app also contains a detailed explanation of how to apply and validate NAF data.

2.5 | Enzyme activities

Enzyme activities of the central carbohydrate metabolism were quantified photometrically as described before with slight modifications (Kitashova et al., 2023). All enzymes were quantified from the same extract, which consisted of 50 mM HEPES-KOH (pH 7.5), 5 mM MgCl$_2$, 2 mM EDTA, 1 mM DTT, 1% (v/v) glycerol, 0.1% (v/v) Triton, and protease inhibitor cocktail for plant cell and tissue extracts in DMSO solution (Sigma-Aldrich®).

Following incubation on ice and centrifugation at 4°C, neutral and acidic invertase activities were determined at 30°C by incubation of supernatants in neutral reaction buffer (20 mM HEPES-KOH pH 7.5, 100 mM sucrose) and acidic reaction buffer (20 mM sodium acetate pH 4.7, 100 mM sucrose), respectively. The reaction was stopped by incubation at 95°C before glucose equivalents were determined photometrically using a coupled glucose oxidase/peroxidase/o-dianisidine assay.

Glucokinase and fructokinase activities were quantified from supernatants using a reaction buffer consisting of 100 mM HEPES-KOH (pH 7.5), 10 mM MgCl$_2$, 2 mM ATP, 1 mM NADP$^+$, 0.5 U glucose 6-phosphate dehydrogenase, and either 5 mM glucose for glucokinase measurement or 5 mM fructose for fructokinase measurement. Production of NADPH was recorded photometrically for 20 min at 30°C and activities were derived from slopes in a linear range of the kinetic.

2.6 | Climate data

Climate data was obtained from a database (https://climatecharts.net/) and comprises values from 1950 until 2019. Temperature mean of a month is given in [°C] and precipitation in [mm month^{-1}].

2.7 | Statistics and data evaluation

Statistics and data evaluation was performed in R (Version 4.2.2) using RStudio, Version 2022.07.2 Build 576 (R Core Team, 2021). Correlation analysis and p-value computation were performed via the *rcorr* function of the *Hmisc* package (Version 5.1–0). Principle component analysis was performed via the *prcomp* function of the base stats package (Version 4.2.2).

3 | RESULTS

3.1 | Fluctuation of linear ETR reveals a longitudinal gradient of natural accessions

After 5 weeks of growth under short-day conditions, plants of 18 natural accessions were acclimated to low (4°C) or elevated (34°C)

temperatures. Maximum quantum yield of PSII (Fv/Fm) and linear ETR were quantified to reveal photosynthetic efficiencies. Detailed information about the accessions is provided in Table S1. Measurements were conducted at the temperature to which plants were acclimated to (i.e., 4°C, 22°C and 34°C). Additionally, plants acclimated at each temperature were exposed to both other temperature regimes for 15 minutes in the dark before, also under these cross-conditions, Fv/Fm and ETR were determined. These cross-condition measurements revealed the effect of a sudden change in temperature regimes on photosynthesis (Figure S1). Linear ETR was found to be both dependent on the measuring and the acclimation temperature. Plants acclimated and measured under 34°C showed the highest mean rates, while plants acclimated at 4°C and measured at 4°C demonstrated the lowest mean rates of ETR.

Particularly, yet not exclusively, from cross-conditional measurements, fluctuations of ETR curves were recognized, which indicate instability in photosynthesis over increasing light intensities. To quantify these fluctuations, a curve following a basic saturation kinetic was fitted to the data (Equation 3):

$$ETR = (PAR \cdot p1)/(PAR + p2), \quad \text{(Eq.3)}$$

with $p1$ and $p2$ being optimized parameters. The resulting residuals between the fit and experimental data then represent a measure for the degree of fluctuation of ETR. Strongest fluctuations were observed at PAR > 500 µmol photons m^{-2} s^{-1}, while only a weak signal-to-noise ratio was identified for PAR < 500 µmol photons m^{-2} s^{-1} (Figure S1). Due to this, residual analysis focused on ETR for PAR > 500 µmol photons m^{-2} s^{-1}. Further, for scaling across measurements, all residuals were normalized to the maximum ETR observed in the respective measurement.

Mean scaled residuals across all accessions became highest for plants acclimated and measured at 4°C (Figure 1A). In general, residuals were observed to be higher for measurements at 4°C than at 22°C and 34°C. Yet, interestingly, cold acclimation resulted in higher residuals than in non-cold or heat-acclimated plants when measured at 4°C. In contrast, heat and cold acclimation resulted in a lower fluctuation level of ETR compared to non-acclimated plants (22°C) when measured at 34°C (Figure 1A, right panel). To test whether scaled residuals can provide information about geographic origin and habitat of natural accessions, they were Spearman-correlated with latitude, longitude, temperature, and precipitation of the first quarter of the year (Figure 1B). This part of the year has recently been found to be indicative of the primary metabolism's regulation of natural *Arabidopsis* accessions (Weiszmann et al., 2023).

When measured at 22°C, plants acclimated to 4°C and 22°C showed similar residuals of ETR, while plants acclimated at 34°C showed the highest fluctuations. When measured at 34°C, plants acclimated at 4°C and 34°C showed the most stable ETR, while 22°C showed higher scaled residuals. This observation indicated a conserved mechanism of temperature acclimation and stabilization of photosynthetic efficiency. Hence, for further temperature acclimation analysis, the difference between the mean scaled residuals of plants acclimated at 22°C and 4°C, both measured at 34°C, was calculated
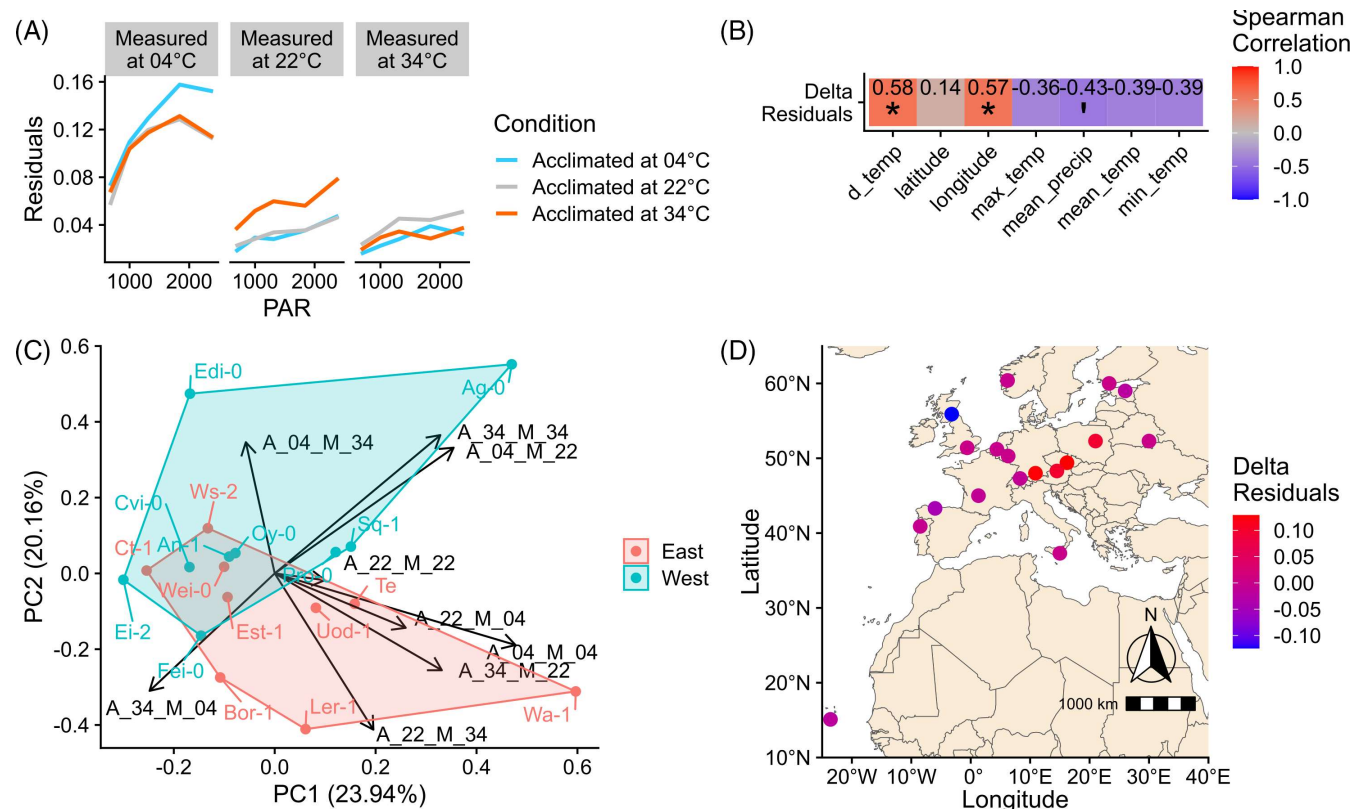
FIGURE 1 Fluctuations of electron transport rates across natural *Arabidopsis* accessions. (A) Overall trends of residuals in each combination of growth and measurement temperatures across all natural accessions. Residuals were normalized to the maximum ETR. (B) Spearman correlation between geographical and climate data to the difference between the mean scaled residuals of plants measured at 34°C after being acclimated at 22°C and 4°C. Climate data comprise the first quarter of the year (i.e., Jan – Mar). d_temp: maximum temperature difference; max_temp: highest temperature; mean_precip: mean precipitation; mean_temp: mean temperature; min_temp: minimal temperature. Details are provided in Table S1. Asterisks indicate significance (Spearman, n ≥ 5): * p < 0.05. Mean precipitation was significantly correlated with residuals to a significance level of 10% (i.e., p < 0.1 indicated as ('). Red colour indicates positive correlation, purple colour indicates negative correlation. (C) PCA of the mean scaled residuals of all conditions. Accessions labeled in blue represent the accessions classified as 'western', while the red label represents 'eastern' accessions. Loadings indicate mean scaled residuals at a certain acclimation (*A*) and measurement (*M*) temperature, e.g.: A_04_M_34: acclimated at 4°C, measured at 34°C. (D) Geographic origins of accessions and the delta in residuals of plants acclimated at 22°C and 4°C, when measured at 34°C.

and described as *Δ(delta) residuals*, indicating the acclimation capacity of photosynthetic electron transport under maximal temperature fluctuation. The *Δresiduals* were correlated to geographical and climate data from the first quarter of the year at the original habitat of the accessions. The analysis revealed a significant correlation between the *Δresiduals* and the longitude, as well as the difference in monthly mean temperatures recorded within the first quarter of the year, i.e., *d_temp = maximum mean temperature – minimum mean temperature*. Due to the significant positive correlation of *Δresiduals* with longitude, accessions were classified as western (50%, i.e., 9 out of 18 accessions) or eastern (50%; Figure 1D). Principal component analysis (PCA) showed that variance on PC1 was explained by measurements at 4°C, while PC2 was explained by measurements at 34°C (Figure 1C). Most distant accessions on PC1 were Ei-2 (Eifel, Germany) and Wa-1 (Warsaw, Poland). Most distant accessions on PC2 were Ag-0 (Argentat, France) and Ler-1 (Landsberg am Lech, Germany).

Maximum quantum yield of PSII (Fv/Fm) did not significantly differ between eastern and western accessions under any of the analyzed conditions (Figure S1). In general, it was lowest for plants acclimated to 4°C (Fv/Fm ∼0.7–0.8) and highest for non-acclimated plants grown and analyzed at 22°C (Fv/Fm ≥0.8). Variance of Fv/Fm was highest for cold acclimated plants, suggesting higher variability of acclimation of PSII among natural accessions than under elevated temperature. The Fv/Fm showed a significant negative correlation with ETR residuals, except for non-acclimated plants or heat-acclimated plants when measured at 4°C (Figure S2). Finally, short-term cold treatment induced higher photosynthetic fluctuations than both long-term and short-term heat exposure.

3.2 | Differential carbohydrate compartmentation during heat and cold acclimation relates to a longitudinal gradient

Amounts of starch, sucrose, glucose, and fructose were quantified across all 18 natural accessions under each acclimation condition.

Soluble carbohydrates significantly increased during cold acclimation, but total amounts varied strongly between accessions (Figure S3). In heat-acclimated plants, sucrose amounts also increased but to a lower extent than in the cold, whereas hexose amounts decreased compared to non-acclimated plants. The sucrose-to-starch ratios, calculated from C6 equivalents, showed distinct patterns across the natural accessions under low and high temperatures. For most accessions, the ratio of sucrose to starch was higher when plants were exposed to heat rather than cold. In Pro-0, Wei-0, and Cvi-0, the sucrose-to-starch ratio in cold-treated plants remained similar to that of non-acclimated plants.

In a PCA, temperature-induced carbohydrate dynamics separated cold-acclimated plants from non-acclimated (22°C) and heat-acclimated plants on PC1, explaining almost 80% of the total variance (Figure 2). On PC2, a separation of eastern and western accessions was observed, which was strongest for cold-acclimated plants and weakest for non-acclimated plants. A differential ratio of starch-to-soluble carbohydrates explained the observed separation on PC2 (~14%). In general, starch accumulation was stronger in western accessions, while soluble carbohydrates were accumulated stronger in eastern accessions. Carbohydrate accumulation was significantly stronger under 4°C than under 34°C, which resulted in a stronger separation of 22°C samples from cold samples than from heat samples (Figures 2 and S3). In average, exposure to elevated temperature resulted in a stronger increase of sucrose-to-starch ratios than under low temperature (Figure S3).
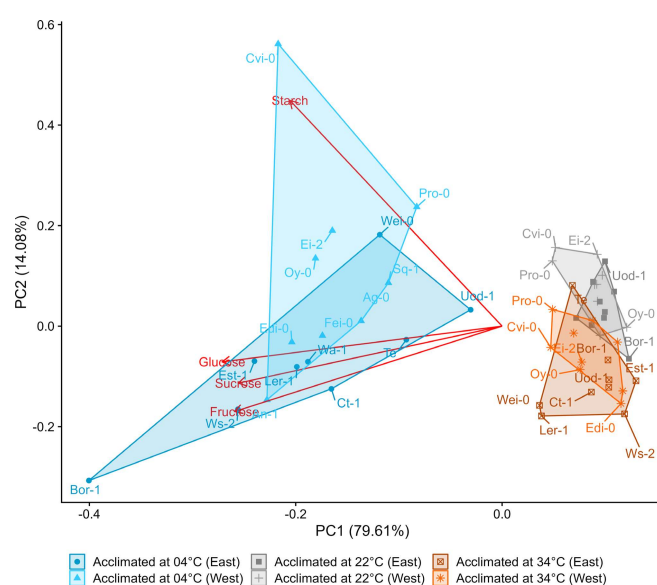

FIGURE 2   **Differential carbohydrate accumulation during heat and cold acclimation in eastern and western accessions.** Dots represent scores of accessions acclimated at different temperatures as indicated by the color (grey: 22°C, blue: 4°C, orange: 34°C). Loadings, i.e., coefficients of the linear combination of carbohydrate concentrations, are shown in red (n ≥ 5). Classification of eastern and western accessions refers to scaled ETR residuals of heat-acclimated plants (see Figure 1).

Subcellular distribution of sucrose, glucose and fructose was determined experimentally by applying a non-aqueous fractionation protocol, which enables the separation of plastidial, cytosolic and vacuolar fractions while metabolism is efficiently and continuously quenched (Fürtauer et al., 2016). A conserved cold response across accessions was an increased proportion of sucrose in plastids and cytosol, while the vacuolar proportion decreased compared to plants at 22°C (Figure 3 A-C). At 34°C, only cytosolic portions increased, while vacuolar sucrose content decreased. The plastidial relative sucrose content remained similar compared to 22°C plants. Relative glucose fractions were highest in the vacuole across all conditions and accessions, and both low and elevated temperatures resulted in an even stronger vacuolar accumulation (Figure 3 F). For fructose, a similar distribution was observed except for plants acclimated to 34°C (Figure 3 G-I). It was observed that the mean fructose portion increased in the plastids and decreased in the vacuole. Further, fructose compartmentation at 34°C was the most variable across accessions, ranging from a similar distribution across all compartments in Cvi-0 to a very strong vacuolar compartmentation in Ct-1, Est-1 and Fei-0 (Figure 3, lower panel).

While relative fructose amount in the cytosol and plastids increased in heat-acclimated plants, vacuolar hexose compartmentation and plastidial sucrose allocation separated cold acclimated accessions from heat and non-acclimated plants (Figure 4). Plastidial sucrose allocation was found to be a conserved cold response across western and eastern accessions. In contrast, vacuolar glucose accumulated stronger in western accessions, while an increase of vacuolar fructose portions was indicative for cold-acclimated eastern accessions. Vacuolar sucrose fractions together with relative amounts of glucose in plastids and cytosol were correlated with plants at 22°C.

Based on the observation of general and specific temperature responses in carbohydrate metabolism, central enzyme activities of carbohydrate metabolism were quantified to reveal if they can explain the observed metabolic output. Enzyme activities were quantified in accessions Cvi-0 and Wa-1, which covered a large geographical range of analysed accessions from southwest to northeast (approx. 5,500 km). Further, subcellular carbohydrate metabolism in both accessions explained a large proportion of PC 1 and PC 2 when comparing temperature acclimation (see Figure 4). In both accessions, neutral invertase activities were found to be significantly increased under elevated temperature (Figure 5A). Acidic invertase activity was significantly reduced at low temperature in Wa-1, while activity significantly increased in Cvi-0 under elevated temperatures (Figure 5B). Fructokinase activity significantly increased during cold acclimation of Wa-1, while no significant temperature effect was observed for Cvi-0, which had lower activities than Wa-1 under all conditions (Figure 5C). Also, mean glucokinase activities were lower in Cvi-0 than in Wa-1, and no significant temperature effect was observed in either accession (Figure 5D).

To estimate the impact of physiologically relevant subcellular carbohydrate concentrations on the stability of photosynthesis, effective subcellular concentrations were calculated from relative metabolite distributions, their absolute amounts and assumptions about
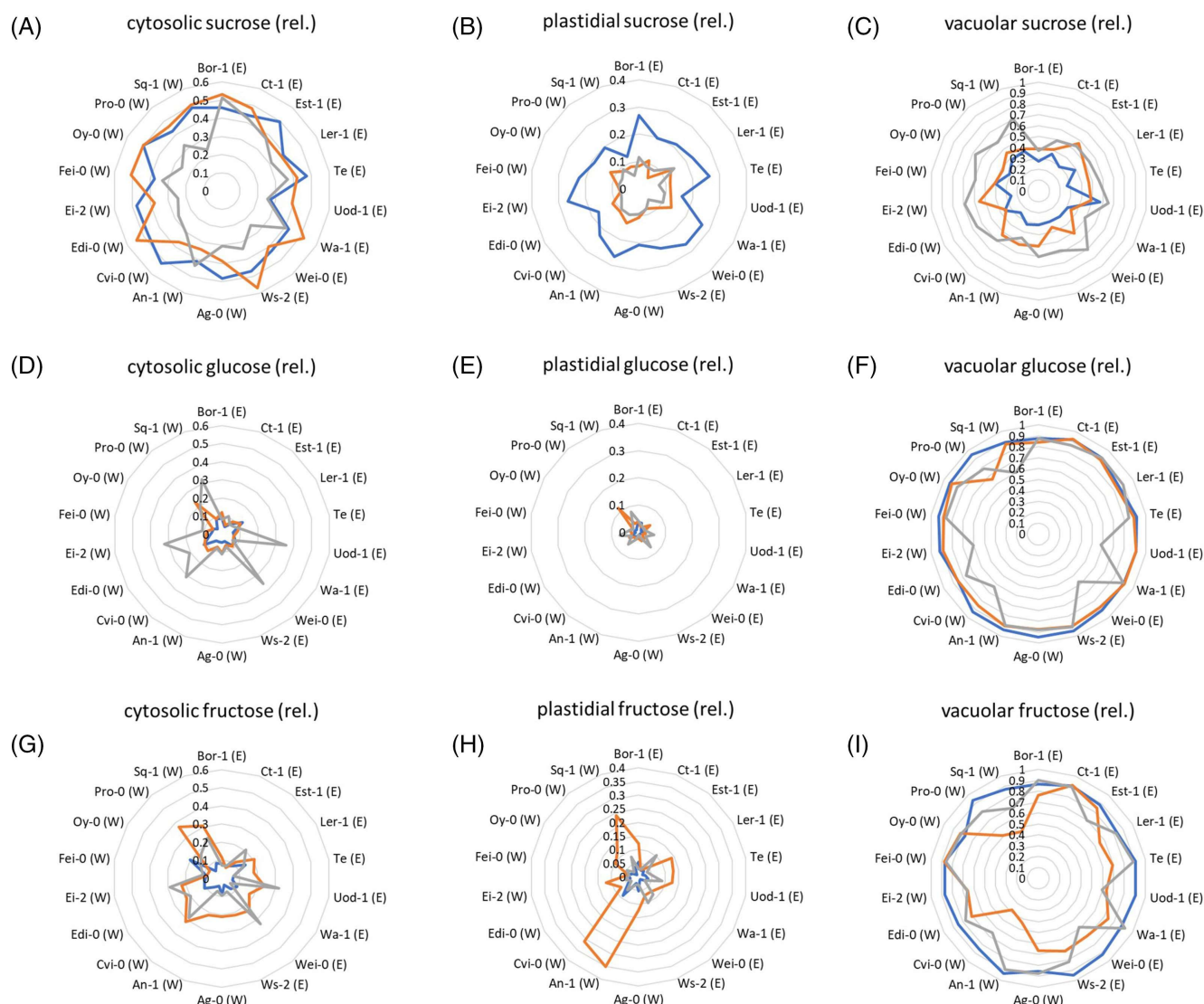
FIGURE 3 Subcellular carbohydrate compartmentation of cold- and heat-acclimated natural accessions. Accessions and classification into eastern I or western (W) are indicated in each diagram. Relative amounts are indicated by circle lines corresponding to values between 0 (0%) and 1 (100%). Grey lines: 22°C; blue lines: 4°C; orange lines: 34°C. (A – C) sucrose proportions in cytosol, plastid and vacuole. (D – F) glucose proportions in cytosol, plastid and vacuole. (G – I) fructose proportions in cytosol, plastid and vacuole. Lines represent mean values (n = 3). All data, including SD, is provided in Table S4.

compartment volumes (Nägele and Heyer, 2013). The volume of plastids was estimated as 20% of the total cellular volume. For cytosol, it was estimated to be 5% and 75% for the vacuole. The estimated compartment-specific concentration was then correlated to Fv/Fm, maximum ETR and residuals of scaled ETR (Figure 6; Tables S3 and S4).

The strongest positive and most significant correlations were observed between the maximum ETR and the effective plastidial sucrose concentration for plants acclimated at 4°C and measured at 34°C, and *vice versa*. Also, vacuolar sucrose concentration correlated significantly with maximum ETR and Fv/Fm for heat-acclimated plants, measured at 4°C and 34°C, respectively. A significant positive correlation was found for cytosolic sucrose concentration and Fv/Fm in plants acclimated to 4°C and measured at 34°C. In plants

acclimated at 22°C, vacuolar fructose concentration was found to be significantly positively correlated to Fv/Fm.

To reveal how subcellular carbohydrate concentrations relate to the ETR residual-based classification of western and eastern accessions, Spearman's rank correlation coefficients were also determined for both accession groups separately (Figure 7). Vacuolar sucrose concentrations were positively correlated with maximum ETR at 22°C in eastern accessions while, under fluctuating temperature (acclimated at 34°C → measured at 4°C, and *vice versa*), plastidial sucrose concentrations significantly correlated with maximum ETR. This was also observed for cold-acclimated western accessions. However, heat-acclimated western accessions measured at 4°C showed a significant negative correlation of plastidial sucrose concentration with Fv/Fm, which contrasted with eastern accessions. Also, plastidial fructose
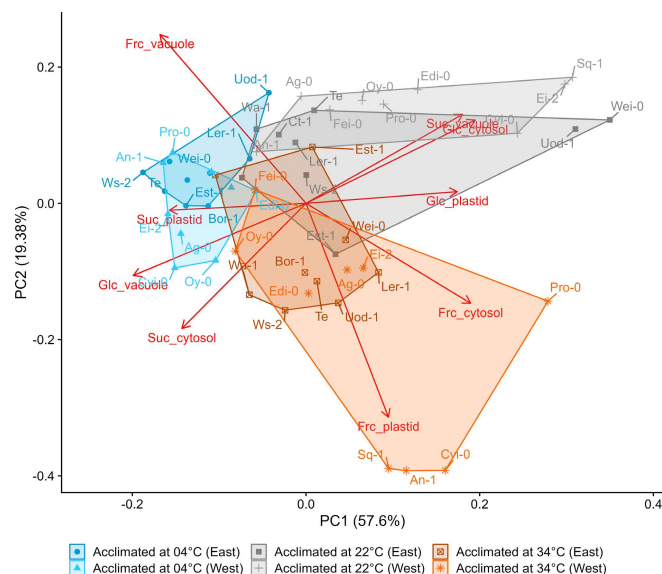
FIGURE 4 Natural variation of subcellular carbohydrate compartmentation during heat and cold acclimation. Dots represent scores of accessions acclimated at different temperatures as indicated by the color (grey: 22°C, blue: 4°C, orange: 34°C). Loadings represent relative carbohydrate distribution across plastids, cytosol and vacuole (n = 3). Classification of eastern and western accessions refers to scaled ETR residuals of heat-acclimated plants (see Figure 1).

concentrations were negatively correlated with Fv/Fm in western accessions when heat-acclimated plants were measured at 4°C. For heat-acclimated western accessions, analysed at 34°C, it was found that vacuolar sucrose concentration was negatively correlated with ETR residuals, indicating a stabilizing function of photosynthesis. In general, those observations suggested that not only photosynthetic efficiencies in a fluctuating environment but also subcellular metabolic acclimation strategies differed between accessions with distinct longitudinal origins.

4 | DISCUSSION

Changing temperature regimes belong to typical environmental dynamics to which plants are exposed on different time scales. Already within a diurnal cycle, temperature changes might comprise large amplitudes. Comparing temperature amplitudes over recent decades has revealed an upward trend of minimum and maximum temperatures and an increased probability of extreme events in the temperate climate zone (Ouyang et al., 2023). Plant physiological and molecular consequences of such a dynamic environment can be estimated by analyzing temperature stress response and acclimation output. Immediate adjustment of photosynthesis and metabolism to
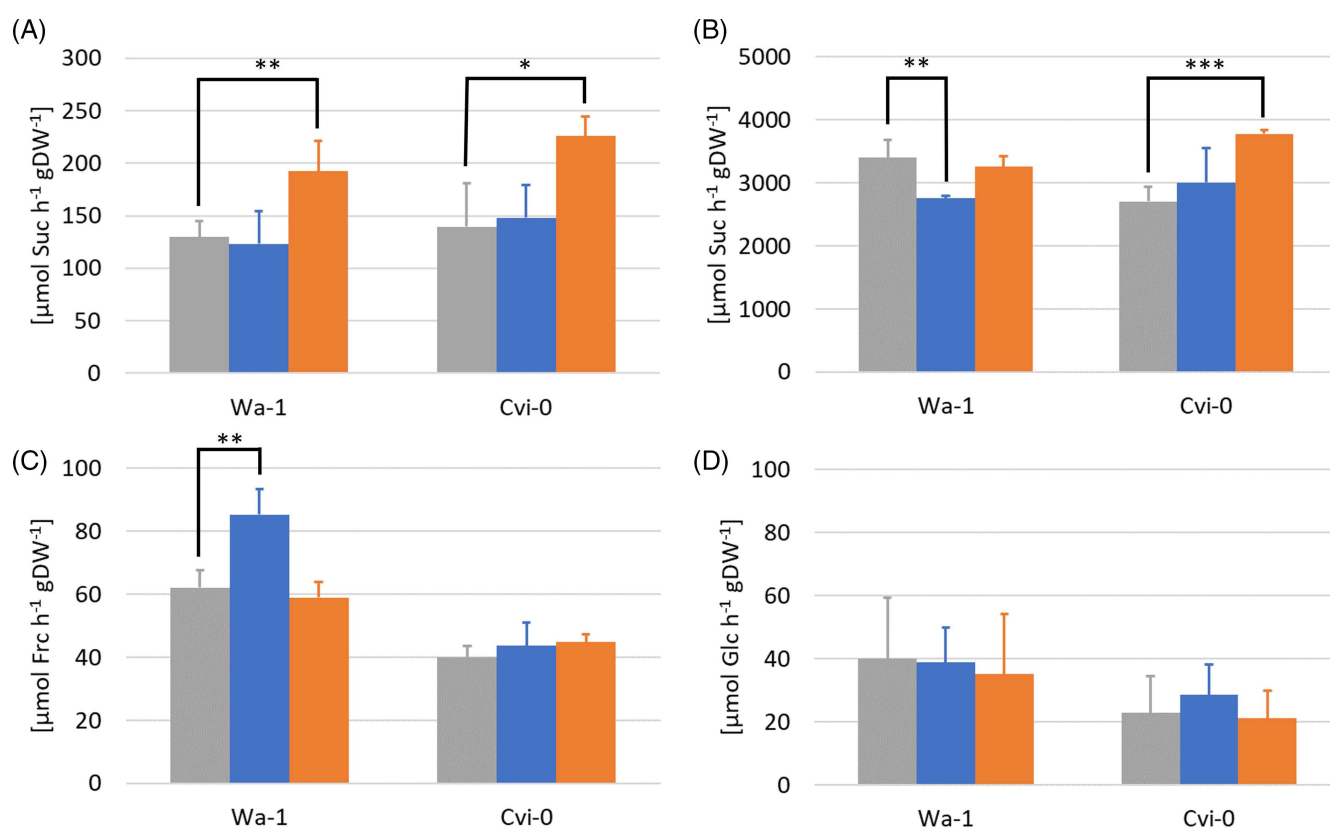
FIGURE 5 Enzyme activities of the central carbohydrate metabolism compared in the two geographically distant *Arabidopsis* accessions **Wa-1 and Cvi-0.** (A) Activity of cytosolic/neutral invertase, (B) activity of vacuolar/acidic invertase, (C) activity of fructokinase, (D) activity of glucokinase. Bars represent means $+/-$ SD (n = 6). Asterisks indicate significance (ANOVA, * p > 0.05; ** p < 0.01; *** p < 0.001). Grey bars: 22°C; blue bars: 04°C; orange bars: 34°C.

FIGURE 6 **Correlation between photosynthetic efficiencies and subcellular carbohydrate concentrations.** Numbers represent Spearman's rank correlation coefficients. Columns relate to experiments to determine *Fv/Fm*, maximal ETR (*max_ETR*) and residuals of scaled ETR (*Residuals*), from left to right: Acclimated at 4°C, Measured at 4°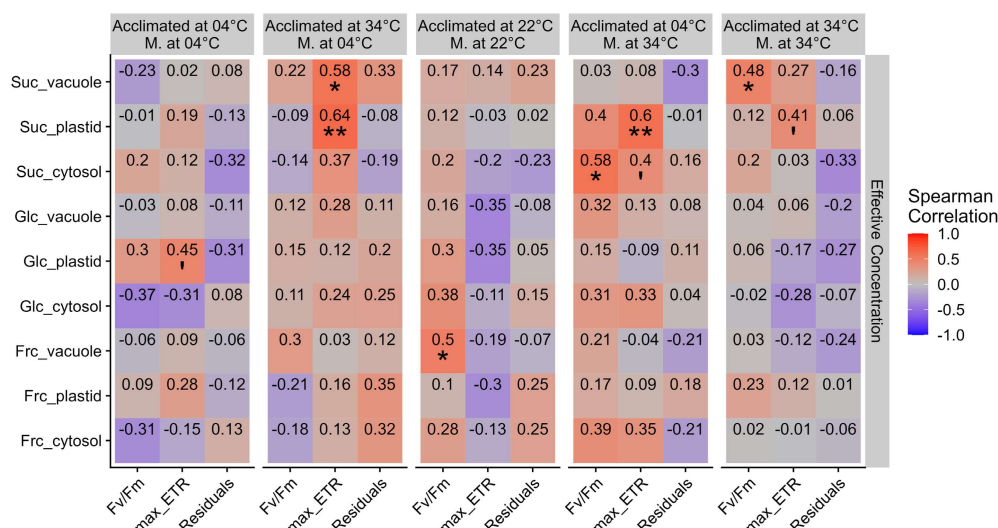C; Acclimated at 34°C, Measured at 4°C; Acclimated at 22°C, Measured at 22°C; Acclimated at 4°C, Measured at 34°C; Acclimated at 34°C, Measured at 34°C. Red color: positive correlation; purple color: negative correlation. Significance codes (Spearman, n ≥ 5): ** 0.001 < p < 0.01; * 0.01 < p < 0.05; ' 0.05 < p < 0.1.

environmental stressors, e.g., significant temperature fluctuation, represents a prerequisite for plant survival and long-term acclimation responses (Kosova et al., 2011). While forward genetic screens, QTL mappings and reverse genetic approaches have essentially contributed to the understanding of plant-environment interactions (Chinnusamy et al., 2003; Panter et al., 2019), the study of natural variation of traits has further contributed important insights. For example, comparing freezing-tolerant to freezing-sensitive accessions revealed a central role of the C-repeat binding factors (CBFs) in adjusting a low-temperature metabolome (Cook et al., 2004). The study of transcriptomes and metabolomes of natural accessions has further revealed negative regulators of freezing tolerance, e.g., auxin- and cytokinin-induced response regulator genes (Hannah et al., 2006). Simulating naturally occurring low-temperature profiles during early vegetative growth showed that seedling growth differs significantly between *Arabidopsis* accessions originating from northern and southern latitudes, which was suggested to reflect local adaptation mechanisms (Clauw et al., 2022). This was supported by substantial reprogramming of the transcriptome and primary metabolome, resulting in differential metabolome plasticity that was found to be negatively correlated to the maximum temperature of the first quarter of the year at the respective natural habitat (Weiszmann et al., 2023). Additionally, in the present study, climate data of the first quarter of the year over almost seven decades was found to correlate negatively with fluctuations of photosynthetic (linear) ETR. Here, measurements at elevated temperatures were considered because they showed the least ETR residuals under temperature fluctuations, suggesting the highest photosynthetic acclimation output across all experiments. Hence, the observed correlation output with climate data suggests that plants originating from habitats with high temperature fluctuation during the first quarter of the year show more efficient photosynthetic

acclimation than accessions from habitats with low temperature fluctuation. This fell together with a longitudinal gradient of the chosen accessions. However, the maximum quantum yield of PSII was found to be stable across the full longitudinal range, which indicates that these conditions are not selective enough to either prevent the growth of eastern accessions in western habitats or *vice versa*.

The ratio of the insoluble storage compound starch to soluble carbohydrates has been found earlier to indicate differential metabolic reprogramming due to temperature changes across natural accessions (Klotke et al., 2004; Guy et al., 2008; Nagler et al., 2015). Here, starch was observed to accumulate stronger in cold-acclimated western accessions, while soluble carbohydrates were associated with eastern accessions. Although neither cold, freezing, nor heat tolerance levels were quantified in the present study due to differential ETR residuals under heat, it might be speculated that western accessions tendentially represent more heat tolerant accessions while eastern accessions might be cold-adapted. If this assumption pertained, reduced starch accumulation in eastern accessions might be due to increased starch degradation capacities to support accumulation of soluble carbohydrates and other cryoprotective compounds (Kaplan et al., 2006; Guy et al., 2008; Sicher, 2011). During heat exposure, starch amounts were found to decrease in most accessions, which is in line with previous findings, and a reasonable explanation might be the inhibition of ADP-glucose pyrophosphorylase and starch synthesis rather than increased capacities of starch degradation (Geigenberger et al., 1998; Awasthi et al., 2014). Interestingly, some accessions showed less heat-sensitive starch metabolism (e.g., Fei-0, Oy-0 or Sq-1) and it might be interesting to analyze differences in starch degradation pathways among these accessions in future studies.

As a result of increased starch degradation and sucrose accumulation under heat, many accessions displayed an increased sucrose-
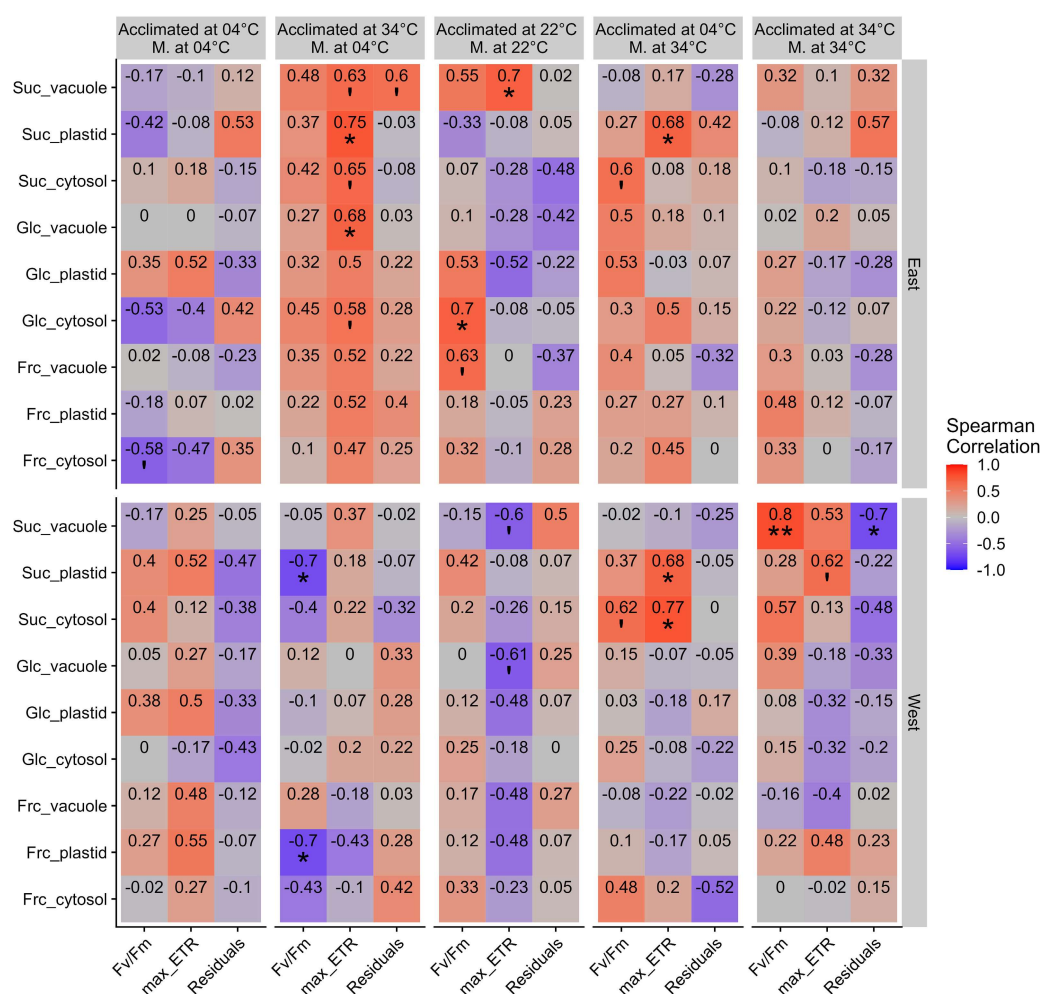
FIGURE 7 — East (top panel)

	Acclimated at 04°C M. at 04°C			Acclimated at 34°C M. at 04°C			Acclimated at 22°C M. at 22°C			Acclimated at 04°C M. at 34°C			Acclimated at 34°C M. at 34°C		
	Fv/Fm	max_ETR	Residuals	Fv/Fm	max_ETR	Residuals	Fv/Fm	max_ETR	Residuals	Fv/Fm	max_ETR	Residuals	Fv/Fm	max_ETR	Residuals
Suc_vacuole	-0.17	-0.1	0.12	0.48	0.63	0.6	0.55	0.7 *	0.02	-0.08	0.17	-0.28	0.32	0.1	0.32
Suc_plastid	-0.42	-0.08	0.53	0.37	0.75 *	-0.03	-0.33	-0.08	0.05	0.27	0.68 *	0.42	-0.08	0.12	0.57
Suc_cytosol	0.1	0.18	-0.15	0.42	0.65	-0.08	0.07	-0.28	-0.48	0.6	0.08	0.18	0.1	-0.18	-0.15
Glc_vacuole	0	0	-0.07	0.27	0.68 *	0.03	0.1	-0.28	-0.42	0.5	0.18	0.1	0.02	0.2	0.05
Glc_plastid	0.35	0.52	-0.33	0.32	0.5	0.22	0.53	-0.52	-0.22	0.53	-0.03	0.07	0.27	-0.17	-0.28
Glc_cytosol	-0.53	-0.4	0.42	0.45	0.58	0.28	0.7 *	-0.08	-0.05	0.3	0.5	0.15	0.22	-0.12	0.07
Frc_vacuole	0.02	-0.08	-0.23	0.35	0.52	0.22	0.63	0	-0.37	0.4	0.05	-0.32	0.3	0.03	-0.28
Frc_plastid	-0.18	0.07	0.02	0.22	0.52	0.4	0.18	-0.05	0.23	0.27	0.27	0.1	0.48	0.12	-0.07
Frc_cytosol	-0.58	-0.47	0.35	0.1	0.47	0.25	0.32	-0.1	0.28	0.2	0.45	0	0.33	0	-0.17

FIGURE 7 — West (lower panel)

	Fv/Fm	max_ETR	Residuals	Fv/Fm	max_ETR	Residuals	Fv/Fm	max_ETR	Residuals	Fv/Fm	max_ETR	Residuals	Fv/Fm	max_ETR	Residuals
Suc_vacuole	-0.17	0.25	-0.05	-0.05	0.37	-0.02	-0.15	-0.6	0.5	-0.02	-0.1	-0.25	0.8 **	0.53	-0.7 *
Suc_plastid	0.4	0.52	-0.47	-0.7 *	0.18	-0.07	0.42	-0.08	0.07	0.37	0.68 *	-0.05	0.28	0.62	-0.22
Suc_cytosol	0.4	0.12	-0.38	-0.4	0.22	-0.32	0.2	-0.26	0.15	0.62	0.77 *	0	0.57	0.13	-0.48
Glc_vacuole	0.05	0.27	-0.17	0.12	0	0.33	0	-0.61	0.25	0.15	-0.07	-0.05	0.39	-0.18	-0.33
Glc_plastid	0.38	0.5	-0.33	-0.1	0.07	0.28	0.12	-0.48	0.07	0.03	-0.18	0.17	0.08	-0.32	-0.15
Glc_cytosol	0	-0.17	-0.43	-0.02	0.2	0.22	0.25	-0.18	0	0.25	-0.08	-0.22	0.15	-0.32	-0.2
Frc_vacuole	0.12	0.48	-0.12	0.28	-0.18	0.03	0.17	-0.48	0.27	-0.08	-0.22	-0.02	-0.16	-0.4	0.02
Frc_plastid	0.27	0.55	-0.07	-0.7 *	-0.43	0.28	0.12	-0.48	0.07	0.1	-0.17	0.05	0.22	0.48	0.23
Frc_cytosol	-0.02	0.27	-0.1	-0.43	-0.1	0.42	0.33	-0.23	0.05	0.48	0.2	-0.52	0	-0.02	0.15

Spearman Correlation scale: 1.0 (red) / 0.5 / 0.0 / -0.5 / -1.0 (purple)

FIGURE 7 Correlation between photosynthetic efficiencies and subcellular carbohydrate concentrations of eastern (top panel) and western (lower panel) accessions. Numbers represent Spearman's rank correlation coefficients. Columns relate to experiments to determine *Fv/Fm*, maximal ETR (*max_ETR*) and residuals of scaled ETR (*Residuals*), from left to right: Acclimated at 4°C, Measured at 4°C; Acclimated at 34°C, Measured at 4°C; Acclimated at 22°C, Measured at 22°C; Acclimated at 4°C, Measured at 34°C; Acclimated at 34°C, Measured at 34°C. Red color: positive correlation; purple color: negative correlation. Significance codes (Spearman, n ≥ 5): ** 0.001 < p < 0.01; * 0.01 < p < 0.05; ' 0.05 < p < 0.1.

to-starch ratio (Figure 8). Enzyme activity measurements in the two accessions Wa-1 and Cvi-0 revealed a significant heat-induced increase of neutral invertase activity in both accessions while, in Cvi-0, also acidic invertase activity increased significantly compared to ambient conditions. This finding proves that increasing sucrose-to-starch ratios can also be observed under increased sucrose cleavage capacities. Previous findings demonstrated that changes in invertase activities hardly predict cleavage rates or fluxes due to efficient feedback-inhibition by cleavage products, i.e., glucose and fructose (Nägele et al., 2010). Hence, the observed increased partitioning of glucose into the vacuole and fructose into the cytosol might crucially repress invertase activities and stabilize sucrose concentrations, while oxidative stress defense is promoted (Xiang et al., 2011).

Subcellular analysis revealed that, at low temperatures, a significant fraction of sucrose was accumulating in the plastids, which would preserve it from being cleaved by cytosolic and/or vacuolar invertases (Klotke et al., 2004; Weiszmann et al., 2018). While invertases have

also been shown to occur in plastids (Vargas et al., 2008), their activity might be much lower than in other compartments. We have shown earlier that plastidial accumulation of sucrose represents a conserved cold acclimation strategy in *Arabidopsis* (Nägele and Heyer, 2013), maybe to support stabilization of thylakoid membranes and photosynthesis similar to raffinose (Knaupp et al., 2011) or to balance carbon allocation throughout the cell (Patzke et al., 2019).

Sucrose accumulation in plastids was observed for all accessions, but eastern accessions accumulated fructose, while western accessions rather accumulated glucose in the vacuole. This finding indicates that not only sucrose biosynthesis and cleavage but also the subsequent metabolism of cleavage products glucose and fructose shows significant natural variation. Indeed, activity measurements of fructo- and glucokinase showed that both selected accessions differed in both absolute activities and temperature-induced dynamics. HEXOKINASE 1 (AtHXK1) catalyzes the phosphorylation of glucose and has recently been shown to improve drought and heat tolerance when

FIGURE 8 Comparing natural variation of metabolic acclimation to low and elevated temperature. Comparisons relate to non-acclimated plants (22°C). Arrow sizes indicate effect strength, arrow color refers to different sugars. Suc – sucrose (blue arrows); Glc – glucose (brown arrows); Frc – fructose (red arrows). Created with BioRender.com.
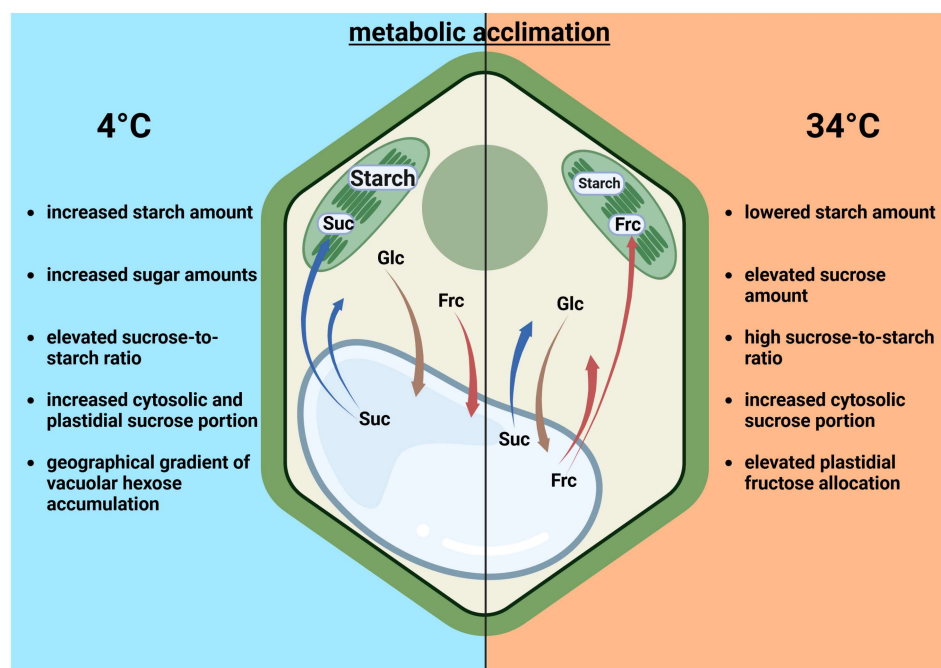
overexpressed in potato (Lehretz et al., 2021). Further, AtHXK1 is a central conserved sugar sensor that might directly affect photosynthesis and transpiration by controlling stomatal aperture (Moore et al., 2003; Granot and Kelly, 2019). Fructokinase catalyzes the carbon flow into the glycolytic pathway and the tricarboxylic acid cycle to provide substrates for amino acid biosynthesis and mitochondrial respiration (Pego and Smeekens, 2000). Hence, natural variation of cold and heat acclimation capacities may, among others, be due to differential hexose phosphorylation capacities, which would also have an impact on respiratory acclimation to a changing temperature regime (Talts et al., 2004; Atanasov et al., 2020).

An increasing body of evidence has revealed that, to comprehensively understand the regulation of photosynthesis and metabolic processes involved in plant temperature response, subcellular data needs to be considered (Hoermiller et al., 2017; Hurry, 2017; Höhner et al., 2021). Yet, estimating effective *in vivo* metabolite concentrations remains challenging not only because of laborious sample fractionation but also due to a lack of information about organellar volumes and their temperature-dependent dynamics. Particularly, such information becomes essential for quantitative analysis of compartment-specific reaction rates and metabolic fluxes because compartmentalization of metabolism directly affects enzymatic activity and function, thus altering regulation and fluxes within a metabolic network (Szecowka et al., 2013; Herrmann et al., 2021; Nägele, 2022). Data of the present study provides further evidence for the importance of estimating subcellular effective concentrations, which enabled the interpretation of physiological effects on photosynthesis. Comparing correlations between subcellular sugar concentrations and photosynthetic efficiencies indicated a split of accessions into east and west. Even under ambient temperature, such a split revealed positive and negative correlation of vacuolar sucrose concentrations with Fv/Fm and maximum ETR in eastern

and western accessions, respectively. Hence, uncovering such effects supports our hypothesis of a physiologically relevant classification due to geographical origin and habitat information.

Finally, many significant correlations between subcellular sugar concentrations and photosynthetic efficiencies were only observed under fluctuating temperatures, which suggests that a subcellular metabolic adjustment during temperature acclimation results in a metabolic state which stabilizes photosynthesis against further environmental deflections. This hints towards the necessity of rethinking the definition of plant (temperature) acclimation, which might rather consider the plasticity of metabolism towards environmental changes than its absolute configuration. It is tempting to speculate that metabolite transport across membranes like the tonoplast or the chloroplast envelope may significantly affect and determine such metabolic plasticity and, by this, temperature acclimation capacities. For example, sucrose transport between chloroplast and cytosol has been shown recently to affect the cold acclimation capacities of *Arabidopsis thaliana* (Patzke et al., 2019). Although the exact *in vivo* function of the pSuT transporter of the inner plastid envelope is still under debate, its activity was found to be essential to maximize freezing tolerance. In the present study, natural variations of subcellular fructose partitioning were observed. Besides differential fructokinase activities, this might also be due to a naturally occurring variation of SWEET17 regulation, which is a homolog of SUGARS WILL EVENTUALLY BE EXPORTED (SWEET) proteins being located to the tonoplast (Guo et al., 2014, Keller et al., 2021). Future studies might decipher the contribution of these transporters and metabolic enzymes to the natural variation of metabolic regulation. In conclusion, using analytical platforms to quantify subcellular primary and secondary metabolism together with studies on metabolite transport promises to promote our understanding of naturally occurring temperature acclimation output.

DATA AVAILABILITY STATEMENT

The data that support the findings of this study are available from the corresponding author upon reasonable request.

ORCID

Dejan Dziubek https://orcid.org/0009-0000-3041-9716
Charlotte Seydel https://orcid.org/0000-0001-9808-0720
Anastasia Kitashova https://orcid.org/0000-0002-4698-3255
Vladimir Brodsky https://orcid.org/0009-0004-7792-2852
Thomas Nägele https://orcid.org/0000-0002-5896-238X

REFERENCES

Atanasov V, Fürtauer L, Nägele T (2020) Indications for a central role of hexokinase activity in natural variation of heat acclimation in *Arabidopsis thaliana*. *Plants* 9: 819

Awasthi R, Kaushal N, Vadez V, Turner NC, Berger J, Siddique KHM, Nayyar H (2014) Individual and combined effects of transient drought and heat stress on carbon assimilation and seed filling in chickpea. *Funct Plant Biol* 41: 1148–1167

Cano-Ramirez DL, Carmona-Salazar L, Morales-Cedillo F, Ramírez-Salcedo J, Cahoon EB, Gavilanes-Ruíz M (2021) Plasma membrane fluidity: an environment thermal detector in plants. *Cells* 10: 2778

Chinnusamy V, Ohta M, Kanrar S, Lee B-h, Hong X, Agarwal M, Zhu J-K (2003) ICE1: a regulator of cold-induced transcriptome and freezing tolerance in Arabidopsis. *Genes Dev* 17: 1043–1054

Choudhury FK, Rivero RM, Blumwald E, Mittler R (2017) Reactive oxygen species, abiotic stress and stress combination. *Plant J* 90: 856–867

Clauw P, Kerdaffrec E, Gunis J, Reichardt-Gomez I, Nizhynska V, Koemeda S, Jez J, Nordborg M (2022) Locally adaptive temperature response of vegetative growth in *Arabidopsis thaliana*. *Elife* 11: e77913

Cook D, Fowler S, Fiehn O, Thomashow MF (2004) A prominent role for the CBF cold response pathway in configuring the low-temperature metabolome of Arabidopsis. *PNAS* 101: 15243–15248

Elias M, Wieczorek G, Rosenne S, Tawfik DS (2014) The universality of enzymatic rate–temperature dependency. *Trends Biochem Sci* 39: 1–7

Fürtauer L, Küstner L, Weckwerth W, Heyer AG, Nägele T (2019) Resolving subcellular plant metabolism. *Plant J* 100: 438–455

Fürtauer L, Weckwerth W, Nägele T (2016) A benchtop fractionation procedure for subcellular analysis of the plant metabolome. *Front Plant Sci* 7: 1912

Garcia-Molina A, Kleine T, Schneider K, Mühlhaus T, Lehmann M, Leister D (2020) Translational components contribute to acclimation responses to high light, heat, and cold in Arabidopsis. *iScience* 23: 101331

Geigenberger P, Geiger M, Stitt M (1998) High-temperature perturbation of starch synthesis is attributable to inhibition of ADP-glucose pyrophosphorylase by decreased levels of glycerate-3-phosphate in growing potato tubers. *Plant Physiol* 117: 1307–1316

Gerhardt R, Heldt HW (1984) Measurement of subcellular metabolite levels in leaves by fractionation of freeze-stopped material in nonaqueous media. *Plant Physiol* 75: 542–547

Gjindali A, Johnson GN (2023) Photosynthetic acclimation to changing environments. *Biochem Soc Trans* 51: 473–486

Granot D, Kelly G (2019) Evolution of guard-cell theories: the story of sugars. *Trends Plant Sci* 24: 507–518

Gray GR, Hope BJ, Qin X, Taylor BG, Whitehead CL (2003) The characterization of photoinhibition and recovery during cold acclimation in *Arabidopsis thaliana* using chlorophyll fluorescence imaging. *Physiol Plant* 119: 365–375

Guo WJ, Nagy R, Chen HY, Pfrunder S, Yu YC, Santelia D, Frommer WB, Martinoia E (2014) SWEET17, a facilitative transporter, mediates fructose transport across the tonoplast of Arabidopsis roots and leaves. *Plant Physiol* 164: 777–789

Guy C, Kaplan F, Kopka J, Selbig J, Hincha DK (2008) Metabolomics of temperature stress. *Physiol Plant* 132: 220–235

Hannah MA, Wiese D, Freund S, Fiehn O, Heyer AG, Hincha DK (2006) Natural genetic variation of freezing tolerance in Arabidopsis. *Plant Physiol* 142: 98–112

Hernandez JS, Nägele T (2022) The trade-off function of photorespiration in a changing environment. isP, diac022

Herrmann HA, Dyson BC, Miller MAE, Schwartz JM, Johnson GN (2021) Metabolic flux from the chloroplast provides signals controlling photosynthetic acclimation to cold in Arabidopsis thaliana. *Plant Cell Environ* 44: 171–185

Herrmann HA, Schwartz J-M, Johnson GN (2019) Metabolic acclimation—a key to enhancing photosynthesis in changing environments? *J Exp Bot* 70: 3043–3056

Hoermiller, II, Naegele T, Augustin H, Stutz S, Weckwerth W, Heyer AG (2017) Subcellular reprogramming of metabolism during cold acclimation in Arabidopsis thaliana. *Plant Cell Environ* 40: 602–610

Höhner R, Day PM, Zimmermann SE, Lopez LS, Krämer M, Giavalisco P, Correa Galvis V, Armbruster U, Schöttler MA, Jahns P, Krueger S, Kunz H-H (2021) Stromal NADH supplied by PHOSPHOGLYCERATE DEHYDROGENASE3 is crucial for photosynthetic performance. *Plant Physiol* 186: 142–167

Huner NPA, Öquist G, Sarhan F (1998) Energy balance and acclimation to light and cold. *Trends Plant Sci* 3: 224–230

Hurry V (2017) Metabolic reprogramming in response to cold stress is like real estate, it's all about location. *Plant Cell Environ* 40: 599–601

Kaplan F, Sung DY, Guy CL (2006) Roles of β-amylase and starch breakdown during temperatures stress. *Physiol Plant* 126: 120–128

Keller I, Rodrigues CM, Neuhaus HE, Pommerrenig B (2021) Improved resource allocation and stabilization of yield under abiotic stress. *J Plant Physiol* 257: 153336

Kitashova A, Adler SO, Richter AS, Eberlein S, Dziubek D, Klipp E, Nagele T (2023) Limitation of sucrose biosynthesis shapes carbon partitioning during plant cold acclimation. *Plant Cell Environ* 46: 464–478

Klotke J, Kopka J, Gatzke N, Heyer AG (2004) Impact of soluble sugar concentrations on the acquisition of freezing tolerance in accessions of Arabidopsis thaliana with contrasting cold adaptation - evidence for a role of raffinose in cold acclimation. *Plant Cell Environ* 27: 1395–1404

Knaupp M, Mishra KB, Nedbal L, Heyer AG (2011) Evidence for a role of raffinose in stabilizing photosystem II during freeze-thaw cycles. *Planta* 234: 477–486

Kohli SK, Khanna K, Bhardwaj R, Abd_Allah EF, Ahmad P, Corpas FJ (2019) Assessment of subcellular ROS and NO metabolism in higher plants: multifunctional signaling molecules. *Antioxidants* 8: 641

Kosova K, Vitamvas P, Prasil IT, Renaut J (2011) Plant proteome changes under abiotic stress - Contribution of proteomics studies to understanding plant stress response. *J Proteomics* 74: 1301–1322

Lehretz GG, Sonnewald S, Lugassi N, Granot D, Sonnewald U (2021) Future-proofing potato for drought and heat tolerance by overexpression of hexokinase and SP6A. *Front Plant Sci* 11

Lundmark M, Cavaco AM, Trevanion S, Hurry V (2006) Carbon partitioning and export in transgenic Arabidopsis thaliana with altered capacity for sucrose synthesis grown at low temperature: a role for metabolite transporters. *Plant Cell Environ* 29: 1703–1714

Maloof JN, Borevitz JO, Dabi T, Lutes J, Nehring RB, Redfern JL, Trainer GT, Wilson JM, Asami T, Berry CC, Weigel D, Chory J (2001) Natural variation in light sensitivity of Arabidopsis. *Nat Genet* 29: 441

Moore B, Zhou L, Rolland F, Hall Q, Cheng WH, Liu YX, Hwang I, Jones T, Sheen J (2003) Role of the Arabidopsis glucose sensor HXK1 in nutrient, light, and hormonal signaling. *Science* 300: 332–336

Morelli R, Russo-Volpe S, Bruno N, Lo Scalzo R (2003) Fenton-dependent damage to carbohydrates: free radical scavenging activity of some simple sugars. *J Agric Food Chem* 51: 7418–7425

Nägele T (2022) Metabolic regulation of subcellular sucrose cleavage inferred from quantitative analysis of metabolic functions. *Quant Plant Biol* 3: e10

Nägele T, Henkel S, Hörmiller I, Sauter T, Sawodny O, Ederer M, Heyer AG (2010) Mathematical modeling of the central carbohydrate metabolism in Arabidopsis reveals a substantial regulatory influence of vacuolar invertase on whole plant carbon metabolism. *Plant Physiol* 153: 260–272

Nägele T, Heyer AG (2013) Approximating subcellular organisation of carbohydrate metabolism during cold acclimation in different natural accessions of Arabidopsis thaliana. *New Phytol* 198: 777–787

Nägele T, Stutz S, Hörmiller II, Heyer AG (2012) Identification of a metabolic bottleneck for cold acclimation in Arabidopsis thaliana. *Plant J* 72: 102–114

Nagler M, Nukarinen E, Weckwerth W, Nägele T (2015) Integrative molecular profiling indicates a central role of transitory starch breakdown in establishing a stable C/N homeostasis during cold acclimation in two natural accessions of *Arabidopsis thaliana*. *BMC Plant Biol* 15: 284

Olas JJ, Apelt F, Annunziata MG, John S, Richard SI, Gupta S, Kragler F, Balazadeh S, Mueller-Roeber B (2021) Primary carbohydrate metabolism genes participate in heat-stress memory at the shoot apical meristem of *Arabidopsis thaliana*. *Mol Plant* 14: 1508–1524.

Ouyang X, Liao W, Luo M (2023) Change of probability density distributions of summer temperatures in different climate zones. *Front Earth Sci.* doi: https://doi.org/10.1007/s11707-022-1006-1

Panter PE, Kent O, Dale M, Smith SJ, Skipsey M, Thorlby G, Cummins I, Ramsay N, Begum RA, Sanhueza D, Fry SC, Knight MR, Knight H (2019) MUR1-mediated cell-wall fucosylation is required for freezing tolerance in *Arabidopsis thaliana*. *New Phytol* 224: 1518–1531

Patzke K, Prananingrum P, Klemens PAW, Trentmann O, Rodrigues CM, Keller I, Fernie AR, Geigenberger P, Bolter B, Lehmann M, Schmitz-Esser S, Pommerrenig B, Haferkamp I, Neuhaus HE (2019) The Plastidic Sugar Transporter pSuT Influences Flowering and Affects Cold Responses. *Plant Physiol* 179: 569–587

Pego JV, Smeekens SC (2000) Plant fructokinases: a sweet family get-together. *Trends Plant Sci* 5: 531–536

Peterbauer T, Richter A (2001) Biochemistry and physiology of raffinose family oligosaccharides and galactosyl cyclitols in seeds. *Seed Sci Res* 1: 185–197

Pommerrenig B, Ludewig F, Cvetkovic J, Trentmann O, Klemens PAW, Neuhaus HE (2018) In concert: orchestrated changes in carbohydrate homeostasis are critical for plant abiotic stress tolerance. *Plant Cell Physiol* 59: 1290–1299

Prasch CM, Sonnewald U (2013) Simultaneous application of heat, drought, and virus to Arabidopsis plants reveals significant shifts in signaling networks. *Plant Physiol* 162: 1849–1866

R Core Team (2021) *R: A language and environment for statistical computing.* R Foundation for Statistical Computing, Vienna, Austria.

Schwenkert S, Fernie AR, Geigenberger P, Leister D, Möhlmann T, Naranjo B, Neuhaus HE (2022) Chloroplasts are key players to cope with light and temperature stress. *Trends Plant Sci* 27: 577–587

Seydel C, Kitashova A, Fürtauer L, Nägele T (2022) Temperature-induced dynamics of plant carbohydrate metabolism. *Physiol Plant* 174: e13602

Sicher R (2011) Carbon partitioning and the impact of starch deficiency on the initial response of Arabidopsis to chilling temperatures. *Plant Sci* 181: 167–176

Strand Å, Foyer CH, Gustafsson P, GardestrÖM P, Hurry V (2003) Altering flux through the sucrose biosynthesis pathway in transgenic Arabidopsis thaliana modifies photosynthetic acclimation at low temperatures and the development of freezing tolerance. *Plant Cell Environ* 26: 523–535

Szecowka M, Heise R, Tohge T, Nunes-Nesi A, Vosloh D, Huege J, Feil R, Lunn J, Nikoloski Z, Stitt M, Fernie AR, Arrivault S (2013) Metabolic fluxes in an illuminated Arabidopsis rosette. *Plant Cell* 25: 694–714

Talts P, Parnik T, Gardestrom P, Keerberg O (2004) Respiratory acclimation in Arabidopsis thaliana leaves at low temperature. *J Plant Physiol* 161: 573–579

Vargas WA, Pontis HG, Salerno GL (2008) New insights on sucrose metabolism: evidence for an active A/N-Inv in chloroplasts uncovers a novel component of the intracellular carbon trafficking. *Planta* 227: 795–807

Wanner LA, Junttila O (1999) Cold-induced freezing tolerance in Arabidopsis. *Plant Physiol* 120: 391–400

Weiszmann J, Fürtauer L, Weckwerth W, Nägele T (2018) Vacuolar sucrose cleavage prevents limitation of cytosolic carbohydrate metabolism and stabilizes photosynthesis under abiotic stress. *FEBS J* 285: 4082–4098

Weiszmann J, Walther D, Clauw P, Back G, Gunis J, Reichardt I, Koemeda S, Jez J, Nordborg M, Schwarzerova J, Pierides I, Nägele T, Weckwerth W (2023) Metabolome plasticity in 241 *Arabidopsis thaliana* accessions reveals evolutionary cold adaptation processes. *Plant Physiol* 193: 980–1000

Xiang L, Le Roy K, Bolouri-Moghaddam M-R, Vanhaecke M, Lammens W, Rolland F, Van den Ende W (2011) Exploring the neutral invertase–oxidative stress defence connection in Arabidopsis thaliana. *J Exp Bot* 62: 3849–3862

SUPPORTING INFORMATION

Additional supporting information can be found online in the Supporting Information section at the end of this article.

> **How to cite this article:** Hernandez, J.S., Dziubek, D., Schröder, L., Seydel, C., Kitashova, A., Brodsky, V. et al. (2023) Natural variation of temperature acclimation of *Arabidopsis thaliana*. *Physiologia Plantarum*, 175(6), e14106. Available from: https://doi.org/10.1111/ppl.14106

2.2 The trade-off function of photorespiration in a changing environment

Jakob Sebastian Hernandez, Thomas Nägele *

The photorespiratory pathway in plants comprises metabolic reactions distributed across several cellular compartments. It emerges from the dual catalytic function of Rubisco, i.e. ribulose-1,5-bisphosphate carboxylase/oxygenase. Rubisco either carboxylates or oxygenates ribulose-1,5-bisphosphate. Carboxylation reactions produce 3-phosphoglycerate molecules which are substrates for the central carbohydrate metabolism. However, oxygenation reactions additionally form 2-phosphoglycolate molecules which are (i) substrate for a multicompartmental recovery process, and (ii) inhibit several enzymes of the Calvin–Benson–Bassham cycle. Here, an approach of structural kinetic modelling is presented to investigate the extent of stabilization of the Calvin–Benson–Bassham cycle and carbohydrate metabolism by photorespiration. This method is based on a parametric representation of the Jacobian matrix of a metabolic system which offers a robust strategy for handling uncertainties associated with in vitro kinetic constants. Our findings indicate that oxygenation of ribulose-1,5-bisphosphate by Rubisco significantly stabilizes the Calvin–Benson–Bassham cycle. Hence, a trade-off function of photorespiration is suggested which reduces carbon assimilation rates but simultaneously stabilizes metabolism by increasing plasticity of metabolic regulation within the chloroplast. Furthermore, our analysis indicates that increasing carbon flux towards sucrose biosynthesis has a stabilizing effect. Finally, our findings shed light on the role of a multicompartmental metabolic pathway in stabilizing plant metabolism against perturbation induced by a dynamic environment.

Corresponding Author: *

in silico
Plants

OXFORD

SPECIAL ISSUE: Multiscale Modelling of Photosynthesis
Original Research

The trade-off function of photorespiration in a changing environment

Jakob Sebastian Hernandez and Thomas Nägele[*]

Ludwig-Maximilians-Universität München, Faculty of Biology, Plant Evolutionary Cell Biology, Großhaderner Str. 2-4, 82152 Planegg, Germany

[*]Corresponding author's e-mail address: thomas.naegele@lmu.de

ABSTRACT

The photorespiratory pathway in plants comprises metabolic reactions distributed across several cellular compartments. It emerges from the dual catalytic function of Rubisco, i.e. ribulose-1,5-bisphosphate carboxylase/oxygenase. Rubisco either carboxylates or oxygenates ribulose-1,5-bisphosphate. Carboxylation reactions produce 3-phosphoglycerate molecules which are substrates for the central carbohydrate metabolism. However, oxygenation reactions additionally form 2-phosphoglycolate molecules which are (i) substrate for a multicompartmental recovery process, and (ii) inhibit several enzymes of the Calvin–Benson–Bassham cycle. Here, an approach of structural kinetic modelling is presented to investigate the extent of stabilization of the Calvin–Benson–Bassham cycle and carbohydrate metabolism by photorespiration. This method is based on a parametric representation of the Jacobian matrix of a metabolic system which offers a robust strategy for handling uncertainties associated with *in vitro* kinetic constants. Our findings indicate that oxygenation of ribulose-1,5-bisphosphate by Rubisco significantly stabilizes the Calvin–Benson–Bassham cycle. Hence, a trade-off function of photorespiration is suggested which reduces carbon assimilation rates but simultaneously stabilizes metabolism by increasing plasticity of metabolic regulation within the chloroplast. Furthermore, our analysis indicates that increasing carbon flux towards sucrose biosynthesis has a stabilizing effect. Finally, our findings shed light on the role of a multicompartmental metabolic pathway in stabilizing plant metabolism against perturbation induced by a dynamic environment.

KEYWORDS: Photorespiration; photosynthesis; plant metabolism; stability; structural kinetic modelling.

1. INTRODUCTION

Cellular metabolism consists of a highly elaborate reaction network which frequently shows complex and non-intuitive dynamical behaviour. This behaviour can be deterministically described by a system of ordinary differential equations, ODEs (Klipp *et al.* 2016). Such a kinetic model can then be used to analyse and simulate consequences of environmental fluctuations, e.g. sudden changes of temperature or light intensity. These perturbations might result in a deviation of the metabolic system from its steady state. The system can then either return to its original state again (stable), exponentially diverge from its original state (unstable) or be metastable (behaviour is indifferent). The formulation of ODEs in a kinetic model is, however, typically challenged by lacking experimental data on enzymatic parameters, which are often laborious and difficult to quantify (Wittig *et al.* 2014). Furthermore, enzymatic activity *in vivo* depends on numerous factors, such as temperature and pH, thus greatly increasing the permissive parameter space which exacerbates the physiological interpretation of *in vitro* data (Bisswanger 2017).

Previously, the approach of structural kinetic modelling (SKM) was developed which allows for quantitative evaluation of dynamic properties without referring to any explicit system of ODEs, and which is achieved by a parametric representation of the Jacobian matrix (Steuer *et al.* 2006). Structural kinetic modelling has been confirmed to be a suitable approach for evaluation of the stability and robustness of metabolic states (Grimbs *et al.* 2007). It has been successfully used in a variety of studies

to analyse metabolism and its regulation (Grimbs *et al.* 2007; Reznik and Segrè 2010; Fürtauer and Nägele 2016). However, evaluation of regulatory interactions between a metabolite and reaction of interest is complicated by the complex interplay found within the highly dynamic system of cellular metabolism. Depending on the regulatory setting, a single regulatory interaction can be beneficial or detrimental for the system stability. Further, although a vast amount of data and information is available on regulatory interplay between genes, proteins and metabolites, e.g., provided by genome-scale metabolic networks (Tang *et al.* 2021), many regulatory and metabolic interactions can be assumed to remain elusive or unknown.

Carbon fixation takes place in the stroma of chloroplasts and is catalysed by the enzyme ribulose-1,5-bisphosphate carboxylase/oxygenase (Rubisco). This enzyme facilitates the carboxylation of ribulose-1,5-bisphosphate (RuBP) and subsequent cleavage between the C_2 and C_3 carbon forming two molecules of 3-phospho-D-glycerate (3-PGA) (Andersson 2008). In succeeding steps, 3-PGA is used in the Calvin-Benson-Bassham Cycle (CBBC) to resynthesize RuBP and supply the cell with triose phosphates which are substrate for starch and sucrose biosynthesis (Bassham *et al.* 1954; Martin *et al.* 2000). As the CBBC is directly connected to the rate of carbon fixation, its regulation is crucial for overall metabolic stability. Stability of the CBBC has, thus, an immediate influence on the plant's ability to cope with environmental fluctuations, e.g. changes in light intensity or temperature.

Perturbed or affected metabolic regulation can have significant effects on the rate of carbon assimilation. For example, accumulation of triose phosphates through a low starch and sucrose synthesis rate would result in low abundance of inorganic phosphate and thus limit RuBP regeneration through a lower rate of photophosphorylation (Sharkey 1985). In contrast, if triose phosphate utilization is too high, the rate at which RuBP needs to be regenerated is jeopardized as the CBBC becomes carbon-starved (Kadereit *et al.* 2014). The rate at which Rubisco fixes carbon depends on both the CO_2 and O_2 concentration at the active site of Rubisco (Warburg 1920; Foyer *et al.* 2009). This is a result of the dual catalytic function of Rubisco, which not only carboxylates RuBP, but also reacts with oxygen to form one molecule 2-PG and one of 3-PGA (Bowes *et al.* 1971; Foyer *et al.* 2009). As 2-PG is a strong inhibitor of several essential enzymes involved in the CBBC and chloroplast metabolism, its degradation is of utmost importance (Anderson 1971; Kelly and Latzko 1976; Flügel *et al.* 2017). Affected enzymes are triose-phosphate isomerase (TPI) which catalyses the interconversion between glyceraldehyde 3-phosphate (GAP) and dihydroxyacetone phosphate (DHAP) (Anderson 1971), SBPase which dephosphorylates sedoheptulose-1,7-bisphosphat (SBP) to sedoheptulose-7-phosphat (Sed7P) (Flügel *et al.* 2017) and phosphofructokinase (PFK) which catalyses steps in glycolysis (Kelly and Latzko 1976).

The multistep pathway responsible for interconversion of 2-PG is known as photorespiration and involves several subcellular compartments (Fig. 1), namely the chloroplast, peroxisome and mitochondria (Foyer *et al.* 2009). In this process, two molecules of 2-PG are converted into one molecule of CO_2 and one molecule of 3-PGA which can then be used in the CBBC and allows for the recovery of 75 % of carbon otherwise lost

(Berry *et al.* 1978; Foyer *et al.* 2009). This process, however, comes at a substantial energetic cost to the cell: fixed carbon is again released and ATP and NAD(P)H are consumed (Foyer *et al.* 2009). Furthermore, ammonium (NH_4^+) is produced during photorespiration from which nitrogen has to be recaptured, adding further costs to the cell in the form of ATP and reduced ferredoxin (Foyer *et al.* 2009).

Historically, oxygenation of RuBP was interpreted as an unavoidable consequence of an oxygen-rich atmosphere, with photorespiration solely being the disposal of 2-PG (Lorimer and Andrews 1973). However, an increasing body of knowledge points to additional important physiological roles. To this extent, it has been suggested that photorespiration has a significant impact on protection from photoinhibition (Heber and Krause 1980; Takahashi *et al.* 2007; Shi *et al.* 2022). Additionally, photorespiration interacts with several other metabolic pathways and operates in a tightly regulated manner with nitrogen, sulfur and C_1 metabolism (Hodges *et al.* 2016). Yet, it still remains elusive what stabilizing or destabilizing effect photorespiration has on the CBBC. It is further questioned if 2-PG, in its function as a key regulator, can mitigate the consequences of environmental perturbations. As regulation of the CBBC is crucial for stability of whole-plant metabolism, this study aimed to investigate and quantify to what extent photorespiration affects the stability of the CBBC. For its analysis, the stability of CBBC and photorespiration was evaluated using SKM. Additionally, a discrete-parameter optimization approach was introduced being based on a modified version of the Branch and Bound (BnB) algorithm (Land and Doig 1960). To demonstrate this approach, we reevaluate the stability of the CBBC, considering regulation by 2-PG in context of other regulatory interactions.

2. MATERIALS AND METHODS

In the following section, vectors are annotated in lowercase, v. Matrices are annotated in capital letters, M.

2.1 Stability of reaction networks

Biochemical reaction networks can be deterministically described over time t by a system of ODEs, $\dot{x} = f(x, k, t)$ with $x = (x_1, ..., x_n)^T$ variables (e.g. substrate concentrations), $f = (f_1, ..., f_n)^T$ functions and $k = (k_1, ..., k_l)^T$ parameters (e.g. kinetic constants) (Klipp *et al.* 2016).

If the point x fulfils the steady-state condition $\dot{x} = 0$ ($\dot{x}_1 = 0, ..., \dot{x}_n = 0$), the system will remain in its current state without external perturbations and x is annotated as $\bar{x}$. If the system x is perturbed, the steady state can either be stable (x returns to steady state), unstable (x leaves steady state) or metastable (behaviour is indifferent) depending on the system behaviour (Klipp *et al.* 2016).

The dynamics of an ODE system $\dot{x}$ close to a stable point $\bar{x}$ can be investigated by means of linearization. To this end, the Jacobian Matrix J is obtained by Taylor expansion of temporal changes of the deviations from the steady state $\bar{x}$ and is evaluated at $\bar{x}$. The best linear approximation of $\dot{x}$ near $\bar{x}$ is then given by $\dot{x} \approx Jx + z$ with $z = (z_1, ..., z_n)^T$ containing inhomogeneities (Klipp *et al.* 2016). For non-homogenous systems (i.e. $z \neq 0$) the linearization can be converted into a homogenous
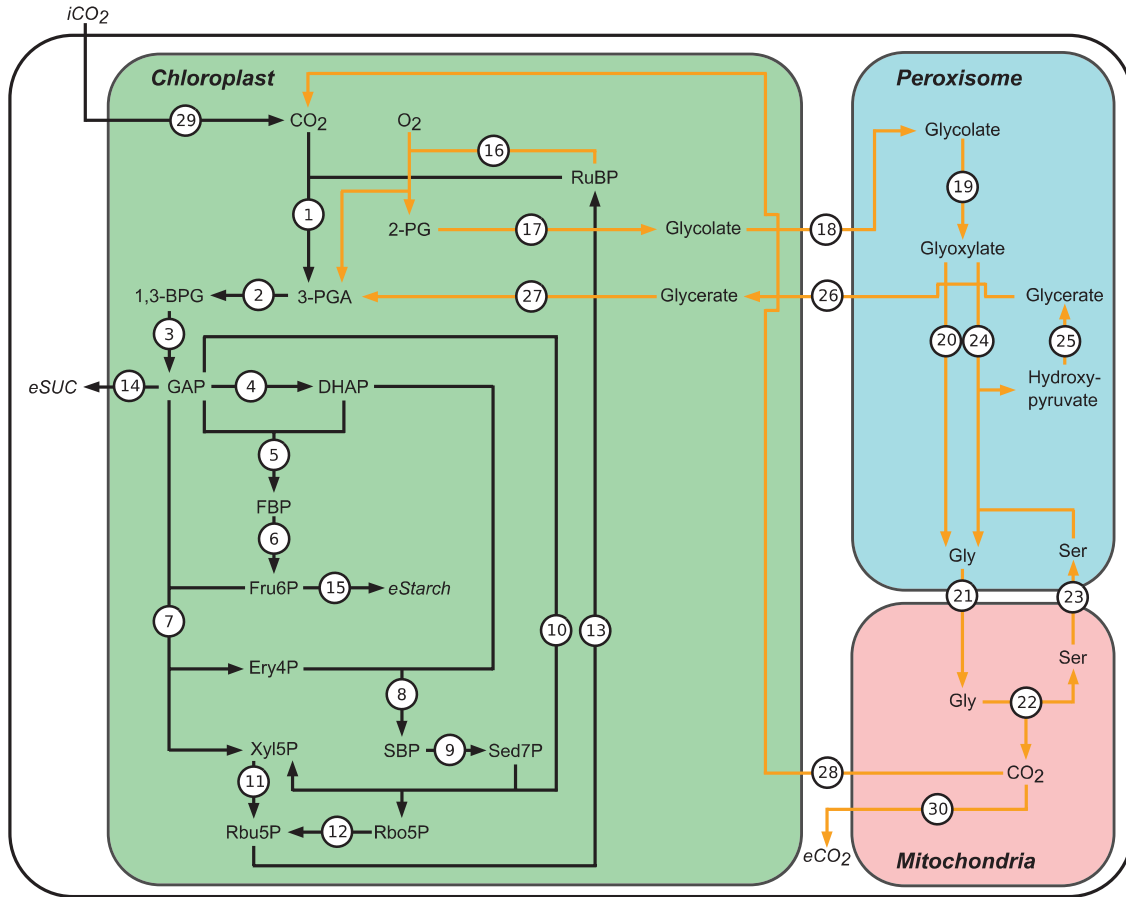
Figure 1. The Calvin–Benson–Bassham cycle (black) and photorespiration (orange). Reactions are catalysed by the following enzymes: 1. Rubisco—ribulose-1,5-bisphosphate carboxylase/oxygenase, 2. PGK—phosphoglycerate kinase, 3. GAPDH—glyceraldehyde 3-phosphate dehydrogenase, 4. TPI—triose-phosphate isomerase, 5. ALD—aldolase, 6. FBPase—fructose 1,6-bisphosphatase, 7. TK—transketolase, 8. ALD—aldolase, 9. SBPase—sedoheptulose-1,7-bisphosphatase, 10. TK—transketolase, 11. RPE—ribulose-phosphate epimerase, 12. RPI—ribose-5-phosphate isomerase, 13. PRK—phosphoribulokinase, 14. GAP export for sucrose synthesis, 15. Fru6P export for starch synthesis, 16. Rubisco—ribulose-1,5-bisphosphate carboxylase/oxygenase, 17. PGP—phosphoglycolate phosphatase, 18. Glycolate transport, 19. GO—glycolate oxidase, 20. GGAT—glutamate-glyoxylate aminotransferase, 21. Glycine transport, 22. GDC and SHMT—glycine decarboxylase complex and serine hydroxymethyltransferase, 23. Serine transport, 24. SGAT—serine-glyoxylate aminotransferase, 25. HPR1—hydroxypyruvate reductase 1, 26. Glycerate transport, 27. GLYK—glycerate kinase, 28. Portion of CO_2 reentering chloroplast, 29. CO_2 entering chloroplast from atmosphere, 30. Portion of CO_2 released to cytoplasm. RuBP—ribulose-1,5-bisphosphate, 3-PGA—3-phospho-D-glycerate, 1,3-BPG—1,3-bisphosphoglyceric acid, GAP—glyceraldehyde 3-phosphate, DHAP—dihydroxyacetone phosphate, FBP—fructose 1,6-bisphosphate, Fru6P—fructose 6-phosphate, Ery4P—erythrose 4-phosphate, Xyl5P—xylulose 5-phosphate, SBP—sedoheptulose-1,7-bisphosphate, Sed7P—sedoheptulose-7-phosphate, Rbu5P—ribulose 5-phosphate, Rbo5P—ribose-5-phosphate, 2-PG—2-phosphoglycolate, Gly—glycine, Ser—serine. The model does not consider refixation of ammonium.

system by the coordination transformation $\hat{x} = x - \bar{x}$ resulting in $(d/dt)\hat{x} = J\hat{x}$ and the general solution for homogenous systems:

$$\hat{x}(t) = \sum_{i=1}^{n} c_i b_i e^{\lambda_i t} \tag{1}$$

with λ_i being the eigenvalues of J and b_i being the corresponding eigenvectors (Klipp *et al.* 2016). The coefficients c_i can be determined by solving $x(0) = \sum_{i=1}^{n} c_i b_i$ (note that $e^{\lambda_i 0} = 1$). As a consequence of $e^{\lambda t} = e^{(a+ib)t} = e^{at}(\cos bt + i \sin bt)$, the stability of the steady state is entirely determined by the real parts of the eigenvalues of J. If all real parts of the eigenvalues are below zero (i.e. $a < 0$) then for $t \to \infty$ the term $e^{\lambda t}$ converges to 0 and thus $\hat{x}(t) \to 0$ and $x(t) \to \bar{x}$. In other words,

after a perturbation the system returns to $\bar{x}$ and the steady state is considered locally asymptotically stable. If any of the eigenvalues has a positive real part (i.e. $a > 0$), the system will exponentially diverge from its steady state.

An important note is that, following the Hartman–Grobman theorem, the linearized system only reflects the local behaviour of the dynamic system if the stable point $\bar{x}$ is hyperbolic (i.e. J cannot have eigenvalues whose real parts equal 0, $a \neq 0$).

2.2 Structural kinetic modelling

In practice, calculation of the Jacobian Matrix J is often complicated by a lack of knowledge on enzymatic rate equations and kinetic parameters (e.g. V_{max}, K_m, K_i) required for the formulation of the ODE system $\dot{x}$. To circumvent this, an approach named 'SKM' was proposed by Steuer and co-workers in which kinetic

parameters are replaced by normalized enzymatic parameters (Steuer *et al.* 2006).

In this approach the system of ODEs is given by:

$$\dot{x} = \frac{dx(t)}{dt} = Nv(x,k)$$

(2)

with $x = (x_1, ..., x_n)^T$ metabolites and $v = (v_1, ..., v_r)^T$ reaction rates. The $n \times r$ dimensional matrix N represents the stochiometric matrix of the considered metabolic reaction network. After defining:

$$c_n(t) := \frac{x_n(t)}{\bar{x}_n}, \quad \Lambda_{nr} := N_{nr} \frac{v_r(\bar{x})}{\bar{x}_n}, and \mu_r(c) := \frac{v_r(x)}{v_r(\bar{x})},$$

(3)

the variable substitution $x_n = c_n \bar{x}_n$ leads to the system being rewritten in terms of $c(t)$ as:

$$\frac{dc}{dt} = \Lambda \mu(c).$$

(4)

Now J can be evaluated at steady state $c^0 = 1$ with:

$$J_c = \Lambda \left. \frac{\partial \mu(c)}{\partial c} \right|_{c^0=1} =: \Lambda \theta_c^\mu.$$

(5)

Thus, the Jacobian is defined as a product of matrices Λ and θ. The matrix Λ consists of the stochiometric matrix N normalized to the flux $v(\bar{x})$ and metabolite concentrations $\bar{x}$ at steady state. The $r \times n$ dimensional matrix θ contains normalized elasticities and represents the degree of saturation of the normalized flux $\mu(c)$ with respect to the normalized concentration $c(t)$. Hence, entries in θ describe to what extend changes in concentration of metabolite n influence the flux rate of reaction r. Depending on the interaction between the considered metabolite and reaction, θ is either defined within the interval $(0; \ 1)$ for activating effects or within $(-1; \ 0)$ for inhibitory effects. A detailed discussion concerning entries of θ has been provided earlier (Steuer *et al.* 2006). Entries in relation to Michaelis–Menten kinetics have been discussed in Reznik and Segrè (2010).

To analyse the system dynamics, the model was repeatedly simulated with parameters for $\theta_{Substrate}^{Reaction}$ being chosen from a uniform distribution in the unit interval $(0; 1)$. This ensured that all possible explicit kinetic models of the observed system are considered. Eigenvalues of randomized Jacobians were calculated and the stability of the model was evaluated. The maximum real part of all eigenvalues represented the spectral abscissa of J.

2.3 Ranking of parameters

Parameters used in the SKM approach were ranked according to their Pearson correlation to the spectral abscissa. Additionally, the distance between the distribution function of stable solution and the original probability density function was used for ranking. Pearson correlation was calculated as follows:

$$r_{\theta b} = \frac{\sum_{i=1}^n (\theta_i - \bar{\theta}) * (b_i - \bar{b})}{\sqrt{\sum_{i=1}^n (\theta_i - \bar{\theta})^2} \sqrt{\sum_{i=1}^n (b_i - \bar{b})^2}}$$

(6)

with $b = max(Re(\lambda))$. The rank for the correlation analysis R_c for a parameter $\theta_{Metabolite}^{Reaction}$ is given in descending order of $|r_{\theta b}|$. The distance was calculated by:

$$d_n = \quad \|F_n - F_0\| = \ sup_x |F_n(x) - F_0(x)|$$

(7)

with F_n being the cumulative distribution function of values of θ resulting in a stable solution. F_0 is the cumulative normal distribution (a normal distribution was used to sample θ). Finally, sup_x is the supremum of the set of distances. The distance d_n was then ranked in descending order, yielding R_d. The overall rank for a parameter was given in ascending order of the mean from the ranks R_c and R_d.

2.4 BnB algorithm

To analyse how regulation affects the observed stability of a model, a discrete-parameter optimization algorithm was developed. It followed the *Branch and Bound* procedure first proposed by (Land and Doig 1960), which allows for the implicit enumeration of all possible combinations of regulatory interactions in a given model. In this approach, the regulatory solutions can be envisioned as forming a tree in which low performing branches are pruned. This is achieved by comparing branching nodes to a boundary value, which is determined by the heuristic solution. The algorithm uses a best-first search strategy with wide branching as reviewed before (Morrison *et al.* 2016). An added challenge arose from the fact that the objective of the optimization problem (proportion of stable solutions) was not easily calculated by a simple cost function but rather had to be determined using a Monte Carlo experiment which is inherently noisy. Owing to this, nodes were pruned by hypothesis testing. As the proportion of stable solutions follows a binomial distribution which can be normally approximated, the Z-test was used ($H_0 : \ p_1 \leq p_2$, the proportion of stable solutions of the heuristic solution is equal or less than that of the considered node. $H_1 : \ p_1 > p_2$, the proportion of stable solutions of the heuristic solution is greater than that of the considered node). The standard score was calculated applying the following equation (Equation 8):

$$z = \quad \frac{\hat{p}_1 - \hat{p}_2}{\sqrt{\hat{p}(1-\hat{p})\frac{2}{n}}}$$

(8)

with $\hat{p}_1$ being the proportion of stable solutions within the best heuristic solution (i.e. the best solution with only discrete parameters). The proportion of stable solutions in the node considered for pruning was given by $\hat{p}_2$. The pooled standard error was calculated using $\hat{p} = (\hat{p}_1 + \hat{p}_2)/2$. The number of samples within each Monte Carlo experiment was given by n. If the value of $z > 2.33$ ($\alpha = 0.01$, one-tailed), then H_0 could be discarded (i.e. the proportion of stable solutions in the heuristic solution is significantly higher than in the observed node) and the considered node was pruned.

For continuous parameter optimization of nodes, particle swarm optimization was applied (Kennedy and Eberhart 1995). The velocity v_i and position x_i of a particle i was updated according to the particles best position p_i and the best global position p_g following:
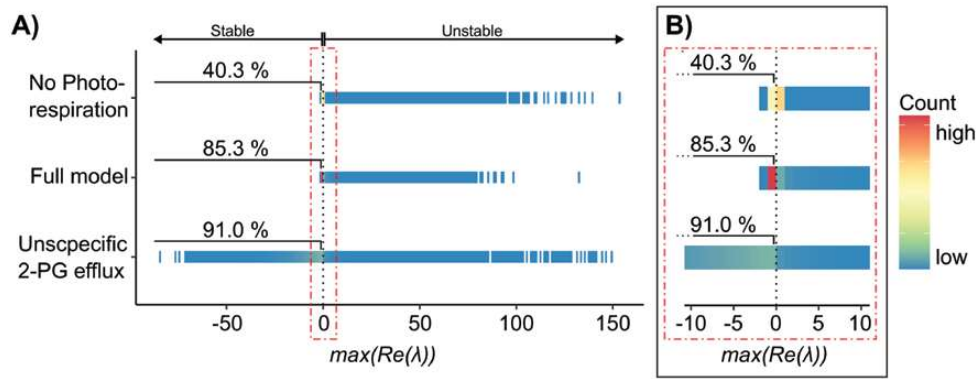
Figure 2. Stability of the CBBC. (A) Full range of spectral abscissa. (B) Enlarged view of range between −10 and 10. Results are shown for models with photorespiration, without photorespiration, and with an unspecific 2-PG efflux. Maximal real eigenvalues below 0 (dotted black line) correspond to stable systems. Each model was simulated 10^6 times. Input and saturation parameters were randomized.

$$\begin{cases} v_i \leftarrow \chi(v_i + u(0, \phi_1) \otimes (p_i - x_i) + u(0, \phi_2) \otimes (p_g - x_i)), \\ x_i \leftarrow x_i + v_i \end{cases}$$
$$(9)$$

with $\phi = \phi_1 + \phi_2 = 4.1$, $\phi_1 = \phi_2$ and $\chi = 2/(\phi - 2 + \sqrt{\phi^2 - 4\phi})$ as proposed by (Clerc and Kennedy 2002) and reviewed in Poli *et al.* (2007). The vector $u(0, \phi)$ contained random numbers uniformly distributed in $[0, \phi]$. The numbers were randomly generated for each particle in each iteration. Component-wise multiplication is indicated by $\otimes$.

Both pseudocode of the algorithm and an accompanying MATLAB® (www.themathworks.com) script are provided in Supporting Information.

3. RESULTS

3.1 Photorespiration affects stability of carbon fixation

As plant metabolism comprises a complex network of pathways which was not possible to consider completely within this study, a simplified mathematical model was developed to simulate fluxes under the steady-state assumption, $\dot{x} = 0$. While a steady-state assumption ignores concentration dynamics in accumulating and/or depleting metabolite pools, it still reflects a helpful approximation of many pathways which show quasi-stationary concentrations without significant fluctuation, e.g., during the light or dark phase of a diurnal cycle (Gibon *et al.* 2004; Küstner *et al.* 2019b). Yet, as outlined earlier, also dynamic pathways might be interpreted based on a steady-state assumption within a (very) short time period which does not show significant alteration of metabolite concentrations (Nägele et al. 2014, 2016). The considered equilibrium point $\bar{x}$ was hyperbolic and, in accordance with the Hartman–Grobman theorem, could be used to analyse the local behaviour of the dynamical system (Hartman 1960), justifying the use of the SKM approach.

Based on real parts of eigenvalues of Jacobian matrices, the stability of the model was then analysed and compared to a model in which Rubisco only catalyses the carboxylation of RuBP (no photorespiration). In a synthetic scenario, stability was analysed under conditions where 2-PG had an unspecific

efflux and no carbon was recovered. A graphical representation of these models can be found in Supporting Information—**Fig. S1**. Model simulations were run 10^6 times with metabolite concentrations and reaction fluxes being based on literature data (Flügel *et al.* 2017; Fürtauer *et al.* 2019; Jablonsky *et al.* 2011; Kitashova *et al.* 2021; Zhu *et al.* 2007; Küstner *et al.* 2019a). In conflicting reports, values from subcellular studies were used. Furthermore, input fluxes and efflux partitioning were perturbed to simulate differing physiological conditions resulting from a changing environment, e.g. stress could impose an increased ATP demand, which was reflected by perturbed efflux partitioning.

In the most basic case of all $\theta_{Substrate}^{Reaction}$ being set to 1 (corresponding to simple irreversible mass-action kinetics), the full model (including all reactions shown in Fig. 1) and the model with an unspecific 2-PG efflux showed a stable steady state. In contrast, the model without photorespiration demonstrated an unstable steady state (Fig. 2).

When allowing $\theta_{Substrate}^{Reaction}$ to move freely in the interval $(0; 1)$, the results indicated that the model without photorespiration was the least stable with only 40.3 % of simulations resulting in a stable solution, i.e. $max(Re(\lambda))$ was negative (Fig. 2). Comparison to the full model showed that including the photorespiratory pathway stabilized the system to 85.3 %. Interestingly, the most stable model was observed with an unspecific efflux of 2-PG where 91.0 % of the spectral abscissa (the maximum real part of all eigenvalues) were below 0. Additionally, this model possessed large negative eigenvalues and thus converged faster than the two other models. It is, however, important to keep in mind that such a scenario is highly artificial and would significantly reduce carbon assimilation rates. Due to the proportion of stable solutions (91 % vs. 40.3 %), these results suggested that oxygenation of RuBP increases stability of the CBBC. Furthermore, the convergence rate was increased resulting in a faster response to perturbations. As this stabilizing effect was seen in both the full model and the model with an unspecific efflux, this suggested that the observed stabilization did not result from the addition of an arbitrary cyclic structure but rather from the oxygenation of RuBP. The multistep process of recuperating carbon from 2-PG again resulted in a slow convergence rate, yet the higher proportion of stable solutions was maintained. Photorespiration

Table I. Ranking of saturation coefficients θ in accordance with their impact on the stability. Rankings are provided both with respect to the full model and the model lacking photorespiration. Rank 1: highest impact, rank 34: lowest impact. θ represents the saturation coefficient between a given metabolite and a reaction. Pearson correlation and the distance measure dn between the cumulative distribution function of values of θ resulting in a stable solution and the original distribution function were used for ranking.

Overall rank	Full model			No Photorespiration		
	θ	*Correlation*	dn	θ	*Correlation*	dn
1	θGAPTPI	-0.28	0.0637	θGAPTPI	-0.07	0.2454
2	θGAPTK	0.15	0.0366	θGAPeSuc	-0.05	0.2892
3	θFru6PTK	-0.12	0.0268	θCO2Rubisco	-0.11	0.0102
4	θGAPeSuc	-0.12	0.0339	θGAPTK	0.04	0.1016
5	θ3PGAPGK	0.08	0.0092	θRuBPRubisco	0.04	0.0028
6	θRuBPRubisco	0.06	0.0058	θFru6PTK	-0.01	0.0121
7	θGAPTK	0.04	0.0074	θ3PGAPGK	0.02	0.0021
8	θGlyoxylateSGAT	0.03	0.0187	θGAPAld	-0.01	0.0026
9	θGlyoxylateGGAT	-0.02	0.0350	θGAPTK	0.02	0.0017
10	θSed7PTK	-0.03	0.0073	θSed7PTK	-0.01	0.0027
11	θDHAPALD	0.04	0.0032	θEry4PALD	0.01	0.0017
12	θSBPSBPase	0.02	0.0037	θFru6PeStarch	0.00	0.0032
13	θSerMitSerT	-0.02	0.0041	θDHAPALD	0.01	0.0014
14	θSerPerSGAT	-0.01	0.0094	θDHAPAld	0.00	0.0024
15	θCO2Rubisco	-0.03	0.0026	θRbo5PRPI	0.01	0.0015
16	θEry4PALD	0.02	0.0028	θ13BPGPGK	0.00	0.0015
17	θGAPAld	-0.03	0.0018	θRbu5PPRK	0.00	0.0017
18	θDHAPAld	-0.01	0.0024	θSBPSBPase	0.01	0.0012
19	θGlycerateChlGLYK	0.01	0.0046	θXyl5PRPE	0.01	0.0012
20	θGlycolateChlGlycoT	0.01	0.0029	θFBPFBPase	0.00	0.0014
21	θHydroxyp.HPR	0.01	0.0035			
22	θCO2_miteCO2	-0.01	0.0044			
23	θRbo5PRPI	0.01	0.0020			
24	θGlyceratePerGlycertaeT	0.01	0.0035			
25	θGlycolatePerGO	0.01	0.0020			
26	θCO2_mitCO2_d	0.01	0.0031			
27	θGlyPerGlyT	0.01	0.0019			
28	θXyl5PRPE	0.01	0.0011			
29	θRbu5PPRK	0.01	0.0010			
30	θGlyMitGDC/SHMT	0.01	0.0011			
31	θ13BPGPGK	0.00	0.0016			
32	θFru6PeStarch	0.00	0.0018			
33	θ2PGPGP	0.00	0.0016			
34	θFBPFBPase	0.00	0.0010			

thus increased the probability of finding a stable steady state at experimentally observed metabolite concentrations and reaction fluxes.

3.2 GAP dynamics are pivotal for system stability

One of the draw backs of the SKM approach lies in the fact that *in vivo* only a subset of the analysed parameter space is present. Owing to this and in order to investigate where the 14.7 % instability observed in the full model originated from, perturbed parameters of the model were ranked in accordance to their impact on the stability of the metabolic network. This allowed us to estimate the physiological relevance of the results. Pearson correlation between parameters and $max(Re(\lambda))$ was

determined. Furthermore, the distribution of perturbed parameter values resulting in a stable solution was compared to their original probability density function, $\|d_n = F_n - F_0\|$. In the full model, the most influential parameters were almost all found to be tied to reactions and metabolites within the CBBC (Table 1). An exception to this were parameters which determine the effect of glycolate on rates of GGAT and SGAT ($\theta_{Glyoxylate}^{GGAT}$, $\theta_{Glyoxylate}^{SGAT}$). These parameters were associated with photorespiration rather than the CBBC. However, the results showed that reactions involving GAP as a substrate (θ_{GAP}^{TPI}, θ_{GAP}^{TK}, θ_{GAP}^{eSuc}) were the most essential in stabilizing the system after perturbation. This observation was true for both the full model as well as the model ignoring photorespiration. To a lesser extent, this was

also observed for the carboxylation and oxygenation of RuBP ($\theta_{RuBP}^{Rubisco}$, $\theta_{CO2}^{Rubisco}$). However, this was more pronounced in the model lacking photorespiration. In conclusion, this suggested that GAP partitioning was the most essential aspect governing CBBC stability.

Interestingly, reactions catalysed by TPI, and to a lesser extend also SBPase, had a considerable impact on the stability of the model. This further suggested a possible benefit of inhibition by 2-PG which inhibits both enzymes.

Comparing parameters between both models revealed a sharp increase in the value of d_n for two parameters, θ_{GAP}^{TPI} and θ_{GAP}^{eSuc}. The d_n value for θ_{GAP}^{eSuc} increased from 0.037 to 0.289, for θ_{GAP}^{TPI} the change was slightly lower, increasing from 0.064 to 0.245. This increase was coupled with a decline in the corresponding correlation coefficients. As d_n represents a shift in the parameter distribution found in stable solutions from the uniform distribution, this was most likely the consequence of a reduced parameter space leading to stable solutions. Values of θ contained in stable solutions were compared between the two models ([Fig. 3](#)).

The lack of photorespiration clearly reduced the parameter space of stable solutions compared to the full model. Values of the saturation parameter θ_{GAP}^{eSuc} were shifted towards 1, while θ_{GAP}^{TPI} was shifted towards 0. This suggested an increasing importance of GAP export in order to stabilize the system, especially in relation to GAP utilization for DHAP synthesis. As starch synthesis occurs downstream of TPI, this indicated that starch synthesis may not be able to stabilize fluctuations effectively. Taken together, the structure and location of photorespiration thus appeared to alleviate the pressure on the GAP export required to stabilize the system.

Previous studies and the rich history of explicit modelling of the CBBC and photorespiration showed that TPI operates close to equilibrium under physiological conditions ([Jablonsky *et al.* 2011](#)). This suggested that θ_{GAP}^{TPI} should be closer to 1 (as

was found in the full model) which indicated that the reduced proportion of stable solutions (see [Fig. 2](#)) was indeed of importance in relation to conditions *in vivo*. However, it is important to consider that this would also be reflected in a value of θ_{DHAP}^{TPI} close to -1, suggesting reversibility. To ensure that reduced parameter space of θ_{GAP}^{TPI} was still relevant under these reversible conditions, the two models were simulated reflecting this change and distributions of θ_{GAP}^{TPI} and θ_{GAP}^{eSuc} were again compared [see **Supporting Information—Fig. S2**]. Previous observations were confirmed with this approach suggesting that the observed stabilizing effect of photorespiration was not an artefact of an irreversibility assumption but indeed relevant under physiological conditions.

Following this, the model was investigated to analyse if starch synthesis was indeed unable to affect the stability of the system. The effect of $\theta_{Fru6P}^{eStarch}$ on the stability was analysed across the two models ([Table 1](#)). Both models showed no apparent effect of $\theta_{Fru6P}^{eStarch}$ for the stability of the system. A change in θ_{GAP}^{eSuc} had a direct effect on the partial derivative $\frac{\partial(f(GAP))}{\partial(GAP)}$ found within the Jacobian matrix. As a result of Equation (5), higher values of θ_{GAP}^{eSuc} resulted in an absolute increase of $\frac{\partial(f(GAP))}{\partial(GAP)}$, thus increasing the effect that a change in the concentration of GAP had upon its own dynamics. Furthermore, θ_{GAP}^{eSuc} only affected $\frac{\partial(f(GAP))}{\partial(GAP)}$, whereas changes in other parameters of GAP also affected other entries in the Jacobian (e.g. θ_{GAP}^{TPI} affects $\frac{\partial(f(GAP))}{\partial(GAP)}$ and $\frac{\partial(f(DHAP))}{\partial(GAP)}$). This could make GAP dynamics more resilient against effects of other metabolites and might constitute an overflow mechanism for excess carbon out of the CBBC without influencing CBBC dynamics. Similarly, an increase in $\theta_{Fru6P}^{eStarch}$ affected $\frac{\partial(f(Fru6P))}{\partial(Fru6P)}$, allowing more control over its own dynamics. However, as mentioned previously, the most crucial junction determining the stability was found to be at GAP and its various pathways. Thus, an increase in the absolute value of $\frac{\partial(f(GAP))}{\partial(GAP)}$ appeared to be more beneficial than an absolute increase in $\frac{\partial(f(Fru6P))}{\partial(Fru6P)}$.
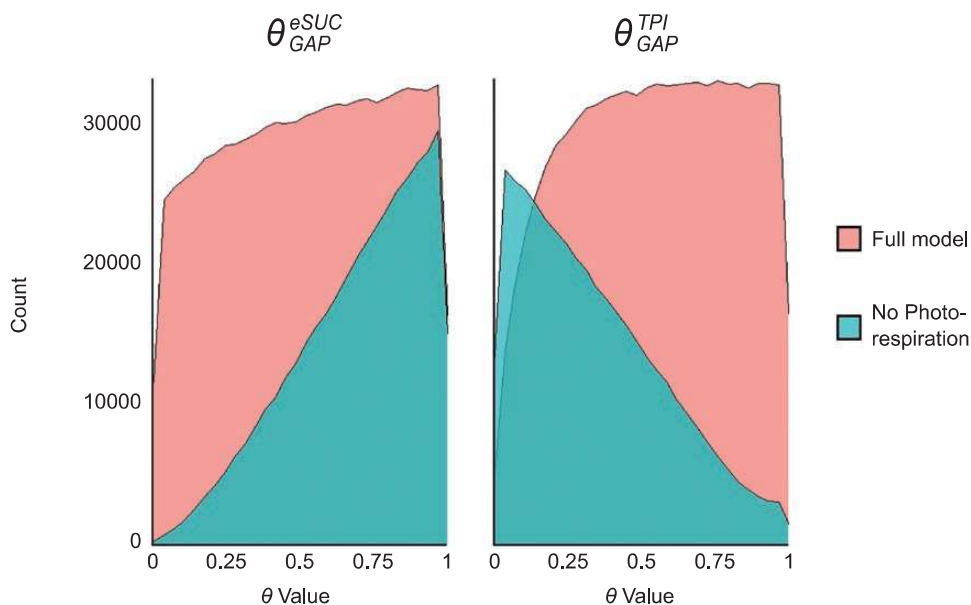

Figure 3. Values of θ found in stable solutions. Parameters are shown in which the model without photorespiration showed the largest deviation from the expected distribution ($d_n\theta_{GAP}^{eSuc} = 0.289$, $d_n\theta_{GAP}^{TPI} = 0.245$). Values for θ are shown for both the full model and the model excluding photorespiration.

3.3 A shift in carbon partitioning towards sucrose synthesis increases metabolic stability

Based on the assumption that an increase in the absolute value of $\frac{\partial(f(GAP))}{\partial(GAP)}$ may stabilize the CBBC, it was suggested that an increase in the ratio of assimilated carbon going to sucrose biosynthesis rather than starch synthesis should increase the stability of the model as well. This would be a consequence of Equation (10).

$$\frac{\partial(f(GAP))}{\partial(GAP)} = \sum_{j=1}^{m} \Lambda_j^{GAP} * \theta_{GAP}^j, \tag{10}$$

The resulted from rules of matrix multiplication when analysing a single element of J following Equation (5). Following the term $\Lambda_{eSuc}^{GAP} * \theta_{GAP}^{Suc} = -1 * \frac{v_{eSuc}\overline{[GAP]}}{[GAP]} * \theta_{GAP}^{Suc}$, a shift of assimilated carbon towards sucrose synthesis rather than starch synthesis increased $v_{eSuc}\overline{[GAP]}$ and, thus, $\frac{\partial(f(GAP))}{\partial(GAP)}$, resulting in a similar effect as observed above. To test this, the ratio of sucrose/starch allocation was shifted in the model by altering the corresponding fluxes and the results were again simulated 10^6 times for each condition.

Supporting the hypothesis, results showed that an increased proportion of sucrose biosynthesis resulted in an increase in the stability of the system (Fig. 4). Interestingly, this effect was more pronounced under deficiency of photorespiration (24.4 % → 46.2 % stability vs. 79.8 % → 86.1 % stability, see Fig. 4).

In addition to increased biosynthesis of soluble sugars, accumulation of secondary metabolites is a well-known stress and acclimation response of plants (see e.g. Winkel-Shirley 2002; Doerfler *et al.* 2013). Following the finding that a shift from starch towards sucrose synthesis was able to stabilize the system, a model was created containing an Ery4P export to simulate the impact that induction of secondary metabolism via the shikimate pathway might have on the CBBC. A graphical representation of this model and a model containing Ery4P export, but no photorespiration, is provided in **Supporting Information— Fig. S3**. Similar as to what was observed for starch metabolism, the value of $\theta_{Ery4P}^{eSecondary\_Metabolism}$ had no significant effect on the stability of the system (Table 2).
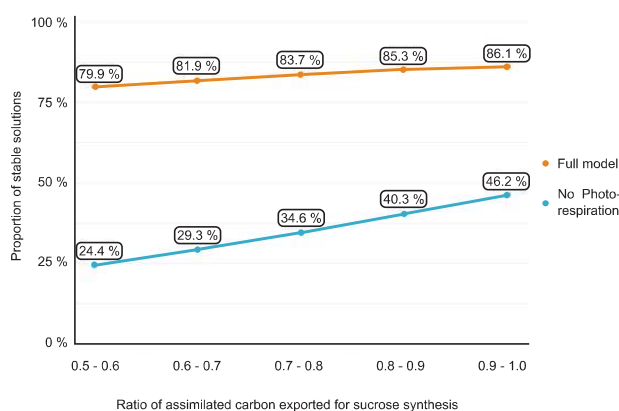

Figure 4. Portion of stable solutions with increasing carbon partitioning going towards sucrose synthesis. Each point was simulated 10^6 times at different ratios of sucrose synthesis randomized within an interval of 0.1; the ratio is given in C6-Sucrose/C6-Starch.

Table 2. Effect of $\theta_{Ery4P}^{eSecondary\_Metabolism}$ on the stability of the CBBC. The rank of $\theta_{Ery4P}^{eSecondary\_Metabolism}$ is shown in relation to all other θ parameters involved in the model. The parameter θ in general represents the saturation coefficient between a given metabolite and a reaction. Ranking was achieved according to its Pearson correlation with the spectral abscissa and the distance measure d_n.

Model	Rank	Pearson correlation	*dn*
Full model	34 of 35	−0.01	0.001
No photorespiration	15 of 21	0.00	0.011

Based on this finding, we hypothesized that GAP export for sucrose synthesis was particularly able to stabilize the system which might result from its direct ability to control GAP dynamics. To test this hypothesis, the ratio of carbon going towards sucrose, starch or secondary metabolites was altered and the proportion of stable solutions under each condition was quantified (Fig. 5).

In presence of the photorespiratory pathway, carbon allocation towards sucrose proved to be the most effective in stabilizing the system (Fig. 5, left panel, full model). In contrast, a lack of photorespiration shifted most stable parameter combinations towards higher activity of secondary metabolism (40–60 %). In both models, carbon channelling into starch biosynthesis contributed least to stability (0–20 %). In summary, these results suggested that the presence of the photorespiratory pathway allows for higher rates of sucrose biosynthesis without compromising the stability of the metabolic network, i.e. a higher carbon flux has to be allocated towards secondary metabolism in the absence of photorespiration in order to increase metabolic stability. Further, the stabilizing effect of GAP export was only found to be efficient if a sufficiently large parameter space for GAP export was present, which might be achieved either through photorespiration or secondary metabolism [**see Supporting Information—Fig. S4**].

3.4 The role of 2-PG in stabilizing the CBBC

To analyse if regulation of the CBBC by 2-PG though inhibition of TPI and/or SBPase may change the carbon partitioning towards a more stable system, a BnB algorithm was applied with the purpose of searching for optimal strategy resulting in stable solutions. This analysis was challenged by the combinatorial problem of testing ~4 * 10^{12} parameter combinations. Here, BnB enabled a computation time of, in total, <700 h (MATLAB® R2021a, Intel® Core™ i7-10700 @ 2.90 GHz).

In a situation where no enzymatic regulation, except for TPI and SBPase, was considered, both inhibition of TPI and SBPase by 2-PG lead to a decrease in stability (Fig. 6A). This effect was strongest for TPI, where the proportion of stable models fell from 85.3 % without inhibition to 6.1 % with strong inhibition. Although less pronounced, a drop of stability from 85.3 % to 80.6 % was also observed for SBPase. This drastically changed when considering full enzymatic regulation of the CBBC, highlighting the importance of the BnB approach (Fig. 6B). In 30 % of near-optimal solutions (no significant difference to the best solution, $P > 0.01$), a weak inhibition of TPI by 2-PG was observed. A weak inhibition by 2-PG of SBPase was observed in 15 % of
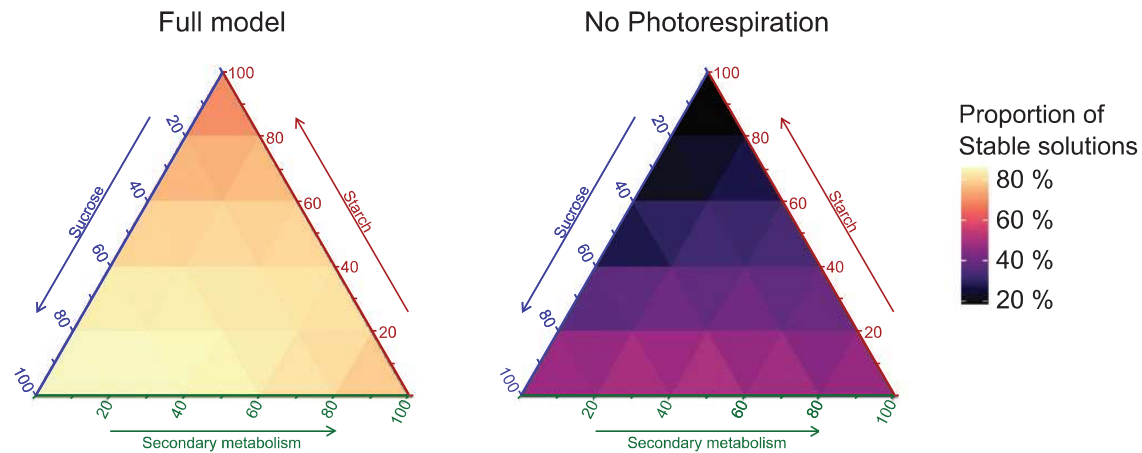
Figure 5. How carbon allocation affects the stability of the CBBC. The ternary plot was constructed from 231 data points each simulated 10^4 times per model. Arrows indicate the proportion of carbon flux in direction of sucrose, starch and/or secondary metabolites. Colour indicates proportion of stable solutions.

all simulated models and strong inhibition in 75 % of solutions. This indicated a positive effect of regulation by 2-PG on the stability of the metabolic network with inhibition of SBPase taking a key role. Although this was more ambiguous for the regulation of TPI, a considerable parameter space existed also for this inhibition (30 % of all scenarios).

4. DISCUSSION

Exposure to a sudden change of environmental conditions, e.g. light intensity or temperature, typically induces stress reactions in organisms to counteract and prevent irreversible damage of cells, tissues or organs. Stabilization of metabolism plays a central role in such stress response because it is preliminary to perceive and integrate environmental signals (Zhang *et al.* 2022). Here, stability might be interpreted as the probability of transition of metabolic steady states, and it has been shown before that stability properties can be determined by network structures themselves, e.g., by metabolic cycles (Reznik and Segrè 2010). Stability properties of a biochemical reaction network can be quantified via an SKM approach (Steuer *et al.* 2006). With this approach, effects of single and/or multiple effectors and regulators on system stability can be estimated to yield non-intuitive information about metabolic pathways, pathway structures (Reznik and Segrè 2010) or metabolic acclimation strategies (Fürtauer and Nägele 2016). In case of an unstable metabolic state, slight modifications of environmental conditions might immediately result in an oscillating, or chaotic, dynamic behaviour of single metabolite concentrations or whole pathways (Fürtauer and Nägele 2016). In photosynthetic metabolism, this might rapidly lead to an imbalance of, e.g., ATP/ADP or NADPH/NADP ratios which can easily cause generation of reactive oxygen species and tissue damage (Noctor and Foyer 2000). To reliably estimate stability properties in metabolic systems, a vast variety of regulatory interactions between proteins and metabolites needs to be considered which rapidly results in extensive combinatorial problems for computation. To overcome some limitations of computation time, we applied a discrete-parameter optimization approach. The importance of such an approach became evident when evaluating the effect of inhibition of CBBC enzymes by

2-PG which finally suggested that photorespiration represents a trade-off between carbon assimilation rate and stability of cellular metabolism. This finding is in line with previous work which came to a similar conclusion using simplified ODE models with mass-action kinetics (Hahn 1991). Furthermore, previously published work in bioengineering found that a bypass, oxidizing glycolate completely in the chloroplast, leads to a 40 % increase in biomass production of tobacco plants in field experiments (South *et al.* 2019). This further suggests that the stabilizing effect resulting from photorespiration is tied to oxygenation of RuBP rather than its innate cyclic structure. This is owing to the fact that, considering fluctuations apparent to field experiments, synthetic plants showed an increase in biomass production as compared to wild-type tobacco.

Our findings supplement and extend the previously suggested regulatory role of 2-PG for adjustment and allocation of chloroplast carbon flow (Flügel *et al.* 2017). The amount of 2-PG is tightly regulated by 2-PG phosphatase, PGLP, and its activity was shown to be essential for efficient carbon fixation and allocation (Flügel *et al.* 2017; Levey *et al.* 2019). Altogether, this suggests a strong impact of PGLP activity on stabilizing whole-cell carbon metabolism after environmental perturbation. Further, simulations revealed that differential allocation of fixed carbon in either soluble carbohydrates, storage compounds or other (secondary) metabolism differentially affects stability of the whole CBBC network. As a consequence, under sudden temperature and/or light changes, when ratios of Rubisco-driven carboxylation and oxygenation significantly deviate from the current homeostasis, metabolism needs to be reprogrammed to maximize stabilization capacities.

The capability of re-stabilizing carbon fixation, and all downstream carbohydrate biosynthesis, is a critical variable in plant ecology and evolution because it significantly determines cell and tissue fate as well as growth and developmental success. Hence, combining biochemical and physiological experiments with stability analysis, e.g. by SKM, represents a promising approach to yield detailed insights into metabolic regulation. This information is essential to interpret experimental data on metabolite dynamics because underlying regulation might comprise non-intuitive patterns, e.g. metabolic
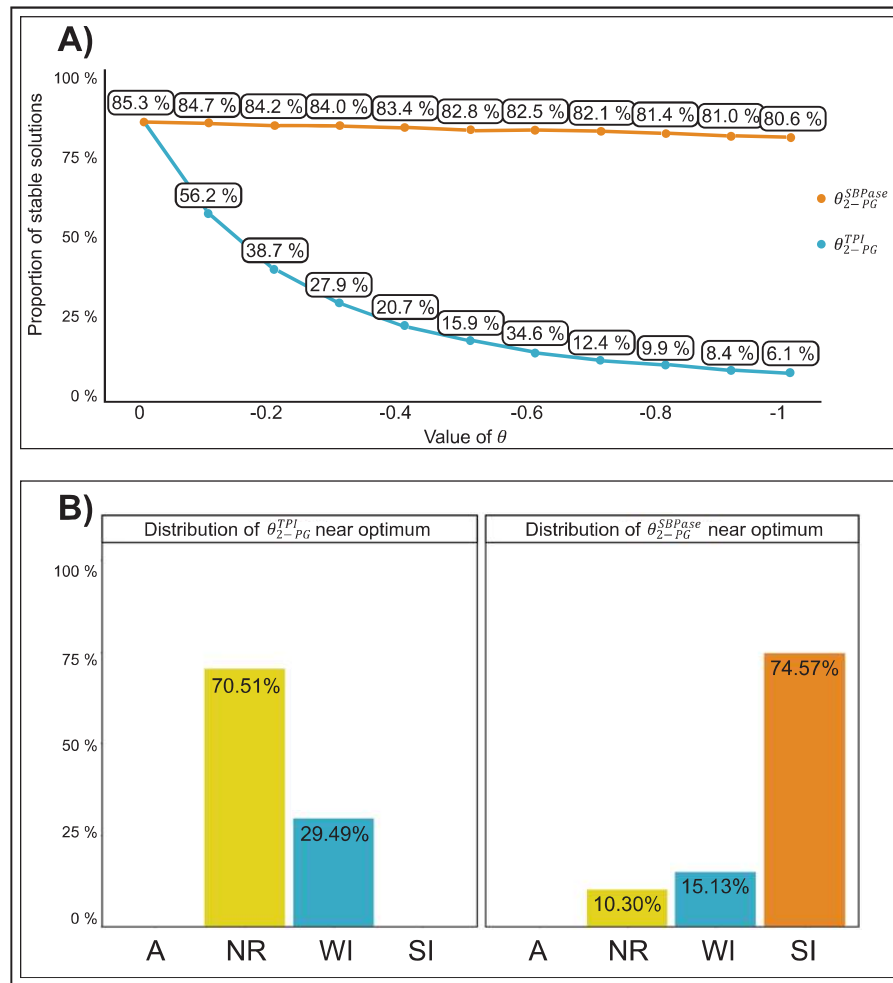
Figure 6. Effects of inhibition of TPI and SBPase by 2-PG. (A) Effects of inhibition by 2-PG without considering regulation of the CBC. Each point was simulated 10^5 times. The blue line represents the effect of 2-PG on TPI. The orange line depicts the effect of 2-PG on SBPase. (B) Effects of inhibition by 2-PG when considering regulation of the CBC. Depicted are results of parameter optimization. The bar plot shows the distribution of regulatory interactions between 2-PG and TPI or SBPase found at the optimal solution and solutions which are not significantly worse ($P > 0.01$). A: activation ($\theta = 1$), NR: no regulation ($\theta = 0$), WI: weak inhibition ($\theta = -0.1$), SI: strong inhibition ($\theta = -0.99$).

cycles (Reznik and Segrè 2010) or nested structures (Schaber *et al.* 2009) which limit interpretation of experimental findings. Further, it indicates the dependency of structural kinetic properties within a metabolic network which interconnects pathways across diverse subcellular compartments. We found that stabilization is achieved by increasing the parameter space of θ_{GAP}^{eSuc} and θ_{GAP}^{TPI} resulting in a stable solution (see Fig. 3). Owing to this and the noticeable correlation of θ_{GAP}^{eSuc} with $max(Re(\lambda))$ but not for $\theta_{Fru6P}^{eStarch}$, a shift from starch accumulation towards sucrose synthesis was able to stabilize the kinetic models (see Table 1 and Fig. 4).

It has been described earlier that under stress, e.g. due to low temperature, carbon allocation is redirected from starch to sucrose biosynthesis (Strand et al. 1997, 1999). While this can be explained by the metabolic role of soluble carbohydrates as substrates for other pathways or osmotically active substances (Obata and Fernie 2012), we hereby provide evidence for an additional role of this metabolic reprogramming in structural kinetic stabilization of carbon metabolism against environmentally induced perturbations. Owing to limitations set by this approach, only a small subset of pathways found within a

cell could be analysed. For example, in the simulated models photorespiration was treated as a closed loop. The addition of further pathways (e.g. nitrogen, sulfate and C_1 metabolism), which are tightly linked to photorespiration, might lead to further regulatory insights (Hodges *et al.* 2016). The speed of convergence towards the steady state could be increased, as reflected by large negative eigenvalues, when photorespiration was treated as an open loop, which would further emphasize the stabilizing effect observed, bringing the model more towards the unrealistic scenario where 2-PG possesses an unspecific efflux (see Fig. 2).

Besides soluble carbohydrates, also secondary metabolites, e.g. flavonoids via the shikimate pathway, are well-known to be involved in plant abiotic stress reactions, acclimation and tolerance mechanisms (Winkel-Shirley 2002; Schulz *et al.* 2016; Naikoo *et al.* 2019). Yet, previously, evidence has also been provided for significant variation of the extent of accumulation of secondary metabolites even across different natural accessions of *Arabidopsis thaliana* (Schulz et al. 2015). While significant correlation between tolerance measures, e.g. freezing tolerance, and flavonoid metabolism has been observed in

these studies, some of the underlying mechanisms remain elusive. For example, transcript levels were found to be associated much stronger to freezing tolerance than absolute metabolite levels (Schulz *et al.* 2015). In context of findings of the present study this might highlight and support the hypothesis of metabolic stabilization by modification of efflux/influx capacities of the CBBC and photorespiratory pathways towards starch, sucrose and secondary metabolism (see Fig. 5). While our analysis revealed that in the full model partitioning of carbon towards sucrose biosynthesis improved the stability more than allocating carbon towards secondary metabolism, secondary metabolism was structurally able to provide a similar effect by increasing the admissive parameter space when oxygenation of RuBP was decreased. Finally, the optimal carbon partitioning was shifted under these conditions towards 40–50 % into secondary metabolism and 50–60 % into sucrose synthesis. Such a scenario might reflect a stress-acclimated state of plant metabolism when rates of photorespiration are decreased again after initial stress response while sugars and secondary metabolites are significantly increased in their amount (Savitch *et al.* 2001; Doerfler *et al.* 2013). It further emphasizes the regulatory interaction between pathways with differential subcellular localization and indicates how stability may affect evolution of metabolism.

In conclusion, our study suggests a stabilizing role of photorespiration on the dynamics of cellular metabolism, thus representing a trade-off between carbon assimilation and metabolic stability in a dynamic environment. Finally, shifting carbon partitioning from starch accumulation towards sucrose synthesis significantly increases system stability which might be related to stress tolerance mechanisms of plants.

SUPPORTING INFORMATION

The following additional information is available in the online version of this article—

Figure S1. Graphical representation of models. (A) Full model. (B) Model lacking photorespiration. (C) Model with unspecific 2-PG efflux.

Figure S2. Values of θ found in stable solutions for TPI reversibility. Values for θ are shown for both the full model and the model excluding photorespiration.

Figure S3. Graphical representation of models with export for secondary metabolism. (A) Full model with Ery4P export. (B) Model lacking photorespiration with Ery4P export.

Figure S4. Effect of carbon partitioning between sucrose synthesis and secondary metabolism. Top: Changes to model stability. Bottom: Effect on admissible parameter space.

MATLAB Scripts. All scripts used in this work. Each model and the Branch and Bound algorithm are present in a separate folder.

Pseudocode BnB. A brief overview of the functions involved in the Branch and Bound algorithm.

SOURCES OF FUNDING

CONFLICT OF INTEREST

None declared.

CONTRIBUTIONS BY THE AUTHORS

Both authors conceptualized the study, performed modelling and calculations, and wrote the paper.

ACKNOWLEDGEMENTS

LITERATURE CITED

Anderson LE. 1971. Chloroplast and cytoplasmic enzymes II. Pea leaf triose phosphate isomerases. *Biochimica et Biophysica Acta (BBA) - Enzymology* 235:237–244.

Andersson I. 2008. Catalysis and regulation in Rubisco. *Journal of Experimental Botany* 59:1555–1568.

Bassham JA, Benson AA, Kay LD, Harris AZ, Wilson AT, Calvin M. 1954. The path of carbon in photosynthesis. XXI. The cyclic regeneration of carbon dioxide acceptor1. *Journal of the American Chemical Society* 76:1760–1770.

Berry JA, Osmond CB, Lorimer GH. 1978. Fixation of 18O$_2$ during photorespiration: kinetic and steady-state studies of the photorespiratory carbon oxidation cycle with intact leaves and isolated chloroplasts of C$_3$ plants 1. *Plant Physiology* 62:954–967.

Bisswanger H. 2017. *pH and temperature dependence of enzymes*. Berlin, Germany: Wiley–VCH Verlag, 145–147.

Bowes G, Ogren WL, Hageman RH. 1971. Phosphoglycolate production catalyzed by ribulose diphosphate carboxylase. *Biochemical and Biophysical Research Communications* 45:716–722.

Clerc M, Kennedy J. 2002. The particle swarm—explosion, stability, and convergence in a multidimensional complex space. *IEEE Transactions on Evolutionary Computation* 6:58–73.

Doerfler H, Lyon D, Nägele T, Sun XL, Fragner L, Hadacek F, Egelhofer V, Weckwerth W. 2013. Granger causality in integrated GC-MS and LC-MS metabolomics data reveals the interface of primary and secondary metabolism. *Metabolomics* 9:564–574.

Flügel F, Timm S, Arrivault S, Florian A, Stitt M, Fernie AR, Bauwe H. 2017. The photorespiratory metabolite 2-phosphoglycolate regulates photosynthesis and starch accumulation in *Arabidopsis*. *The Plant Cell* 29:2537–2551.

Foyer CH, Bloom AJ, Queval G, Noctor G. 2009. Photorespiratory metabolism: genes, mutants, energetics, and redox signaling. *Annual Review of Plant Biology* 60:455–484.

Fürtauer L, Küstner L, Weckwerth W, Heyer AG, Nägele T. 2019. Resolving subcellular plant metabolism. *The Plant Journal* 100:438–455.

Fürtauer L, Nägele T. 2016. Approximating the stabilization of cellular metabolism by compartmentalization. *Theory in Biosciences* 135:73–87.

Gibon Y, Blasing OE, Palacios-Rojas N, Pankovic D, Hendriks JH, Fisahn J, Hohne M, Gunther M, Stitt M. 2004. Adjustment of diurnal starch turnover to short days: depletion of sugar during the night leads to a temporary inhibition of carbohydrate utilization, accumulation of sugars and post-translational activation of ADP-glucose pyrophosphorylase in the following light period. *The Plant Journal* 39:847–862.

Grimbs S, Selbig J, Bulik S, Holzhütter H-G, Steuer R. 2007. The stability and robustness of metabolic states: identifying stabilizing sites in metabolic networks. *Molecular Systems Biology* 3:146.

Hahn BD. 1991. Photosynthesis and photorespiration: modelling the essentials. *Journal of Theoretical Biology* 151:123–139.

Hartman P. 1960. A lemma in the theory of structural stability of differential equations. *Proceedings of the American Mathematical Society* 11:610–620.

Heber U, Krause GH. 1980. What is the physiological role of photorespiration? *Trends in Biochemical Sciences* 5:32–34.

Hodges M, Dellero Y, Keech O, Betti M, Raghavendra AS, Sage R, Zhu X-G, Allen DK, Weber APM. 2016. Perspectives for a better understanding of the metabolic integration of photorespiration within a complex plant primary metabolism network. *Journal of Experimental Botany* 67:3015–3026.

Jablonsky J, Bauwe H, Wolkenhauer O. 2011. Modeling the Calvin–Benson cycle. *BMC Systems Biology* 5:185.

Kadereit JW, Körner C, Kost B, Sonnewald U. 2014. *Strasburger – lehrbuch der pflanzenwissenschaften*. Heidelberg: Springer Spektrum Berlin.

Kelly GJ, Latzko E. 1976. Inhibition of spinach-leaf phosphofructokinase by 2-phosphoglycollate. *FEBS Letters* 68:55–58.

Kennedy J, Eberhart R. 1995. Particle swarm optimization. Proceedings of ICNN'95-International Conference on Neural Networks, Perth, WA, Australia. 4:1942–1948. doi:10.1109/ICNN.1995.488968.

Kitashova A, Schneider K, Fürtauer L, Schröder L, Scheibenbogen T, Fürtauer S, Nägele T. 2021. Impaired chloroplast positioning affects photosynthetic capacity and regulation of the central carbohydrate metabolism during cold acclimation. *Photosynthesis Research* 147:49–60.

Klipp E, Liebermeister W, Wierling C, Kowald A. 2016. *Systems biology: a textbook*. Weinheim: Wiley-VCH.

Küstner L, Fürtauer L, Weckwerth W, Nägele T, Heyer AG. 2019a. Subcellular dynamics of proteins and metabolites under abiotic stress reveal deferred response of the *Arabidopsis thaliana* hexokinase-1 mutant gin2-1 to high light. *The Plant Journal* 100:456–472.

Küstner L, Nägele T, Heyer AG. 2019b. Mathematical modeling of diurnal patterns of carbon allocation to shoot and root in *Arabidopsis thaliana*. *npj Systems Biology and Applications* 5:4.

Land A, Doig A. 1960. An automatic method of solving discrete programming problems. *Econometrica* 28:497–520.

Levey M, Timm S, Mettler-Altmann T, Luca Borghi G, Koczor M, Arrivault S, Pm Weber A, Bauwe H, Gowik U, Westhoff P. 2019. Efficient 2-phosphoglycolate degradation is required to maintain carbon assimilation and allocation in the C_4 plant *Flaveria bidentis*. *Journal of Experimental Botany* 70:575–587.

Lorimer GH, Andrews TJ. 1973. Plant photorespiration—an inevitable consequence of the existence of atmospheric oxygen. *Nature* 243:359–360.

Martin W, Scheibe R, Schnarrenberger C. 2000. The Calvin cycle and its regulation. In: Leegood RC, Sharkey TD, von Caemmerer S, eds. *Photosynthesis: physiology and metabolism*. Dordrecht: Kluwer Academic Publishers, 9–51.

Morrison DR, Jacobson SH, Sauppe JJ, Sewell EC. 2016. Branch-and-bound algorithms: a survey of recent advances in searching, branching, and pruning. *Discrete Optimization* 19:79–102.

Nägele T, Fürtauer L, Nagler M, Weiszmann J, Weckwerth W. 2016. A strategy for functional interpretation of metabolomic time series data in context of metabolic network information. *Frontiers in Molecular Biosciences* 3:6.

Nägele T, Mair A, Sun X, Fragner L, Teige M, Weckwerth W. 2014. Solving the differential biochemical Jacobian from metabolomics covariance data. *PLoS One* 9:e92299.

Naikoo MI, Dar MI, Raghib F, Jaleel H, Ahmad B, Raina A, Khan FA, Naushin F. 2019. Chapter 9—role and regulation of plants phenolics in abiotic stress tolerance: an overview. In: Khan MIR, Reddy PS, Ferrante A, Khan NA, eds. *Plant signaling molecules*. Sawston, CA: Woodhead Publishing, 157–168.

Noctor G, Foyer CH. 2000. Homeostasis of adenylate status during photosynthesis in a fluctuating environment. *Journal of Experimental Botany* 51:347–356.

Obata T, Fernie AR. 2012. The use of metabolomics to dissect plant responses to abiotic stresses. *Cellular and Molecular Life Sciences* 69:3225–3243.

Poli R, Kennedy J, Blackwell T. 2007. Particle swarm optimization. *Swarm Intelligence* 1:33–57.

Reznik E, Segrè D. 2010. On the stability of metabolic cycles. *Journal of Theoretical Biology* 266:536–549.

Savitch LV, Barker-Astrom J, Ivanov AG, Hurry V, Oquist G, Huner NP, Gardestrom P. 2001. Cold acclimation of *Arabidopsis thaliana* results in incomplete recovery of photosynthetic capacity, associated with an increased reduction of the chloroplast stroma. *Planta* 214:295–303.

Schaber J, Liebermeister W, Klipp E. 2009. Nested uncertainties in biochemical models. *IET Systems Biology* 3:1–9.

Schulz E, Tohge T, Zuther E, Fernie AR, Hincha DK. 2015. Natural variation in flavonol and anthocyanin metabolism during cold acclimation in *Arabidopsis thaliana* accessions. *Plant, Cell and Environment* 38:1658–1672.

Schulz E, Tohge T, Zuther E, Fernie AR, Hincha DK. 2016. Flavonoids are determinants of freezing tolerance and cold acclimation in *Arabidopsis thaliana*. *Scientific Reports* 6:34027.

Sharkey TD. 1985. Photosynthesis in intact leaves of C_3 plants: physics, physiology and rate limitations. *The Botanical Review* 51:53–105.

Shi Q, Sun H, Timm S, Zhang S, Huang W. 2022. Photorespiration alleviates photoinhibition of photosystem I under fluctuating light in tomato. *Plants* 11:195.

South PF, Cavanagh AP, Liu HW, Ort DR. 2019. Synthetic glycolate metabolism pathways stimulate crop growth and productivity in the field. *Science* 363:eaat9077.

Steuer R, Gross T, Selbig J, Blasius B. 2006. Structural kinetic modeling of metabolic networks. *Proceedings of the National Academy of Sciences of the United States of America* 103:11868–11873.

Strand A, Hurry V, Gustafsson P, Gardeström P. 1997. Development of *Arabidopsis thaliana* leaves at low temperatures releases the suppression of photosynthesis and photosynthetic gene expression despite the accumulation of soluble carbohydrates. *The Plant Journal* 12:605–614.

Strand A, Hurry V, Henkes S, Huner N, Gustafsson P, Gardeström P, Stitt M. 1999. Acclimation of *Arabidopsis* leaves developing at low temperatures. Increasing cytoplasmic volume accompanies increased activities of enzymes in the Calvin cycle and in the sucrose-biosynthesis pathway. *Plant Physiology* 119:1387–1398.

Takahashi S, Bauwe H, Badger M. 2007. Impairment of the photorespiratory pathway accelerates photoinhibition of photosystem II by suppression of repair but not acceleration of damage processes in *Arabidopsis*. *Plant Physiology* 144:487–494.

Tang M, Li B, Zhou X, Bolt T, Li JJ, Cruz N, Gaudinier A, Ngo R, Clark-Wiest C, Kliebenstein DJ, Brady SM. 2021. A genome-scale TF–DNA interaction network of transcriptional regulation of *Arabidopsis* primary and specialized metabolism. *Molecular Systems Biology* 17:e10625.

Warburg O. 1920. Uber die Gesehwindigkeit der photochemichen. *Biochemische Zeitschrift* 103:188–217.

Winkel-Shirley B. 2002. Biosynthesis of flavonoids and effects of stress. *Current Opinion in Plant Biology* 5:218–223.

Wittig U, Rey M, Kania R, Bittkowski M, Shi L, Golebiewski M, Weidemann A, Müller W, Rojas I. 2014. Challenges for an enzymatic reaction kinetics database. *The FEBS Journal* 281:572–582.

Zhang B, Pan C, Feng C, Yan C, Yu Y, Chen Z, Guo C, Wang X. 2022. Role of mitochondrial reactive oxygen species in homeostasis regulation. *Redox Report* 27:45–52.

Zhu X-G, de Sturler E, Long SP. 2007. Optimizing the distribution of resources between enzymes of carbon metabolism can dramatically increase photosynthetic rate: a numerical simulation using an evolutionary algorithm. *Plant Physiology* 145:513–526.

2.3 Regulation of plant metabolism under elevated CO$_2$

Danial Shokouhi [§], Jakob Sebastian Hernandez [§], Dirk Walther, Gabriele Kepp, Serena Schwenkert, Dario Leister, Jürgen Gremmels, Ellen Zuther, Jessica Alpers, Thomas Nägele [*], Arnd G. Heyer [*]

Plant responses to changing environments afford complex regulation at transcriptome and proteome level to maintain metabolic homeostasis. Homeostasis itself constitutes a complex and dynamic equilibrium of metabolic reactions and transport processes among cellular compartments. In the present study, we aimed at the highest possible resolution of this network by combining analysis of transcriptome, proteome and subcellular resolved metabolome of plants exposed to rising carbon dioxide concentrations over a time course of one week. To prove suitability of our approach, we included mutants affected in photorespiratory metabolism and, thus, should deviate from the wild type in their response to elevated CO2. Our multi-omics analysis revealed that the *hpr1-1* mutant, defective in peroxisomal hydroxypyruvate reduction, is also affected in cytosolic pyruvate metabolism, reaching out to cysteine synthesis, while the hexokinase mutant *hxk1* displays a disturbed redox balance upon changing CO2 levels. For the third mutant, defective in the mitochondrial protein BOU, we found compelling evidence that the function of this transporter is related to lipoic acid metabolism, thus challenging current interpretations. This demonstrates that the combined omics approach introduced here opens new insights into complex metabolic interaction of pathways shared among different cellular compartments.

Corresponding Author: *

Authors contributed equally: §

Regulation of plant metabolism under elevated CO$_2$

Danial Shokouhi [1,§], Jakob Sebastian Hernandez [2,§], Dirk Walther [3], Gabriele Kepp [1], Serena Schwenkert [4,5], Dario Leister [4,5], Jürgen Gremmels[3], Ellen Zuther[3], Jessica Alpers[3], Thomas Nägele [2,*], Arnd G. Heyer [1,*]

[1] University of Stuttgart, Institute of Biomaterials and Biomolecular Systems, Department of Plant Biotechnology, Pfaffenwaldring 57, 70569 Stuttgart, Germany

[2] LMU München, Faculty of Biology, Plant Evolutionary Cell Biology, Großhaderner Str. 2-4, 82152 Planegg, Germany

[3] Max-Planck-Institute of Molecular Plant Physiology, Bioinformatics, Potsdam Science Park, Am Mühlenberg 1, 14476 Potsdam, Germany.

[4] LMU München, Faculty of Biology, Plant Molecular Biology, Großhaderner Str. 2-4, 82152 Planegg, Germany

[5] LMU München, Faculty of Biology, MSBioLMU, Großhaderner Str. 2-4, 82152 Planegg, Germany

[§] authors contributed equally

[*] shared correspondence:
thomas.naegele@lmu.de
arnd.heyer@bio.uni-stuttgart.de

ORCID
DS: 0000-0002-0696-5204
JSH:
DW: 0000-0002-5755-9265
SS: 0000-0003-4301-5176
DL: 0000-0003-1897-8421
TN: 0000-0002-5896-238X
AGH: 0000-0003-2074-3234

Key words: *Arabidopsis thaliana*; photosynthesis; photorespiration; carbon dioxide; subcellular metabolism

Abstract

Plant responses to changing environments afford complex regulation at transcriptome and proteome level to maintain metabolic homeostasis. Homeostasis itself constitutes a complex and dynamic equilibrium of metabolic reactions and transport processes among cellular compartments. In the present study, we aimed at the highest possible resolution of this network by combining analysis of transcriptome, proteome and subcellular resolved metabolome of plants exposed to rising carbon dioxide concentrations over a time course of one week. To prove suitability of our approach, we included mutants affected in photorespiratory metabolism and, thus, should deviate from the wildtype in their response to elevated CO_2. Our multi-omics analysis revealed that the *hpr1-1* mutant, defective in peroxisomal hydroxypyruvate reduction, is also affected in cytosolic pyruvate metabolism, reaching out to cysteine synthesis, while the hexokinase mutant *hxk1* displays a disturbed redox balance upon changing CO_2 levels. For the third mutant, defective in the mitochondrial protein BOU, we found compelling evidence that the function of this transporter is related to lipoic acid metabolism, thus challenging current interpretations. This demonstrates that the combined omics approach introduced here opens new insights into complex metabolic interaction of pathways shared among different cellular compartments.

Introduction

Studying regulation of plant metabolism under changing atmospheric conditions is complicated by the high level of compartmentalization of plant cells, but also by the redundancy of pathways in different compartments, e.g., glycolysis, oxidative pentose phosphate pathway or synthesis of various amino acids in the cytosol, plastids and mitochondria. To disentangle overlapping reactions, mutants lacking specific isoforms of enzymes are frequently utilized that disrupt metabolite conversion in a specific compartment. While this strategy enabled insight into the complex interactions of metabolic pathways, knowledge is still limited due to high intracellular mobility of metabolic intermediates and also because of so-called pleiotropic effects of mutations, which are unexpected based on current knowledge of functions of the mutated genes [1].

In the present study we aimed at combining data sets from the transcriptional and proteomic level with metabolite profiles for different subcellular compartments in a time series on plants exposed to an increased CO_2 concentration. By applying the highest analytical resolution possible by now, we asked whether this could solve the problem of pleiotropy. We used three different mutants of Arabidopsis reported to be affected in photorespiratory metabolism.

Photorespiration is, next to photosynthetic CO_2 fixation within the Calvin-Benson-Bassham cycle (CBBC), the second most important metabolic route in green tissues of plants with regard to turnover during the light phase and has an important function also in nitrogen acquisition [2]. It involves at least four different cellular compartments, i.e. plastids, cytosol, peroxisomes and mitochondria, but recent findings point to a function of the vacuole in photorespiration, too [3]. Photorespiration is initialized by oxygenation of ribulose-1,5-bisphosphate that results from the dual use of substrates, carbon dioxide and oxygen, by the enzyme Ribulose-Bisphospate-Carboxylase/Oxygenase (Rubisco). Oxygenation leads to the production of phosphoglycolate, which inhibits activity of enzymes in the CBBC [4]. After dephosphorylation, glycolate is oxidized to glyoxylate and transaminated to yield glycine in the peroxisomes. Two molecules of glycine are converted to serine in the mitochondria, releasing carbon dioxide and ammonia, which must be re-fixed into glutamine in the plastids. Serine is deaminated to hydroxypyruvate again in the peroxisome, which is then reduced to glycerate that, after

80 phosphorylation, can re-enter the CBBC in the plastids. The *hpr1-1* mutant of Arabidopsis is impaired in the last step of the pathway, i.e. reduction of hydrxypyruvate, and is one of the few examples of photorespiratory mutants able to survive at ambient CO_2 concentration, at least in part due to the presence of a cytosolic isoform of the enzyme [5]. While HPR is directly involved in the photorespiratory cycle, hexokinase-1 (HXK1) is involved in the phosphorylation of glucose and fructose produced from sucrose by the action of invertase and has a role as a sugar sensor in plant

85 metabolism [6, 7]. Its involvement in photorespiration has been concluded from experiments with the *hxk1* mutant under high light intensity, where increased photorespiratory turnover led to an accumulation of serine in mitochondria of wild type plants, while it resided in the cytosol of *hxk1* [8]. The third mutation in the set is "a bout de souffle" (*bou*, out of breath), which is blocked in development under ambient CO_2 concentration, thus showing a severe photorespiratory phenotype,

90 accompanied by a very high glycine-to-serine ratio [9]. The BOU enzyme is a mitochondrial transporter the substrate of which is not unequivocally clear. *In vitro* evidence for transport of glutamate has been presented, and it has been hypothesized that its knockout might interfere with poly-glutamylation of dihydrofolate reductase that is needed for glycine decarboxylation [10]. However, the mutant shows a very complex phenotype, and the presence of additional

95 mitochondrial glutamate transporters [11] might argue against a lack of glutamate as sole reason for the mutant phenotype.

In the present study, we aimed at analyzing changes in metabolic regulation resulting from increased atmospheric CO_2 concentration. To this end, we transferred plants from ambient (450 ppm) to about two-fold higher (1000 ppm) CO_2 levels and recorded changes in gene expression,

100 protein abundance and compartment-specific metabolite levels over a time course of seven days. This experimental design allowed for an investigation of the effects of environmental changes related to the anthropogenic climate change. In addition, organelle interaction that was affected by the change in the ratio of photosynthesis to photorespiration could be analyzed. Combined transcriptomics, proteomics, and compartment specific metabolomics provided detailed information

105 on mutant effects and enabled new understanding of metabolic interactions in a changing environment.

Results and Discussion

The metabolic phenotype of *hpr1-1* mutants comprises strong effects on cytosolic glycerate and pyruvate metabolism

110 To gain a detailed understanding of how the metabolic mutants were affected in primary metabolites with relation to the photorespiratory pathway, the *OmicsDB* was created in conjunction with an application programming interface to allow for fast data exploration and straightforward hypothesis testing (see Methods). Extracting subcellular metabolome information with direct relation to photorespiration revealed that *hpr1-1* plants showed the expected strong photorespiratory metabolic

115 phenotype under ambient CO_2 (aCO_2) which clearly separated them in a principal component analysis (PCA) from all other genotypes (Supplementary Figure S1). After transfer to elevated CO_2 (eCO_2), this effect was diminished but *hpr1-1* samples still clearly separated from Col-0. Both, glycine and serine had a high influence on separating *hpr1-1* from Col-0 under aCO_2 (Supplementary Figure S1 B). However, to a similar extent, elevated glycerate levels, especially in

120 mitochondria, differentiated *hpr1-1* from all other genotypes (Figure 1). This was counter-intuitive, because HPR1 contributes to glycerate biosynthesis, and thus a reduction in this metabolite could be

expected. A similar, yet unexplained, observation was already made at whole-cell level and was shown not to depend on the cytosolic isoenzyme HPR2 [5].
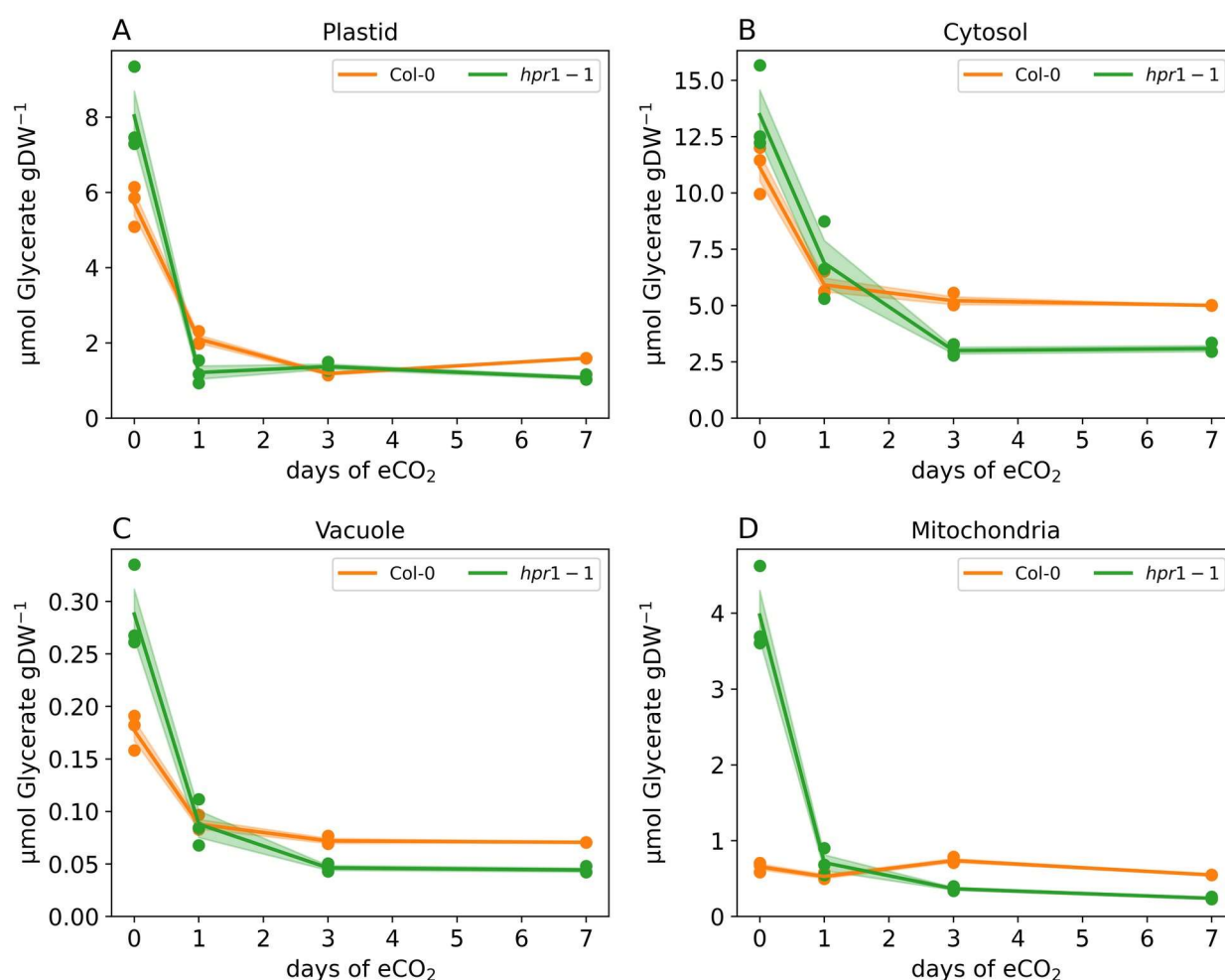

Figure 1. Compartment specific glycerate dynamics. Ordinates reflect glyceric acid amounts in µmol gDW^{-1}, abscissae show time of exposure to eCO$_2$ in days. (A) plastid; (B) cytosol; (C) vacuole, (D) mitochondria. Genotypes are indicated by color (orange − Col-0; green − *hpr1-1*). Filled circles indicate mean values, shaded areas indicate standard deviation, (n = 3)

125 Compartment-specific metabolomics revealed low glycolate in plastids, but accumulation in the cytosol of *hpr1-1* at aCO$_2$ (Supplementary Figure 2 A). This suggested an alternative, so-far undescribed cytosolic route in *hpr1-1* from glycolate to glycerate, which then could be transported into the plastid, probably via the plastidial glycolate /glycerate antiporter PLGG1 (AT1G32080) or the bile acid/sodium symporter BASS6 (AT4G22840). Compared to Col-0, transcripts of PLGG1

130 were slightly elevated in *hpr1-1* and immediately responded to eCO$_2$, suggesting a direct photorespiratory role. The alternative pathway would involve cytosolic pyruvate and cysteine, both being strongly elevated in *hpr1-1* at eCO$_2$ (Figure 2 A, B). Cysteine dynamics were uncoupled from serine and glycine (Figure 3 A), indicative of an alternative metabolic role of cysteine as an intermediate in the pathway from serine to glycerate, thus bypassing hydroxypyruvate

135 (Supplementary Figures S3, S4). Key enzymes on this route, O-acetylserine-thiolyase (OASA1) and L-cysteine desulfhydrase 1 (DES1 - AT5G28030), which catalyzes the interconversion of cysteine to pyruvate releasing ammonia and sulfide, were upregulated at transcript level (log2FC: 0.532; adj. p val. < 0.00001 for one sided z-test, n = 3; Figure 3 B, C).

Cytosolic pyruvate, a product of glycolysis, is supposed to be transported into mitochondria as
140   substrate for the TCA cycle. If involved in the aforementioned pathway, reduced influx into mitochondria would be expected. Indeed, mitochondrial pyruvate carriers 1, 3 and 4 (MPC1 - AT5G20090, MPC3 - AT4G05590, MPC4 - AT4G22310; Figure 2 C - E) displayed slightly lower transcript levels in *hpr1-1* compared to Col-0. This trend was most pronounced in MPC3 that showed a log2FC of -0.977 (adj. p val. 0.067 for one sided z-test, n = 3) under ambient conditions.
145   Transfer to eCO$_2$ resulted in a log2FC of -0.292 after one day of exposure. In line with this, the transcript of pyruvate dehydrogenase kinase (PDK - AT3G06483), an inhibitor of the pyruvate dehydrogenase complex, was significantly upregulated (Supplementary Figure S5).
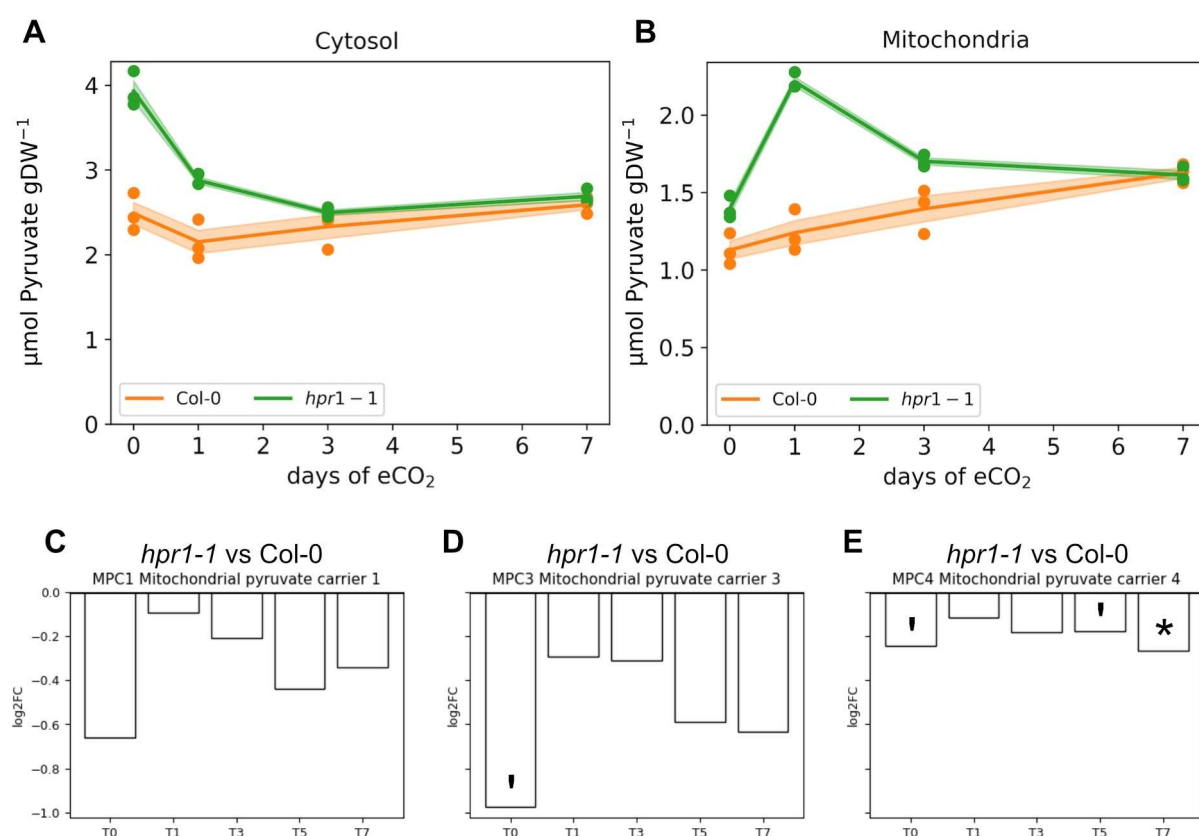

Figure 2. **Subcellular pyruvate concentration of the cytosol and mitochondria, with log2FCs of associated transporters. (A)** Dynamics of cytosolic pyruvate concentration, **(B)** Dynamics of mitochondrial pyruvate concentration. Ordinates reflect pyruvate amounts in μmol gDW^{-1} (mean ± SD; n = 3), abscissae show time of exposure to eCO$_2$ in days. **(C) – (E)** Log2FC between *hpr1-1* and Col-0 for MPC1, MPC3 and MPC4, respectively (* - p value < 0.05, ' - p value < 0.1; n = 3).

In addition to serine, malate from various sources could serve to replenish glycerate, either via
150   pyruvate, depending on malic enzyme, or via oxaloacetate and phosphoenolpyruvate (PEP), involving malate dehydrogenase and phosphoenolpyruvate carboxykinase (PCK), thus explaining the accumulation of cytosolic malate in *hpr1-1*. Depending on the source of pyruvate and acetyl-CoA such a bypass could achieve similar carbon recuperation rates as the base photorespiratory pathway. In such a scenario, acetyl-CoA could originate from either citrate via activity of ATP-
155   citrate lyase (ACL), or acetate depending on the compartment of cysteine synthesis. Indeed, cytosolic citrate was found to accumulate in *hpr1*-1 and transcripts for enzymes related to acetyl-CoA synthesis were found to be upregulated, too (Supplementary Figure S6). In summary, the combined Omics analysis opened the perspective of a new route to glycerate regeneration under photorespiratory conditions, which could make a substantial contribution in the *hpr1-1* mutant.
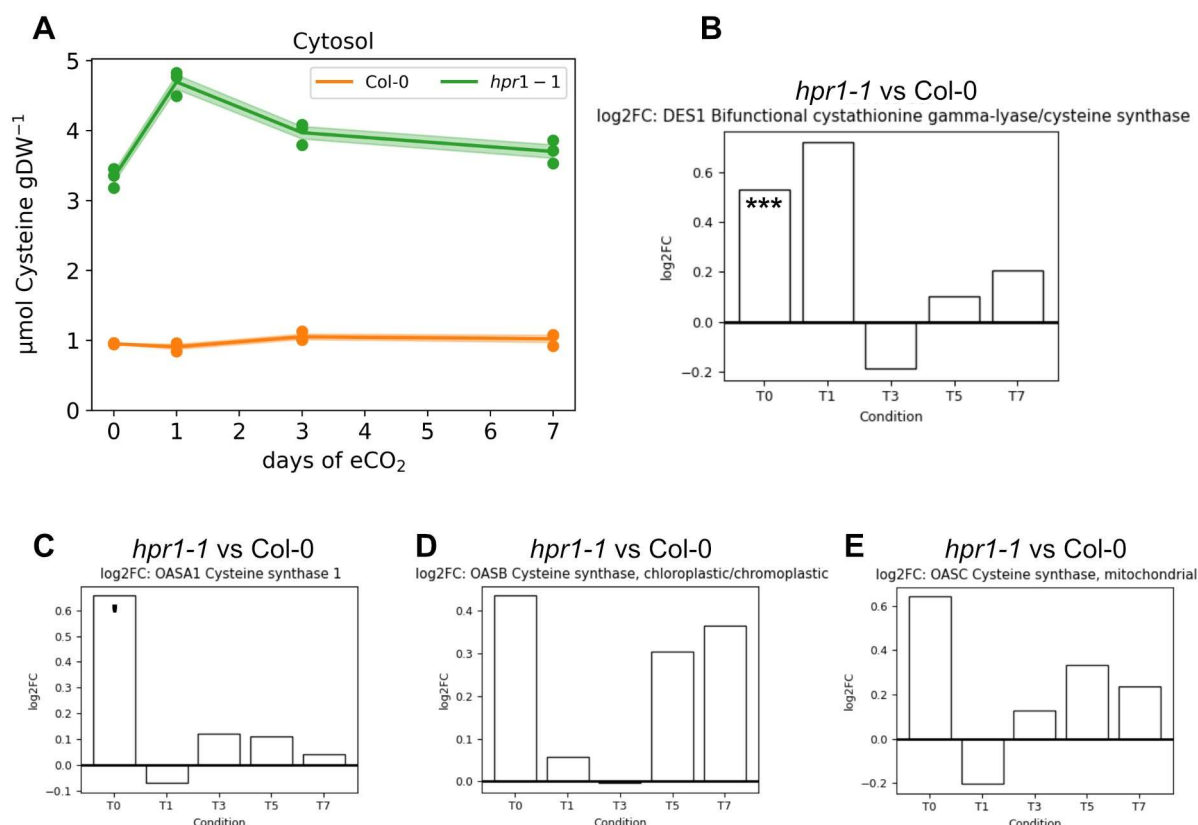
Figure 3. Cytosolic cysteine dynamics with associated enzymes. (A) Dynamics of cytosolic cysteine concentrations. Ordinate reflects cysteine amounts in μmol gDW^{-1} (mean ± SD; n = 3), abscissa shows time of exposure to eCO$_2$ in days. **(B)** Log2FC of DES1 comparing *hpr1-1* to Col-0, **(C) − (E)** Log2FC of enzymes for cysteine biosynthesis enzymes. replicates (*** ‒ p value < 0.001, ' ‒ p value < 0.1; n = 3).

Mutation of HXK1 affects cellular redox balance under photorespiratory conditions

An outstanding feature characterizing metabolic changes in the *hxk1* mutant at eCO$_2$ was a significant increase in soluble sugars. Hexoses increased specifically in the cytosol of *hxk1* while sucrose accumulated in the vacuole, indicating an expectable slow-down in sucrose cycling as a consequence of reduced HXK1 activity.

Looking deeper into the subcellular metabolomes of Col-0 and *hxk1* indicated opposite trends of pyruvate allocation under eCO$_2$ between chloroplasts and mitochondria (Figure 4). Under aCO$_2$, plastidial pyruvate in *hxk1* exceeded that in Col-0, indicating different activity of plastidial glycolysis. Glycolytic and TCA cycle activity have earlier been shown to be inversely related to ambient CO$_2$/O$_2$ ratio and dependent on redox power [12]. Although glycolytic flux in illuminated leaves may only partially depend on cytosolic hexose phosphorylation, because sugar phosphates are directly available from the triose phosphate export from plastids [13], the shift to plastidial pyruvate points out that, under aCO$_2$, deficiency of HXK1 may indeed impair glycolytic flux, which would in turn affect the redox status of the NAD pool. Thus, protein levels of the gene ontology (GO) terms "cell redox homeostasis" and "TCA cycle" were correlated genotype-wise in a PCA (Supplementary Figure S7). The proteomes of all genotypes but *hxk1* showed a clear separation of aCO$_2$ (time point T0) and the first day at eCO$_2$ (T1), while response was substantially delayed in *hxk1*. A strong effect of the HXK1 mutation was observed for peroxisomal catalase 2 (CAT2,

AT4G35090), which dissipated hydrogen peroxide produced in photorespiration. CAT2
180 significantly decreased within the first day of eCO_2 in all genotypes except *hxk1*, where it declined with a significant delay until day 5 of eCO_2 (Supplementary Figure S8).
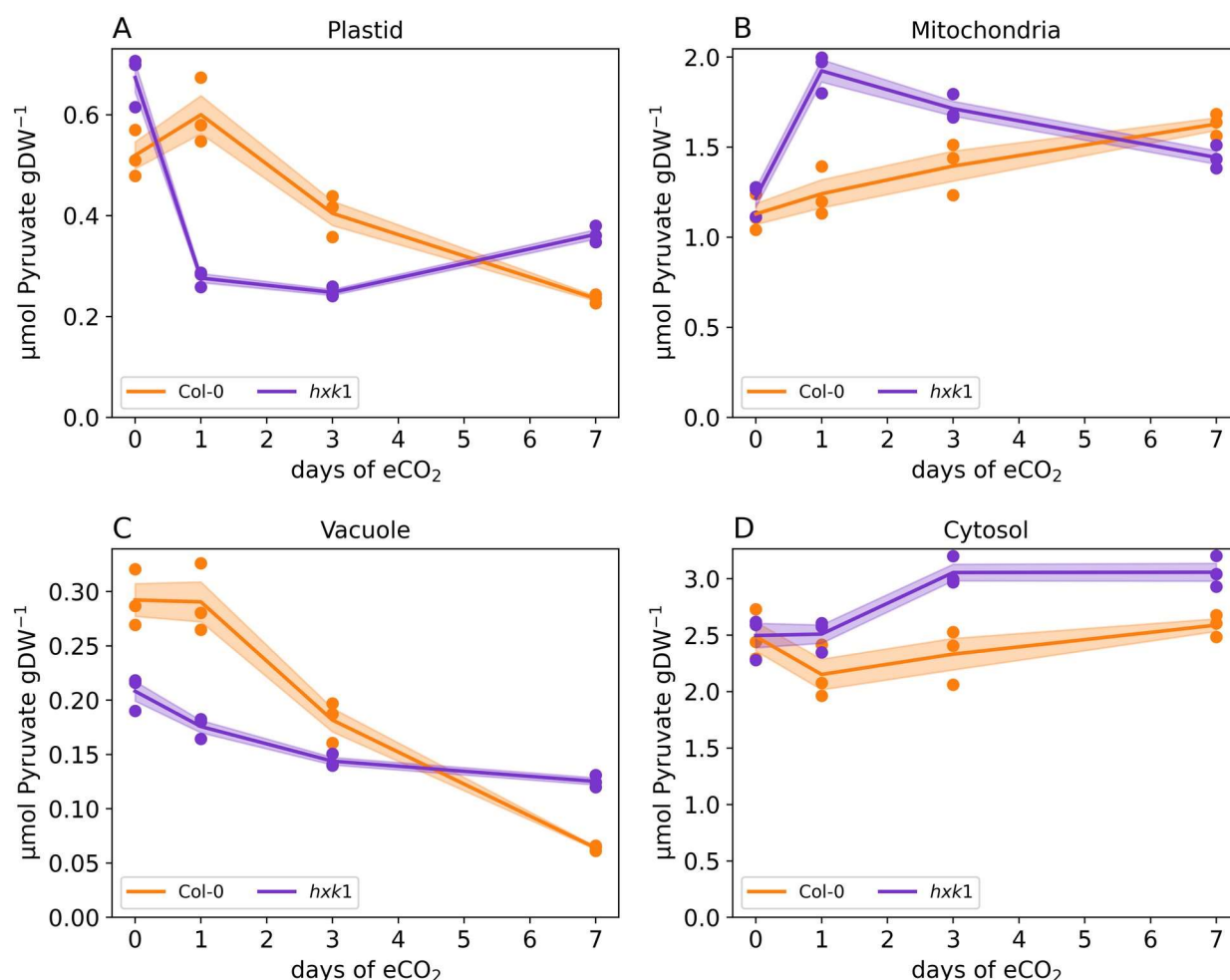

Figure 4. Compartment-specific pyruvate dynamics. Ordinates reflect pyruvate amounts in μmol gDW^{-1}, abscissae show time of exposure to eCO_2 in days. (A) plastid; (B) mitochondria; (C) vacuole, (D) cytosol. Genotypes are indicated by color (orange – Col-0; purple – *hxk1*). Filled circles indicate mean values, shaded areas indicate standard deviation, (n = 3).

It has been reported that, during the photorespiratory cycle, redox equivalents are shuttled between mitochondria, cytosol and peroxisomes [14,] where they are used for the reduction of hydroxypyruvate
185 to glycerate [15.] Peroxisomal malate dehydrogenase, pMDH2 (AT5G09660), that is involved in this shuttle was down regulated in *hxk1* at early eCO_2, but not in the wildtype (Figure 5 D). Downregulation at eCO_2 could follow lowered photorespiratory activity, but the delayed downregulation of peroxisomal catalase CAT2 in *hxk1* during eCO_2 exposure opens an alternative view. During photorespiration, glycolate is oxidized to yield glyoxylate thereby producing H_2O_2, the
190 substrate for catalase-driven disproportionation. If hydroxypyruvate is not reduced by HPR and malate dependent pMDH2, it can non-enzymatically be oxidized to glycolate and subsequently to formate with H_2O_2 as oxidant [15]. This reaction is relevant in the *hpr1-1* mutant, but may also take place in *hxk1*. Strikingly, both mutants show very high levels of malate in the vacuole, where it is not available as a redox shuttle to the peroxisome. This holds true for *hpr1-1* under all conditions,
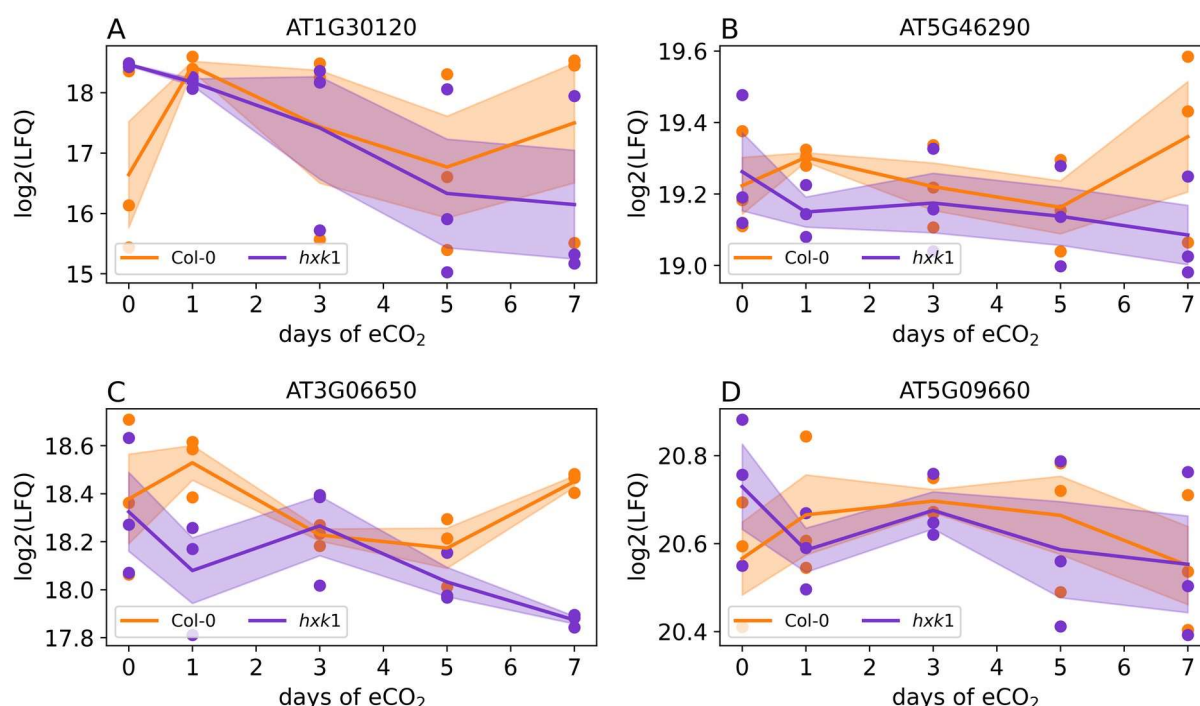195 but only at eCO_2 in *hxk1*.

Figure 5. CO_2-dependent protein dynamics of fatty acid biosynthesis and peroxisomal malate dehydrogenase. (A) plastidial pyruvate dehydrogenase E1 component (AT1G30120), (B) 3-oxoacyl-[acyl-carrier-protein] synthase I (AT5G46290), (C) ATP-citrate synthase B-1 (AT3G06650), (D) peroxisomal NAD-Malate dehydrogenase 2 (AT5G09660). orange: Col-0; purple: *hxk1*. lines and shaded areas represent means +/- SE (n = 3).

It has been reported earlier that oxylipins interact and modulate proteins of ROS synthesis and scavenging, among others also CAT2 (an overview is provided in [16]). Oxylipins are bioactive lipid derivatives which are synthesized from polyunsaturated fatty acids (PUFAs). They are involved in diverse plant-environment interactions, their functions ranging from phytohormone biosynthesis to retrograde signaling [16]. While, to the best of our knowledge, until today no direct regulatory interaction between HXK1 and oxylipins has been described, it might be speculated that an HXK1-mediated re-allocation of carbon flux from cytosolic to plastidial glycolysis might also affect oxylipin metabolism through biosynthesis of PUFAs. Because the oxylipin OPDA (12-oxophytodienoic acid) is precursor of jasmonic acid (JA), this would add an additional layer of the complex interaction of HXK1 with phytohormones. [17], in their pioneering work on the role of HXK1 as a glucose sensor, demonstrated reduced sensitivity of the *gin2-1* mutants to auxins. Since both, JA and auxin, use shared components in their signaling cascade, JA is considered to reduce auxin responsiveness through recruitment of such shared components [18].

In addition to redox homeostasis, inverse dynamics of plastidial and mitochondrial pyruvate in *hxk1* may also impact fatty acid biosynthesis in chloroplasts. The proteome of this biosynthetic pathway revealed opposite trends for *hxk1* and wildtype of central enzymes during early eCO₂. Plastidial pyruvate dehydrogenase (pPDH) E1 component (AT1G30120), 3-oxoacyl-[acyl-carrier-protein] synthase I (AT5G46290) and ATP-citrate synthase B-1 (AT3G06650) were upregulated in Col-0 but downregulated in *hxk1* under eCO₂ (Figure 5 A-C). Also, carboxylic acid metabolism, for which pyruvate represents a central substrate, was affected in *hxk1* at the proteome level (Supplementary Figure S9). All together, these observations demonstrate that HXK1 reaches out far beyond cytosolic carbohydrate metabolism, influencing subcellular redox balance, fatty acid and lipid metabolism and may also integrate ROS metabolism with phytohormonal response.

Metabolite dynamics in a heterozygous *bou* mutant point to a new function of this mitochondrial transporter

The design of the present study was not compatible with the use of the homozygous *bou* mutant, which does not grow at ambient CO_2 levels used as starting conditions. Thus, we made use of heterozygous mutant plants, *h-bou*, which still have an 85% growth reduction as compared to the wild type (Supplementary Figure S10), but are able to develop mature leaves at ambient CO_2 levels. As expected, glycine significantly accumulated in mitochondria of *h-bou* at aCO_2, although not as pronounced as reported for homozygous mutants (Figure 6A). In line with glycine accumulation, the H subunit of the glycine cleavage system (AT2G35370) exhibited lower expression levels in *h-bou* and remained consistently lower than wildtype under all conditions (Figure 6B). Opposite trends were observed in expression of other subunits of the GDC system (AT4G33010 and AT2G26080; Figure 6 C, D) revealing a significant decrease in *h-bou*, but increased expression and a final stabilization in wildtype. Serine accumulated slowly in plastids of *h-bou* plants after transfer to eCO_2 (Figure 7 A, B), pointing to a shift of serine production from photorespiratory to the plastidial phosphorylated pathway (PPSB). This was supported by a higher expression rate of SHMT3 (AT4G32520) in *h-bou* samples as compared to Col-0 (Figure 7 C), and also by glycine accumulation in plastids of *h-bou*.
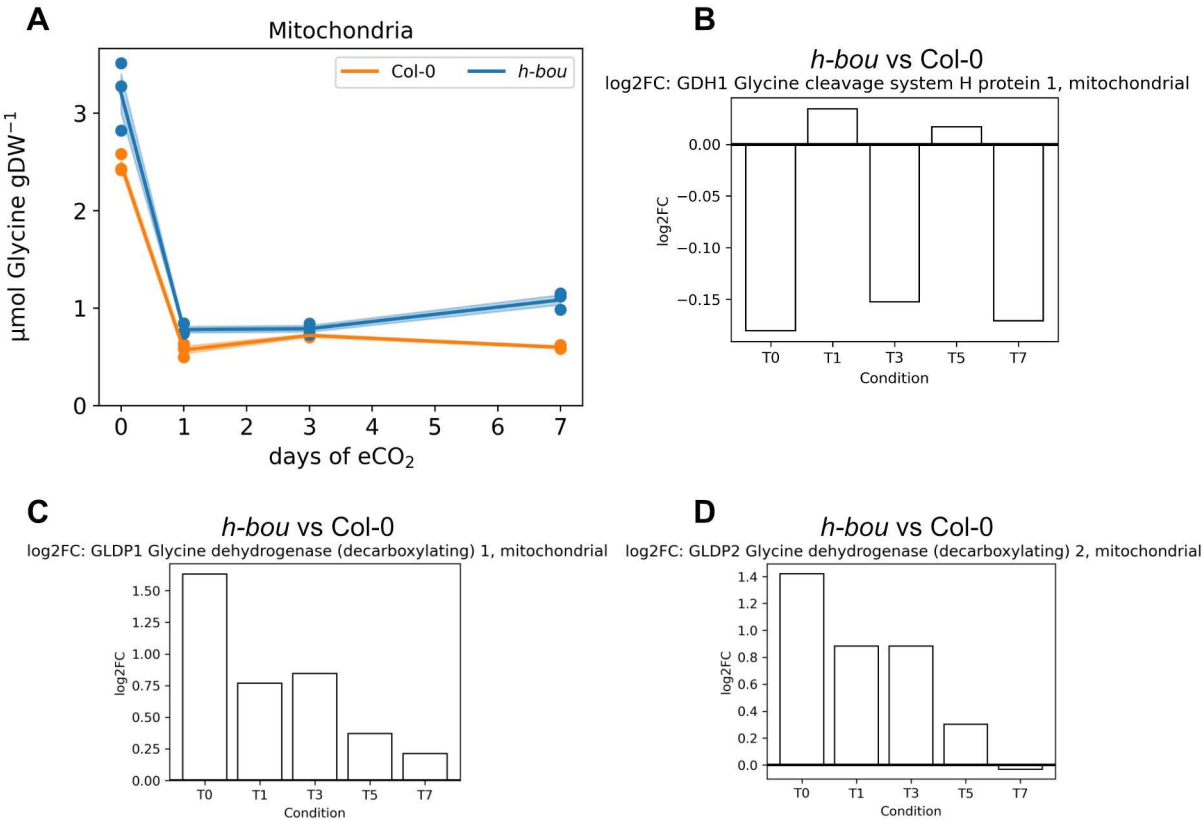

Figure 6. Mitochondrial glycine dynamics with transcripts of associated enzymes. (A) Dynamics of mitochondrial glycine concentrations in *h-bou* (blue) and Col-0 (orange). Ordinate reflects glycine amounts in µmol gDW^{-1}, abscissa shows time of exposure to eCO2 in days. (B) Log2FC of GDC-H (AT2G35370) comparing *h-bou* to Col-0, (C) Log2FC of GDC-P1 (AT4G33010) comparing *h-bou* to Col-0– (D) Log2FC of GDC-P2 (AT2G26080) comparing *h-bou* to Col-0; n = 3.

Considering the reported function of BOU as a mitochondrial glutamate transporter necessary for polyglutamylation of THF [10], an elevated, not reduced, glutamate concentration in *h-bou* mitochondria at aCO_2 was unexpected (Supplementary Figure 11 A). However, already in 2002, it

was reported that the BOU protein belongs to the family of carnitine /acylcarnitine transporters [19] that transport fatty acid carnitine esters into the mitochondrial matrix, where they are involved in lipoylation of decarboxylase enzymes, including the glycine cleavage system [20]. Although lipoic acid was not measured in this study, strong evidence for disturbed homeostasis in *h-bou* comes from significant differences in expression levels of transcripts involved in lipoic acid *de novo* synthesis, LIP1 (AT2G20860) and LIP2 (AT1G04640). Under ambient conditions, LIP1 showed higher expression in *h-bou*, and expression significantly dropped and fell below wild type levels upon transfer to eCO_2 (Figure 7 D). There was no marked difference in the expression pattern of LIP2 between *h-bou* and the wild type, but the level of gene expression in *h-bou* was generally decreased (Figure 7 E).
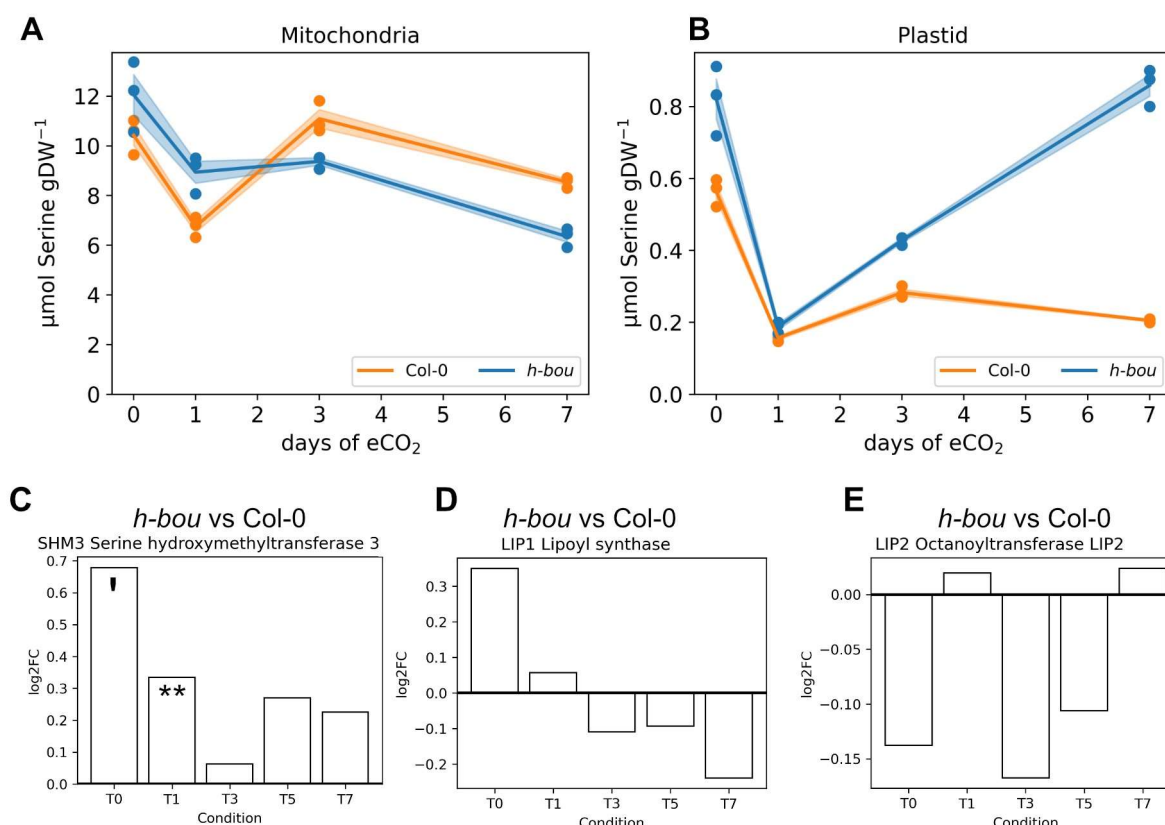

Figure 7. Subcellular serine dynamics in mitochondria and plastids, with transcripts of relevant enzymes. (A) Dynamics of mitochiondrial serine concentration in *h-bou* (blue) and Col-0 (orange), (B) Dynamics of plastidial serine concentration in *h-bou* (blue) and Col-0 (orange). Ordinates reflect serine amounts in µmol gDW^{-1}, abscissae show time of exposure to eCO2 in days. (C) – (E) Log2FC between *h-bou* and Col-0 for SHMT3, LIP1 and LIP2, respectively (** - p value < 0.01, ' - p value < 0.1; n = 3 replicates).

If lipoate availability was reduced in mitochondria of *h-bou*, other mitochondrial decarboxylases featuring E2 subunits, e.g., PDH, 2OGDH and the branched-chain α-ketoacid dehydrogenase complex (BCKDC) involved in catabolism of branched chain amino acids, should be affected [21]. Indeed, we observed elevated pyruvate levels in mitochondria of *h-bou* at aCO_2, indicating reduced turnover (Figure 2B) despite a higher expression level of three different PDH subunits (AT1G48030, AT3G52200, AT1G59900), including the lipoate depending E2 subunit AT1G48030 (Supplementary Figure 12). Upon transition to eCO_2, a significant decrease in expression of these subunits was observed, which, in conjunction with decreasing pyruvate levels, points to a more efficient turnover, possibly because of a released competition for lipoic acid between the glycine cleavage system and PDH when photorespiratory activity declined. A significant decrease in the

transcript level of the E2 subunit of PDH (LTA3, AT3G52200) at eCO_2, indicating return to normal TCA function, supports this view.
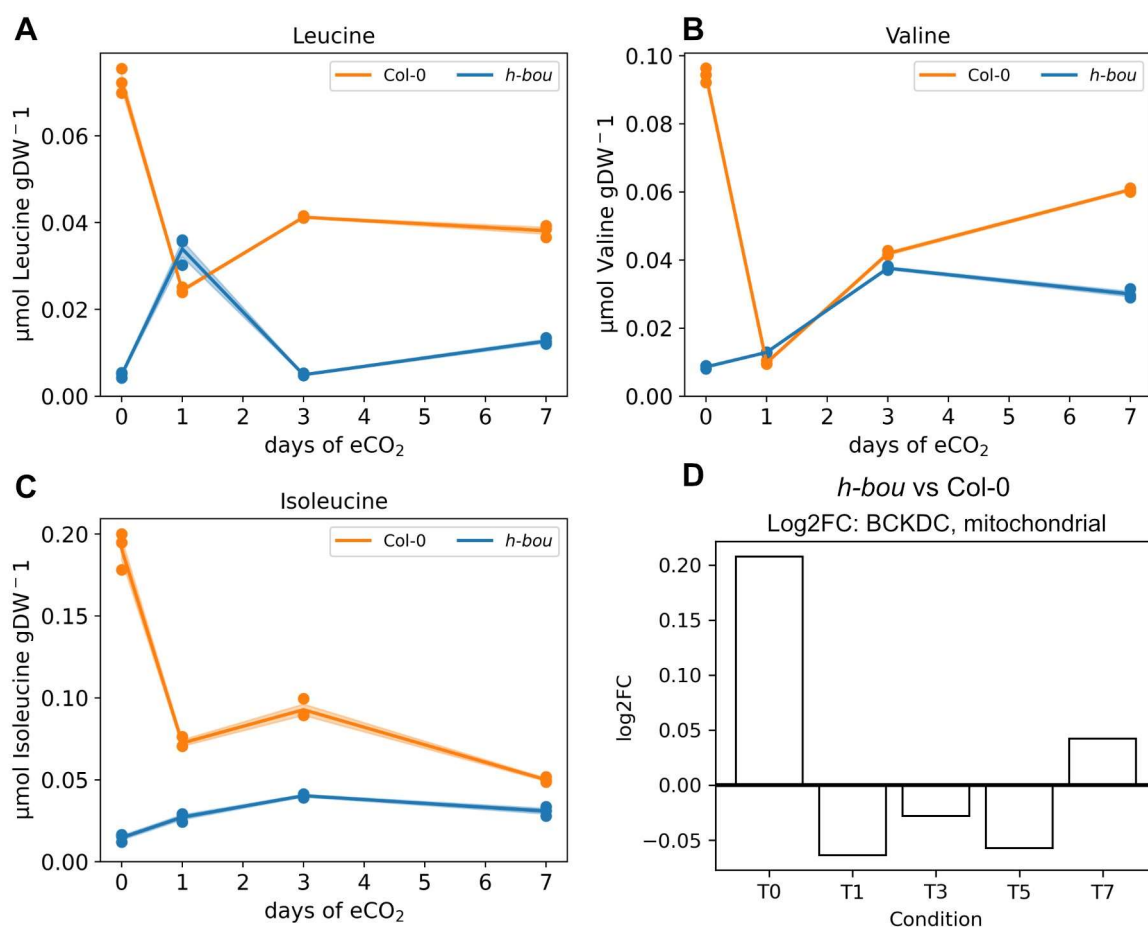

Figure 8. Mitochondrial concentrations of branched chain amino acids, with transcripts of catabolic enzyme BCKDC. (A) Dynamics of mitochiondrial leucine concentration in *h-bou* (blue) and Col-0 (orange), (B) Dynamics of mitochondrial valine concentration in *h-bou* (blue) and Col-0 (orange). (C) Dynamics of mitochondrial isoleucine concentration in *h-bou* (blue) and Col-0 (orange). Ordinates reflect amounts in µmol gDW^{-1}, abscissae show time of exposure to eCO2 in days. (D) Log2FC between *h-bou* and Col-0 for BCKDC (AT3G06850); n = 3.

265   Expression of the E2 subunit of 2-oxoglutarate dehydrogenase, another consumer of lipoate, displayed an increasing trend after transition to eCO_2 (Supplementary Figure S11 C, D), accompanied by an increase in its substrate 2-oxoglutarate, reaching wildtype levels at day 3 (Supplementary Figure S11 B). The low mitochondrial 2-oxoglutarate concentration at aCO_2 indicated a disruption of normal TCA cycle function. Low conversion of 2-oxoglutarate to succinyl-
270   CoA affords replenishment through anaplerotic reactions, an example being catabolism of the branched chain amino acids (BCAA) leucine, valine and isoleucine, all of which were significantly depleted in *h-bou* mitochondria under aCO_2 and gradually accumulated upon transition to eCO_2 (Figure 8, A-C). It is worth mentioning that BCAA catabolic reactions are also coupled to the transamination of 2-oxoglutarate to glutamate [22]. The enzyme BCKDC, involved in catabolism of
275   BCAA, is another consumer of lipoate, thus creating a complex network of competition, were elevated transcript levels of BCKDC (Figure 8 D) at aCO_2 and its decline at eCO_2 contribute to the view of disturbed lipoic acid homeostasis in the *h-bou* mutant. Interestingly, all three branched chain amino acids accumulated in the homozygous *bou* mutant when shifted from high to aCO_2 [23]. Under this condition, a high demand for GDC activity is created, thus restricting lipoate availability
280   for other enzymes. [23] pointed out that the alteration in BCAA levels were not the result of low

nitrate supply causing re-channeling of amino acids, and they also demonstrated that the E2 subunit of BCKDC was elevated at aCO_2. While this is in line with the phenotype of homozygous *bou* being stronger than in the heterozygous condition, the question still remains, why mitochondrial Glu levels were even higher in *h-bou* than in the wildtype. One obvious explanation is the transamination of 2-oxoglutarate to glutamate in the course of BCAA catabolism needed to replenish succinyl-CoA [24, 25], which would also explain low 2-oxoglutarate. Another, though less likely, explanation would be a metabolic transition to the import and use of glutamate for 2-oxoglutarate production in the mitochondria in order to fill up the TCA cycle at limiting PDH activity. Both are compatible with limiting lipoate availability in mitochondria as a result of BOU dysfunction, and thus we conclude that the combined omics approach applied here gives strong evidence to a function of BOU as carnitine/acylcarnitne transporter.

Taken together, our combined and subcellular resolved omics approach revealed additional, new information on complex effects of mutations and helps to elucidate non-obvious phenotypes. It clearly shows that metabolome analysis at the whole cell level reaches limits when it comes to reaction pathways like, e.g., photorespiration, that are shared among various cellular compartments.

Material and Methods

Plant material and growth condition

Arabidopsis thaliana (L.) Heynh. Col-0 as wild type, and mutants *hpr1-1* (SALK067724), *hxk1* (*gin2-1*, Salk_034233c, At4g29130) and heterozygous *bou* (GK-079D12.01, At5g46800) were used in this study. All plants were grown in fully controlled growth chambers at Stuttgart University for six weeks in soil (seedling substrate, Klasmann-Deilmann GmbH) under ambient carbon dioxide (450 ± 20 ppm) and short day (8 h/16 light/dark, 100 µmol m^{-2} s^{-1}, 60% relative humidity, temperature 22/16 °C). Standard NPK fertilizer was applied immediately after thinning seedlings and then every 2 weeks until harvest. After 6 weeks, one set of plants (9 per genotype) was sampled (day 0), and the rest transferred to elevated CO_2 (1000 ± 20 ppm) at the same environmental settings. Consecutive sampling was done at days 1, 3, 5 and 7, each time 4 h into the light phase at the middle of a short day. For each genotype, three biological replicates were harvested, each consisting of a pool of three full rosettes (3 replicates per each genotype and time points, totally 60 samples). Aliquots of fresh plant material were prepared for Proteomics and Transcriptomics analysis, and the rest subjected to lyophilization (Heto PowerDry LL3000; Thermo Electron C.) for subcellular fractionation.

RNA-seq analysis

Between 16 and 24 million, 100 bp, paired-end reads per sample were quality checked using FastQC (https://www.bioinformatics.babraham.ac.uk/projects/fastqc/), and adapter trimming or low-quality filtering were done using Trimmomatic [26]. Filtered reads were mapped to the Arabidopsis genome assembly with Tophat2 [27]. Counting and normalization of mapped reads and analysis of differential expression were done using the cufflinks suite [28].

Proteome analysis by mass spectrometry

Protein extraction and trypsin digestion were carried out following the protocol of (Marino et al. 2019). Liquid chromatography-tandem mass spectrometry (LC-MS/MS) was conducted as previously described, with peptides separated over a 90-minute linear gradient of 5–80% (v/v) CAN [29]. Raw data files were processed using MaxQuant software version 2.4.14.0 [30]. Peak lists were

searched against the Arabidopsis reference proteome (Uniprot, www.uniprot.org) using default settings, with the 'match-between-runs' feature enabled. Protein quantification was performed using the label-free quantification (LFQ) algorithm [30]. Subsequent analysis was executed using Perseus version 2.0.11 [31]. Potential contaminants, proteins identified only by site modification, and reverse hits were excluded from further analysis. Only protein groups quantified by the LFQ algorithm in at least three out of four replicates in at least one condition were considered. LFQ intensities were log2-transformed, and missing values were imputed from a normal distribution using Perseus with standard settings.

Nonaqueous fractionation

Subcellular fractionation of lyophilized plant samples by NAF procedures was performed as earlier described [32, 33]. Briefly, approximately 80-100 mg of lyophilized leaf homogenate were suspended in 10 ml of ice-cold mixture of tetrachloroethylene-heptane (solvent A, ρ = 1.36 g cm^{-3}) and sonified on ice bath for intervals of 5 s with 15 s pauses over a total time course of 12 min (Branson Sonifier 250, Branson, USA; output control 3). Under constant cooling, sonified homogenate was sieved through nylon gauze, pore size 30 µm, and the filtrate was centrifuged for 10 min at 2350 g, 4 °C Supernatant was discarded and pellet resuspended in 1.5 ml of fresh cold solvent A, subsequently loaded onto the ice-cold non-aqueous linear gradient combination of organic solvents initiated by solvent A (ρ = 1.36 g cm^{-3}), and ending up to pure tetrachloroethylene (ρ = 1.6 g cm^{-3}). Gradients were subjected to ultracentrifugation (Optima^{TM} L-90K, BeckMan Coulter, Ireland) for 3 h at 121,000 g, 4 °C. Fractionation of centrifuged gradient was performed into nine 1 ml fractions and each fraction aliquoted to 5 equal subfractions and immediately dried under vacuum condition for subsequent metabolite and marker enzyme analysis. Alkaline pyrophosphatase served as plastidial marker, UGPase as cytosolic marker, succinyl-CoA-synthetase as mitochondrial marker, and acid phosphatase as vacuolar marker enzyme as described earlier [32-34].

Metabolic profiling

For metabolite analysis, one aliquot of NAF and a respective whole cell sample was subjected to carbohydrate determination by HPLC (Dionex ICS 6000, ThermoFisher Scientific, USA), yielding concentrations of glucose, fructose, sucrose and raffinose as described by [35]. Briefly, extraction was performed in 80% ethanol at 80 °C, followed by vacuum drying. Dried extracts were resuspended in Honeywell chromatographic grade water and subjected to HPLC analysis on Dionex CarboPac PA1 BioLC column (4 x 250 mm, ThermoFisher Scientific, USA). Carboxylic acids, including pyruvate, malate, fumarate and citrate as well as minerals (nitrate, phosphate, sulfate) were quantified by anion-exchange chromatography using another aliquot of samples as described [35]. Briefly, extraction was done in 1 ml of 55 °C Honeywell water and incubation at 95 °C, followed by separation on Dionex IonPac AS11-HC RFIC column (4 x 250 mm, ThermoFisher Scientific, USA).

Amino acid measurements were performed by quantitative GC-MS/MS as described [36-38] with a few modifications using a third sample aliquot. Basically, a modified solid phase extraction of amino acids was performed by suspending NAF samples in 1 ml of 10 mM HCl and 10 min shaking at RT, followed by 2 min centrifugation at 14,000 g, RT. Hundred microliter of supernatant in addition to 10 nmol of norvaline (Acros Organics) as internal standard were subjected to amino acid purification, using homogenized suspension of 100 mg ml^{-1} of ion-exchange resin (DOWEX 50WX4, 200-400 mesh) in 10 mM HCl, incubated for 15 min at RT in Mobicol spin classic tubes equipped with 10 µm pore sized filters (MoBiTec GmbH, Germany), followed by centrifugation 5

min at 1,000 g, RT. Resin was washed twice by 80% methanol and 1 min centrifugation each time at 1,000 g, RT to remove non-amino acid metabolites. Subsequently, resin containing purified amino acids was suspended in 150 µl of 1:1 mixture of methanol and 8 M ammonia and centrifuged for 2 min at 5,000 g, RT. Eluent containing purified amino acids was dried in a speed vacuum concentrator (ScanSpeed 32, Denmark). Upon drying, derivatization was done by adding 50 µl of both MTBSTFA (Sigma Aldrich) and acetonitrile, 1 h incubation at 95 °C followed by 2 h at RT and subsequent analysis by GC-MS/MS (TQ8040, Shimadzu, Japan). One microliter of the derivatized samples was injected to device, applying helium as carrier gas at a flow of 1.12 ml/min. Stationary phase was a 30 m Optima 5MS-0.25 µm fused silica capillary column. Ion source, column oven and injection temperature were set up at 250 °C, 100°C and 250 °C respectively. A split 10 gradient program was applied with initial column temperature of 100 °C for 1 min, followed by 15 °C increment per minute till 290 °C, holding for 3 min, again followed by same increment rate to reach the final temperature as 330 °C and holding for 10 min. Subsequent to 5 min solvent delay, spectra of MS device were recorded in Q3 scanning mode.

All other metabolites including carbohydrates, sugar alcohols, carboxylic acids and polyamines were measured using the last remaining sample aliquots by GC-MS/MS as described earlier [39]. Briefly, extraction on ice into methanol-chloroform-water mixture, 2.5:1:0.5 (v/v/v) was followed by centrifugation. Polar phase was separated and along with norvaline as internal standard, dried in a speed vacuum concentrator equipped with cold trap (ScanVac, Denmark). After drying, methoximation was performed using 20 µl of methoxamine dissolved in pyridine (40 mg ml^{-1}) by 90 min incubation at 30 °C followed by silylation, using 80 µl of MSTFA (Sigma Aldrich) and 30 min incubation at 50 °C. Detection was done by the same GC-MS/MS device as amino acids and a different split 10 gradient program as 70 °C for initial temperature and one min holding, followed by 15 °C increment per minute till reaching to final 330 °C, and holding for 10 min. Ion source, column oven and injection temperature were set up at 250 °C, 70°C and 230 °C, respectively, and after 4.7 min solvent delay, spectra were recorded in Q3 scanning mode.

OmicsDB Tech Stack

In order to quickly access omics data in a reliable and reproducible manner, an SQLite Database (OmicsDB) was created, which can be accessed via a custom API (OmicsAPI) in python (Version 3.11.5). When utilizing this API in order to submit data to the OmicsDB, the API sends a URL request to the API of Panther knowledgebase (PANTHER 18.0) in order to retrieve the associated GO terms of a transcript or a protein [40]. In addition to this, the organism-specific locus name is gathered via the API of the UniProt knowledgebase (Release 2024_01) [41]. In order to associate proteins and transcripts to metabolites, GO terms where matched to KEGG modules (Release 108.1), from which information on metabolites was obtained via the associated API [42-44]. The data stored in the OmicsDB can now be accessed via the OmicsAPI in a Go Term specific manner, e.g. "Photorespiration" or "Chloroplast". For fast and easy data exploration, an additional analysis API (ExplorerAPI) was created which can perform principle component analysis (PCA), partial least squares regression (PLS) between Datasets, and time-lagged cross correlation analysis (TLCC). This API should be used in a Jupyter Notebook. Both PCA and PLS can be performed in a sparse manner and use scikit-learn (Version 1.3.2) or in the case of sPLS, the R package mixOmics (Version 6.22.0) in combination with rpy2 (Version 3.5.15) in order to make it accessible in python. Methods related to the TLCC were coded inhouse. In Addition, the ExplorerAPI provides basic plotting methods for individual Omics samples.

The entire codebase and database are available under https://git.nfdi4plants.org/thomas.naegele/OMICS_DB. Additional requirements regarding packages and package versions can be also viewed on GitHub.

The metabolite list associated with photorespiration was further extended to include glutamine, aspartate, malate, and asparagine.

Statistics

Statistics were performed in python (Version 3.11.5). In order to calculate significance of log2FC, z-tests were performed after calculating the geometric mean and the propagation of error as suggested in [45]. In addition, the p-value was adjusted for multiple testing using Bonferroni correction. The script was coded in house, in order to integrate with the OmicsAPI and is available on the same GitHub page.

Acknowledgement

Competing interests

The authors declare no competing interests

Author contributions

TN, AGH and DW designed the study. DS and JSH performed the experiments and analyzed the data. JG, EZ and JA performed transcriptome analysis. SS and DL performed and supervised proteomics analysis. All authors contributed to data evaluation and manuscript preparation. All authors read the manuscript and consent to its content.

Data availability statement

Original data is available at

https://git.nfdi4plants.org/thomas.naegele/Subcellular_analysis_of_metabolic_network_dynamics_under_elevated_CO2

Supplementary Figures

Supplementary Figure S1. Principle component analysis of metabolites associated with photorespiration after exposure to elevated CO_2. (A) Scatter plot of scores. The color of points indicates the genotype (Blue – *h-bou*, Orange – Col-0, Green – *hpr1-1*, Red -*hxk-1)*, while the shape indicates days of elevated CO_2 (1000 ppm) treatment (Circle – T0, Triangle – T1, Square – T3, Pentagon – T7). T0 represents ambient conditions (approx. 400 ppm) before transfer to eCO_2. Replicates: n = 3. (B) Metabolites showing the highest loadings, i.e., contribution to the principle components. The cut off for this table was set to 80% of the highest loading of each component. Loadings are sorted in descending order.

Supplementary Figure S2. Subcellular glycolate concentration and associated transporters. (A) Dynamics of glycolic acid in plastids, (B) Dynamics of glycolic acid in the cytosol. Ordinates reflect glycolic acid amounts in μmol gDW^{-1} (means ± SE; n = 3), abscissae show time of exposure to eCO_2 in days. (C) Log2FC of PLGG1 between *hpr1-1* and Col-0, (D) log2FC of BASS6 between *hpr1-1* and Col-0 (* - p value < 0.05, n = 3).

Supplementary Figure S3. Hypothetical bypass of HPR1. Expression data is given in log2FC between *hpr1-1* and Col-0. Order of squares represent order of conditions (1: aCO_2, 2: 1 day eCO_2, 3: 3 days eCO_2, 4: 5 days eCO_2, 5: 7 days eCO_2). The top row represents transcriptomics data, while the bottom row represents proteomics data (* - p-val < 0.05; n = 3).

Supplementary Figure S4. Model of a data-derived suggested cytosolic bypass in *hpr1-1*.

Supplementary Figure S5. log2FC of PDK between *hpr-1* and Col-0 (*** - p value < 0.0001; n = 3).

Supplementary Figure S6. Cytosolic citrate dynamics (A) and Log2FC between *hpr1-1* and Col-0 of enzymes involved in citrate metabolism (means ± SE; n = 3). (B) Log2FC between *hpr1-1* and Col-0 of citrate synthase subunits. (C) Log2FC between *hpr1-1* and Col-0 of acetyl coenzyme A synthase and acetate/butyrate CoA ligase.

Supplementary Figure S7. Principal component analysis of eCO_2 response in the proteomes of TCA cycle and cellular redox homeostasis. **(A)** Col-0, **(B)** *hxk1*, **(C)** *hpr1-1*, **(D)** *h-bou*. Colors and shapes indicate different time points of eCO_2 exposure. Red filled circles: 0 days at eCO_2, i.e., aCO_2; olive filled triangles: 1 day at eCO_2; green filled squares: 3 days at eCO_2; blue cross: 5 days at eCO_2; magenta crossed square: 7 days at eCO_2. Data was scaled (z-scale, i.e., zero mean, unit variance).

Supplementary Figure S8. Dynamics of peroxisomal CATALASE2 (CAT2, AT4G35090) under eCO_2. **(A)** Col-0**, (B)** *hxk1*, **(C)** *hpr1-1*, **(D)** *h-bou*.

Supplementary Figure S9. Principal component analysis of proteins involved in carboxylic acid metabolism. (A) PCA without loadings; (B) PCA with loadings. Colours indicate genotypes (red: Col-0; cyan: *hxk1*). Symbols represent duration of eCO_2 treatment.

Supplementary Figure S10. Phenotype of the homozygous *bou* mutant **(A),** the heterozygous mutant *h-bou* **(B)** and the Col-0 wildtype **(C).** Plants were grown for six weeks in soil under ambient carbon dioxide (450 ± 20 ppm) and short day (8 h/16 light/dark, 100 μmol m-2 s-1, 60% relative humidity, temperature 22/16 °C) before photography.

Supplementary Figure S11. Mitochondrial glutamate and oxoglutarate dynamics with transcripts of associated enzymes. (A) Dynamics of mitochondrial glutamate concentrations in *h-bou* (blue) and Col-0 (orange). Ordinate reflects glutamate amounts in μmol gDW^{-1} (means ± SE; n = 3), abscissa shows time of exposure to eCO_2 in days. (B) Dynamics of mitochondrial oxoglutarate concentrations in *h-bou* (blue) and Col-0 (orange). Ordinate reflects 2-oxoglutarate amounts in μmol gDW^{-1} (means ± SE; n = 3), abscissa shows time of exposure to eCO_2 in days. (C) Log2FC of OGDH-E2 (AT4G26910) comparing *h-bou* to Col-0– (D) Log2FC of OGDH2-E2 (AT5G55070) comparing *h-bou* to Col-0; n = 3.

Supplementary Figure S12. Log2FCs of PDH subunits for *h-bou* as compared to Col-0 enzymes. (A) Log2FC between *h-bou* and Col-0 for the lipoate containing E2 subunit (AT1G48030). (B) Log2FC between *h-bou* and Col-0 for subunit 2-1 (AT3G52200). (C) Log2FC between *h-bou* and Col-0 for the E1 subunit (AT1G59900); n = 3.

475 References

[1] Serrano-Mislata, A. & Bencivenga, S. et al.DELLA genes restrict inflorescence meristem function independently of plant height. *Nature Plants* 3, 749-754 (2017).

[2] Busch, F. A. & Sage, R. F. et al.Plants increase CO2 uptake by assimilating nitrogen via the photorespiratory pathway. *Nature Plants* 4, 46-54 (2018).

480 [3] Lin, Y.-C. & Tsay, Y.-F.Study of vacuole glycerate transporter NPF8.4 reveals a new role of photorespiration in C/N balance. *Nature Plants* 9, 803-816 (2023).

[4] Dellero, Y. & Jossier, M. et al.Photorespiratory glycolate-glyoxylate metabolism. *J Exp Bot* 67, 3041-3052 (2016).

[5] Timm, S. & Nunes-Nesi, A. et al.A Cytosolic Pathway for the Conversion of Hydroxypyruvate
485 to Glycerate during Photorespiration in Arabidopsis. *The Plant Cell* 20, 2848-2859 (2008).

[6] Li, L. & Sheen, J.Dynamic and diverse sugar signaling. *Current Opinion in Plant Biology* 33, 116 - 125 (2016).

[7] Roth, M. S. & Westcott, D. J. et al.Hexokinase is necessary for glucose-mediated photosynthesis repression and lipid accumulation in a green alga. *Communications Biology* 2, 347 (2019).

490 [8] Küstner, L. & Fürtauer, L. et al.Subcellular dynamics of proteins and metabolites under abiotic stress reveal deferred response of the Arabidopsis thaliana hexokinase-1 mutant gin2-1 to high light. *The Plant Journal* 100, 456-472 (2019).

[9] Eisenhut, M. & Planchais, S. et al.Arabidopsis A BOUT DE SOUFFLE is a putative mitochondrial transporter involved in photorespiratory metabolism and is required for meristem
495 growth at ambient CO2 levels. *The Plant Journal* 73, 836-849 (2013).

[10] Porcelli, V. & Vozza, A. et al.Molecular identification and functional characterization of a novel glutamate transporter in yeast and plant mitochondria. *Biochimica et Biophysica Acta (BBA) - Bioenergetics* 1859, 1249-1258 (2018).

[11] Monné, M. & Daddabbo, L. et al.Uncoupling proteins 1 and 2 (UCP1 and UCP2) from
500 Arabidopsis thaliana are mitochondrial transporters of aspartate, glutamate, and dicarboxylates. *Journal of Biological Chemistry* 293, 4213-4227 (2018).

[12] Tcherkez, G. & Hodges, M.How stable isotopes may help to elucidate primary nitrogen metabolism and its interaction with (photo)respiration in C3 leaves. *J Exp Bot* 59, 1685-1693 (2008).

505 [13] Szecowka, M. & Heise, R. et al.Metabolic Fluxes in an Illuminated Arabidopsis Rosette . *Plant Cell* 25, 694-714 (2013).

[14] Lim, S.-L. & Voon, C. P. et al.In planta study of photosynthesis and photorespiration using NADPH and NADH/NAD+ fluorescent protein sensors. *Nature Communications* 11, 3238 (2020).

[15] Cousins, A. B. & Pracharoenwattana, I. et al.Peroxisomal Malate Dehydrogenase Is Not
510 Essential for Photorespiration in Arabidopsis But Its Absence Causes an Increase in the Stoichiometry of Photorespiratory CO2 Release . *Plant Physiol* 148, 786-795 (2008).

[16] Knieper, M. & Viehhauser, A. et al.Oxylipins and Reactive Carbonyls as Regulators of the Plant Redox and Reactive Oxygen Species Network under Stress. *Antioxidants* 12, (2023).

[17] Moore, B. & Zhou, L. et al.Role of the Arabidopsis Glucose Sensor HXK1 in Nutrient, Light,
515 and Hormonal Signaling. *Science* 300, 332-336 (2003).

[18] Hoffmann, M. & Hentrich, M. et al.Auxin-oxylipin crosstalk: relationship of antagonists.. *Journal of integrative plant biology* 53, 429-45 (2011).

[19] Lawand, S. & Dorne, A.-J. et al.Arabidopsis A BOUT DE SOUFFLE, Which Is Homologous with Mammalian Carnitine Acyl Carrier, Is Required for Postembryonic Growth in the Light. *Plant*
520 *Cell* 14, 2161-2173 (2002).

[20] Bauwe, H.Photorespiration - Rubisco's repair crew. *Journal of Plant Physiology* 280, 153899 (2023).

[21] Taylor, N. L. & Heazlewood, J. L. et al.Lipoic Acid-Dependent Oxidative Catabolism of α-Keto Acids in Mitochondria Provides Evidence for Branched-Chain Amino Acid Catabolism in Arabidopsis. *Plant Physiol* 134, 838-848 (2004).

[22] Hildebrandt, T. & Nunes Nesi, A. et al.Amino Acid Catabolism in Plants. *Molecular Plant* 8, 1563-1579 (2015).

[23] Samuilov, S. & Brilhaus, D. et al.The Photorespiratory BOU Gene Mutation Alters Sulfur Assimilation and Its Crosstalk With Carbon and Nitrogen Metabolism in Arabidopsis thaliana. *Frontiers in Plant Science* 9, (2018).

[24] Binder, S. & Knill, T. et al.Branched-chain amino acid metabolism in higher plants. *Physiologia Plantarum* 129, 68-78 (2007).

[25] Binder, S.Branched-Chain Amino Acid Metabolism in Arabidopsis thaliana.. *The arabidopsis book* 8, e0137 (2010).

[26] Bolger, A. M. & Lohse, M. et al.Trimmomatic: a flexible trimmer for Illumina sequence data. *Bioinformatics* 30, 2114-2120 (2014).

[27] Kim, D. & Pertea, G. et al.TopHat2: accurate alignment of transcriptomes in the presence of insertions, deletions and gene fusions. *Genome Biology* 14, R36 (2013).

[28] Trapnell, C. & Roberts, A. et al.Differential gene and transcript expression analysis of RNA-seq experiments with TopHat and Cufflinks. *Nature Protocols* 7, 562-578 (2012).

[29] Espinoza-Corral, R. & Schwenkert, S. et al.Characterization of the preferred cation cofactors of chloroplast protein kinases in Arabidopsis thaliana.. *FEBS open bio* 13, 511-518 (2023).

[30] Cox, J. & Hein, M. Y. et al.Accurate Proteome-wide Label-free Quantification by Delayed Normalization and Maximal Peptide Ratio Extraction, Termed MaxLFQ*. *Molecular & Cellular Proteomics* 13, 2513-2526 (2014).

[31] Tyanova, S. & Albrechtsen, R. et al.Proteomic maps of breast cancer subtypes. *Nature Communications* 7, 10259 (2016).

[32] Fürtauer, L. & Küstner, L. et al.Resolving subcellular plant metabolism. *The Plant Journal* 100, 438-455 (2019).

[33] Hoermiller, I. I. & Funck, D. et al.Cytosolic proline is required for basal freezing tolerance in Arabidopsis. *Plant Cell Environ* 45, 147-155 (2022).

[34] Knaupp, M. & Mishra, K. B. et al.Evidence for a role of raffinose in stabilizing photosystem II during freeze-thaw cycles. *Planta* 234, 477-486 (2011).

[35] Friedrichs, N. & Shokouhi, D. et al.Flux Calculation for Primary Metabolism Reveals Changes in Allocation of Nitrogen to Different Amino Acid Families When Photorespiratory Activity Changes. *International Journal of Molecular Sciences* 25, (2024).

[36] Molnár-Perl, I. & Katona, Z. GC-MS of Amino Acids as Their Trimethylsilyl/t-butyldimethylsilyl Derivatives: in Model Solutions III. *Chromatographia* 51, S-228 - S-236 (2000).

[37] Sobolevsky, T. G. & Revelsky, A. I. et al.Comparison of silylation and esterification/acylation procedures in GC-MS analysis of amino acids. *J. Sep. Science* 26, 1474-1478 (2003).

[38] Guo, M. & Shi, T. et al.Investigation of amino acids in wolfberry fruit (Lycium barbarum) by solid-phase extraction and liquid chromatography with precolumn derivatization. *Journal of Food Composition and Analysis* 42, 84-90 (2015).

[39] Krämer, K. & Kepp, G. et al.Acclimation to elevated CO_2 affects the C/N balance by reducing de novo N-assimilation. *Physiologia Plantarum* 174, (2022).

[40] Thomas, P. D. & Ebert, D. et al.PANTHER: Making genome-scale phylogenetics accessible to all. *Protein Science* 31, 8-22 (2022).

[41] UniProt-Consortium, T.UniProt: the Universal Protein Knowledgebase in 2023.. *Nucleic acids research* 51, D523-D531 (2023).

570   [42] Kanehisa, M. & Goto, S.KEGG: kyoto encyclopedia of genes and genomes.. *Nucleic acids research* 28, 27-30 (2000).

[43] Kanehisa, M.Toward understanding the origin and evolution of cellular organisms.. *Protein science : a publication of the Protein Society* 28, 1947-1951 (2019).

[44] Kanehisa, M. & Furumichi, M. et al.KEGG for taxonomy-based analysis of pathways and
575   genomes.. *Nucleic acids research* 51, D587-D592 (2023).

[45] Quackenbush, J.Microarray data normalization and transformation. *Nature Genetics* 32, 496-501 (2002).

3. Discussion

This dissertation provides a computational and experimentally validated framework for assessing stability of plant carbon assimilation in a dynamic environment. Subcellular analysis of the central carbohydrate metabolism has been combined with statistical analysis and pattern recognition of photosynthetic efficiency to assess natural variation of temperature acclimation capacities in *Arabidopsis thaliana*. Based on structural kinetic modelling, a combinatorial problem of metabolic regulation of the CBBC could be solved indicating a trade-off function of photorespiration. Finally, a data analysis pipeline has been developed and applied for integrated analysis of a comprehensive experimental data set on plant metabolic regulation under elevated atmospheric CO_2 concentrations. This revealed an alternative pathway of glycerate biosynthesis under such growth conditions.

3.1 Subcellular metabolite distribution in the context of photosynthetic performance

The first publication presented in this dissertation aimed at understanding how an acclimated subcellular metabolic homeostasis is related to the plant's photosynthetic efficiency. At low temperature, reprogramming of carbon partitioning and a tight regulation of resource allocation have been shown earlier to significantly contribute to photosynthetic cold acclimation (see e.g., Herrmann et al., 2019). It has been reported that an increased capacity of sucrose biosynthesis promoted photosynthetic stability under cold (Lundmark et al., 2006; Nägele et al., 2012; Strand et al., 2003). Furthermore, a stabilizing role of vacuolar sucrose cleavage for photosynthesis was suggested, indicating a central role of subcellular sugar allocation (Nägele, 2022; Weiszmann et al., 2018). While such studies were previously also conducted for plants acclimated to high temperatures (Atanasov et al., 2020), it remains unclear to what extent acclimatory patterns are conserved between conditions of low and elevated temperature. To reveal conserved and specific strategies of plant temperature acclimation, 18 natural accessions of *A. thaliana* originating from a wide geographic distribution, were either acclimated to low (4°C) or high (34°C) temperatures, or left at ambient temperatures (22°C). The (linear) electron transport rates (ETRs) were then quantified by pulse-amplitude modulation to assess photosynthetic efficiencies, both at the acclimated temperatures as well as at cross conditions (e.g., acclimated at 4°C and measured at 34°C).

The ETRs were determined in rapid light curve measurements, in which the photosynthetically active radiation (PAR) was increased from 0 to 1200 µmol photons m^{-2} s^{-1}. When plotting such ETR curves, stressed plants exhibited fluctuating patterns rather than smooth curves (Fig. 5 A, B). Quantifying the degree of such fluctuation was the first challenge addressed in this dissertation, which was solved by fitting a saturation curve to the data (Eq. 11):

$$ETR = \frac{PAR * p1}{PAR + p2} \qquad (11)$$

This allowed for the calculation of residuals between the curve fit and experimental data, which directly corresponds to the degree of fluctuation. To compare these fluctuations between conditions, the absolute value of the residuals was scaled by the maximum ETR. The physiological relevance of quantifying such fluctuations becomes evident when analyzing how the ETR is calculated in a PAM protocol:

$$ETR = Y(II) * E * A * 0.5 \qquad (12)$$

Here, $Y(II)$ represents the effective photochemical quantum yield of PS II, E is the incident irradiance, and A is the absorptance. Thus, observed fluctuations were directly related to perturbations of $Y(II)$. In general, quantum yield can be split into three fractions, which are the photochemical yield $Y(II)$, the yield of light-induced non-photochemical quenching $Y(NPQ)$, and the yield of unregulated heat dissipation and fluorescence emission $Y(NO)$ (Klughammer & Schreiber, 2008). Because the yields are connected via $1 = Y(II) + Y(NPQ) + Y(NO)$, this means that perturbations of $Y(II)$ will be reflected in either $Y(NPQ)$ or in $Y(NO)$. Indeed, dynamics of $Y(II)$ are directly mirrored in $Y(NPQ)$ but not in $Y(NO)$ (Fig. 5 C-E). This was reflected in the strong correlation between $Y(II)$ and $Y(NPQ)$ (Fig. 5 F). This trend is continued in the whole data set, with the average correlation between $Y(II)$ and $Y(NPQ)$ being -0.94 when plants where acclimated and measures at 4°C which represents the condition with the highest degree of fluctuations. The correlation between $Y(II)$ and $Y(NO)$ on the other hand was only 0.48.

The observations suggested that the fluctuations of the ETR curves were correlated to fluctuations of $Y(NPQ)$. The quantum yield of NPQ is directly dependent on the proton gradient, ΔpH, across the thylakoid membrane and responds to light changes in a time frame of seconds (Müller et al., 2001). An increase in illumination results in an increased ΔpH which, in turn, activates the xanthophyll cycle and protonates proteins of PSII, allowing for a higher portion of excitation energy to be dispersed safely as heat, preventing the formation of triplet Chl and formation of ROS (Müller et al., 2001). Owing to this, fluctuations of $Y(NPQ)$ are related to perturbations of the ΔpH, which in turn hints towards fluctuations in the metabolism of ATP. As a consequence, the observed fluctuations in the ETR curves suggested an impaired metabolic homeostasis and carbon assimilation process.
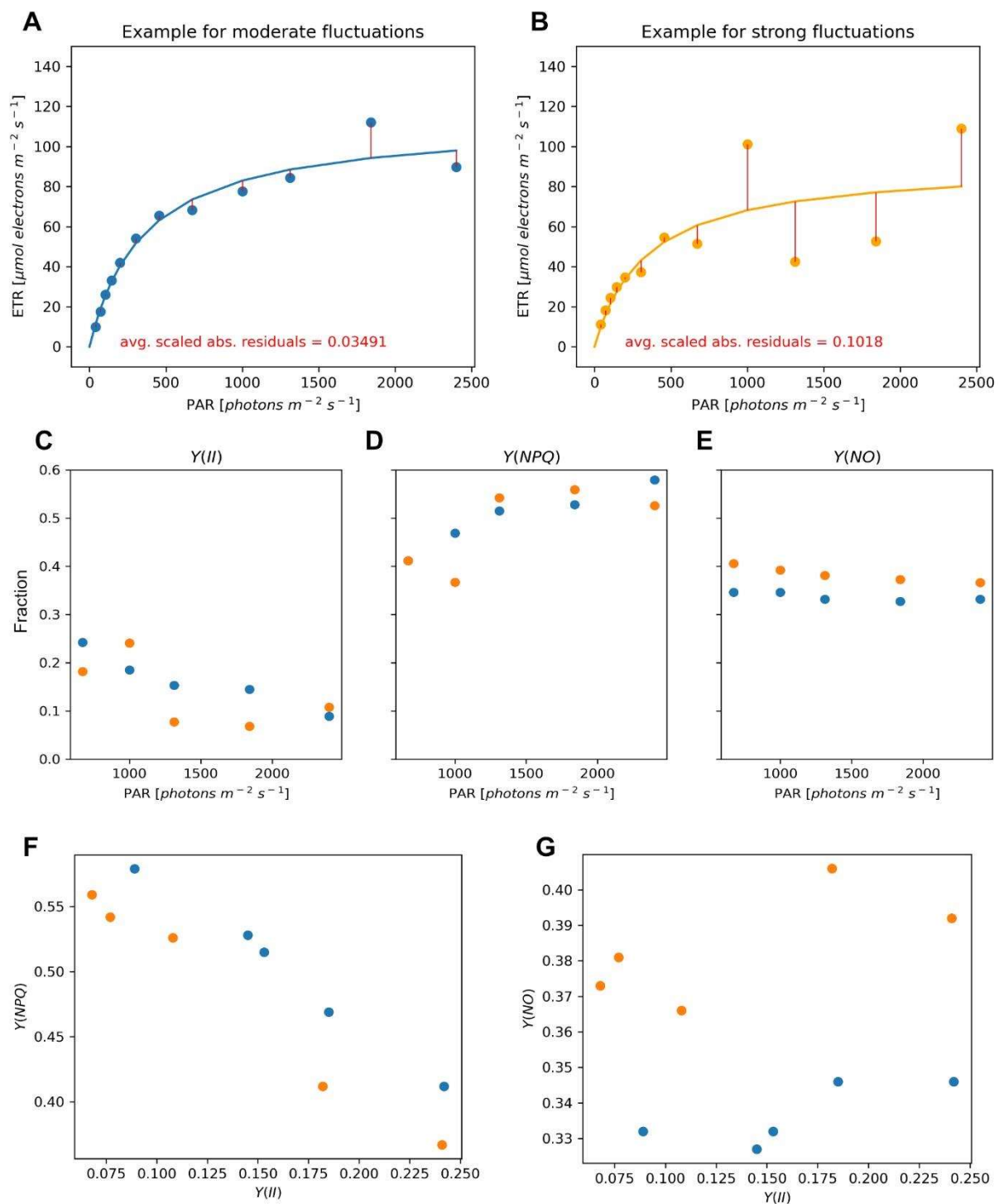
Fig. 5: Analysis of the fluctuations of the electron transport rate (ETR) across PSII. A) Example ETR showing moderate fluctuations. The curve is mostly smooth except for the last two points. B) Example ETR with strong fluctuations. The curve starts oscillating at a PAR of 400 photons m^{-2} s^{-1}, resulting in higher scaled residuals. The degree of fluctuation can be determined by fitting a saturation curve through the data and quantifying the residuals. In order to allow for comparison between conditions, the residuals are scaled to the maximum ETR. The fluctuations tend to be the most pronounced at high PAR values. C) $Y(II)$ at high PAR values. D) $Y(NPQ)$ at high PAR values. E) $Y(NO)$ at high PAR values. F) $Y(II)$ vs $Y(NPQ)$. G) $Y(II)$ vs $Y(NO)$.

With the help of this fluctuation data, the study showed that, after temperature acclimation, the capacity to stabilize photosynthesis against environmental perturbations could separate accessions originating from continental eastern parts of Europe from accessions of coastal western accessions. This geographic distribution might be linked to a higher degree of temperature change in the first quarter of the year (https://climatecharts.net/). This indicates that, in accessions originating from a natural habitat which experiences high temperature dynamics, the capacity to stabilize against temperature fluctuations is increased. Such an effect may thus represent a trade-off between optimizing an acclimated homeostasis for photosynthetic efficiency at a given temperature and preparing for future temperature changes by increasing stabilizing capacity. However, this also indicates that not only the absolute configuration of a given homeostasis has to be considered when judging the acclimation capacity of a plant, but also its ability to buffer environmental fluctuations. Such considerations are particularly important in vegetation and crop sciences, which heavily rely on models to predict photosynthetic output (Kaiser et al., 2015). Such models tend to reflect controlled steady conditions and perform poorly under fluctuating conditions, resulting in an overestimation of photosynthesis (Kaiser et al., 2015). By integrating information on the stability of photosynthetic performance, these models may be further improved to reflect a dynamic environment.

To further analyze how stability of photosynthesis is linked to the stability of a metabolic homeostasis, subcellular sugar concentrations were correlated to the degree of ETR fluctuation and other photosynthetic parameters. This analysis was, however, complicated by the challenges associated with obtaining subcellular metabolite data. The relative compartmental distribution of a metabolite can be obtained via a non-aqueous fractionation (NAF) technique (Fürtauer et al., 2016). In brief, the plant material is separated into subcellular clusters of proteins, lipids and metabolites via sonication. These clusters have differing densities and can be separated along a non-aqueous density gradient into different fractions (Fig. 6). Compartmental marker enzymes can then be used to quantify the distribution of subcellular compartments across these fractions. The subcellular distribution of a target metabolite can be inferred based on the distribution of these compartment specific marker enzymes.
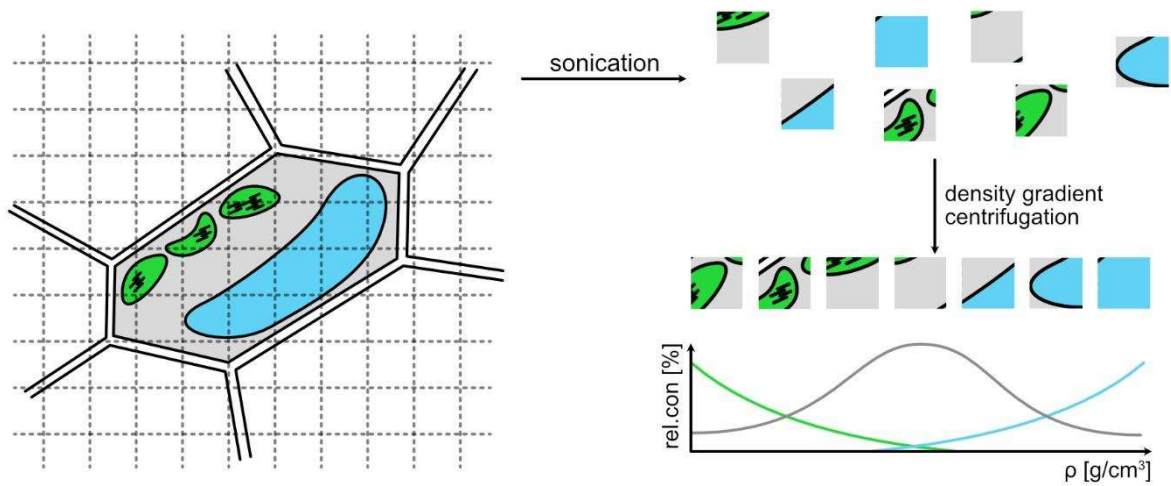
Fig. 6: Schematic representation of the NAF protocol. The cell is separated into subcellular clusters via sonication. These clusters are then sorted based on their density, with compartment specific marker enzymes showing the overall distribution.

In the most basic case, the concentration of a target enzyme can be calculated by solving the following equation of linear combinations (Eq. 13):

$$\begin{bmatrix} p_1 & c_1 & v_1 \\ p_2 & c_2 & v_2 \\ p_3 & c_3 & v_3 \\ p_4 & c_4 & v_4 \\ p_5 & c_5 & v_5 \end{bmatrix} * \begin{pmatrix} x_p \\ x_c \\ x_v \end{pmatrix} = \begin{pmatrix} m_1 \\ m_2 \\ m_3 \\ m_4 \\ m_5 \end{pmatrix} \tag{13}$$

This represents an $Ax = b$ problem, with A being a matrix containing the relative distribution of compartment markers in each column, x the target vector of relative metabolite distributions, and b the known vector of relative metabolite concentration in each fraction. The vector x can be obtained via least-squares fitting, resulting in the subcellular distribution of the target metabolite. This, however, is challenged by a technical error of approximately 10% which needs to be considered for further estimations. As a consequence, the vector x can take up values which are mathematically correct, but physiologically impossible, such as negative values or values very close to or exceeding 1. In addition, the sum of the vector x must always equal 1 as it represents the fraction of each compartment.

Owing to this, several methods have been proposed to make the values of x better reflect the physiological reality of a cell. Generally, there exist at least two possibilities to calculate the values of x, one based on constraining the values of x to the interval $(0,1)$ and the other by comparing the slopes between fractions (Fürtauer et al., 2016). In this study, a new method of calculating x was developed, which is proposed to improve interpretability and performance. It is based on a Monte-Carlo simulation, which adds noise to reflect the experimental uncertainty, and thus reveals the physiologically permissive parameter space of x. As the core of this method uses linear-least squares fitting constrained to $x \in (1,0)$, the interpretation of results is straight forward and easier to understand compared to methods

based on the slopes between fractions. Both this novel method and a previously published method based on slopes (Fürtauer et al., 2016) were introduced into an R-shiny app, allowing fast and convenient calculation of subcellular distributions. The app was released on GitHub along with the publication of the first project (https://github.com/cellbiomaths/NAFalyzer).

Table 1: Evaluation of two methods for calculating relative subcellular distribution from NAF data. The performance was analyzed on a toy data set with known distribution. Here, percent refers to the unit of measurement for relative distributions (e.g. 30% plastid, 20% cytosol, 50% vacuole). As such, the error is given as the average deviation from the known outcome (e.g. 33% calculated − 30% known = 3% error) and is not the proportion of error. Each category was calculated with at least n=9 examples and is given with the standard deviation. Monte-Carlo refers to the approach presented in this study, while Slopes refers to a previously published method (Fürtauer et al., 2016). The degree of separation refers to how well the distribution of marker enzymes diverged from one another.

	Avg. error Monte-Carlo	Avg. error Slopes
Perfect Separation	0.89 +/- 0.35%	4.98 +/- 2.88%
Good Separation	3.00 +/- 1.78%	9.45 +/- 9.21%
Average Separation	4.23 +/- 3.51%	12.28 +/- 11.46%
Bad Separation	7.67 +/- 6.45%	15.34 +/- 11.88%

In order to evaluate the Monte-Carlo approach, the performance was analyzed on a toy data set with known distributions. The error was then compared to the existing method based on slopes (Table 1). The approach based on a Monte-Carlo simulation demonstrated a reduced average error compared to the previously published method. The slopes-based method demonstrated a high error when dealing with data that showed accumulation in one compartment (e.g. 5% plastid, 10% cytosol, 85% vacuole). In such an instance, the slopes-based method tended to even out the distribution between compartments, while the Monte-Carlo based approach was capable of accurately reflecting such patterns. In addition, the Monte-Carlo based approach contains direct feedback on the quality and reliability of results, as the theoretically possible parameter space of x can be directly analyzed (Fig 7). This allows for possible artifacts to be detected and removed, which is currently not possible with the slopes-based approach.
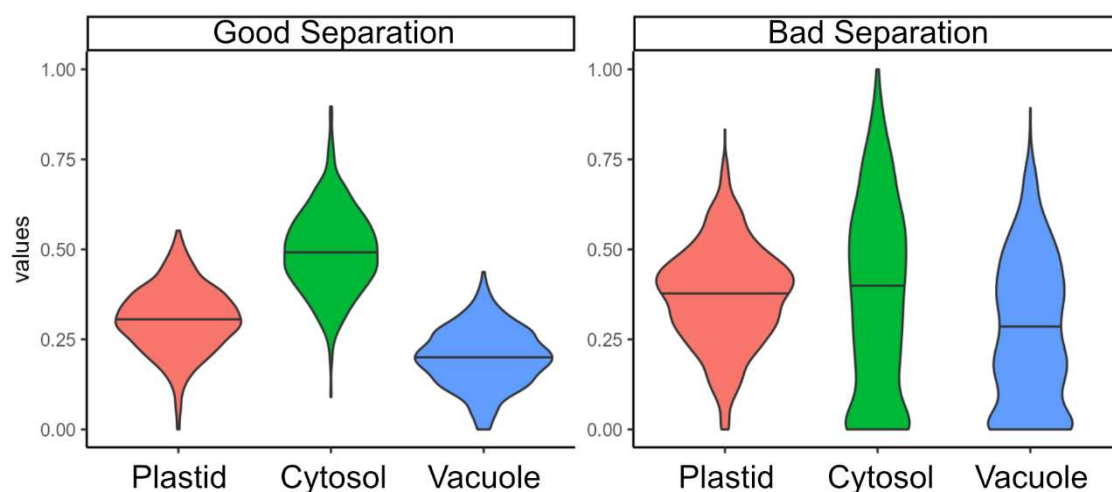
Fig. 7: Evaluation of separation and reliability of NAF. The calculation was performed using experimentally obtained NAF gradients on a toy metabolite with a known distribution of 30%, 50%, and 20%. A good separation between marker enzymes is able to reliably detect compartment distribution with an assumed experimental error of 10%. A bad separation of marker enzymes results in a high degree of uncertainty and multiple possible compartment distributions, as can be observed by the multiple peaks in the violin plot demonstrating underlying multimodal data.

By utilizing this novel approach, the subcellular metabolism of the natural accessions in an acclimated and unacclimated state could be resolved. This allowed for the identification of both specialized and conserved acclimatory patterns of metabolism in natural accessions (see chapter 2.1). One of the most significant effects which were observed was the differential subcellular sucrose allocation between accessions of eastern and western Europe. Under ambient conditions, sucrose was found to be located mainly in the cytosol and the vacuole, with eastern accessions favoring a higher cytosolic fraction and western accessions a higher vacuolar fraction. Under elevated temperatures, a portion of vacuolar sucrose was reallocated towards the cytosol, with this effect being more pronounced in western accessions resulting in similar distributions to eastern accessions. In cold, vacuolar sucrose was remobilized towards the cytosol and plastids across all accessions. Indeed, the resulting effective sucrose concentrations across compartments was found to significantly correlate with photosynthetic performance in a wide range of analyzed conditions. In particular, the concentration of sucrose in the plastid was significantly positively correlated to the maximum ETR in conditions of maximal temperature perturbation. This raises the question of how sucrose is capable of accumulating in the plastid and if it is involved in improving photosynthetic performance.

Currently, based on genome scale reconstructions, there are no described pathways capable of synthesizing sucrose in the plastid. This suggests that metabolite transporters are likely involved in promoting the cold induced accumulation of plastidial sucrose. Recently, pSuT (Plastidic Sugar Transporter) was reported to transport both glucose and sucrose across the inner membrane of the chloroplast (Patzke et al., 2019). As it was reported that pSuT is involved in cold response, it is tempting to speculate that sucrose compartmentation into the plastid is controlled via this transporter. It was,

however, demonstrated that knockout mutants of pSuT had a higher fraction of plastidial sucrose, thus indicating an export rather than import function (Patzke et al., 2019). While this does not answer the question of how sucrose is mobilized into the plastid, it demonstrates that the balance of plastidial sucrose is tightly regulated and a balanced flux between import (or synthesis) and export is required to ensure optimal acclimation to cold. Finally, the role of sucrose in the plastid remains allusive as well. While it has been reported, that plastidial sugars, such as raffinose, can stabilize thylakoid membranes under cold stress (Knaupp et al., 2011), such function has been reported for sucrose only *in vitro* (Hincha et al., 2003).

A distinct accumulation of fructose in eastern accessions and glucose in western accessions was observed in the vacuole under cold, which indicated that the enzymatic pathways governing the metabolism of these sugars may be of importance as well. Notably, the phosphorylation of glucose and fructose by HXK1 and fructokinase(s), respectively, is a central reaction in plant metabolism and plays an important role in plant stress response. HXK1 has been linked to enhanced heat and drought tolerance and functions as a conserved sugar sensor, possibly regulating stomatal aperture and impacting photosynthesis directly (Granot & Kelly, 2019; Lehretz et al., 2021; Moore et al., 2003). On the other hand, fructokinases drive carbon flow into essential metabolic pathways such as glycolysis and the tricarboxylic acid cycle, providing substrates for respiration and amino acid synthesis. The observed differences in enzyme activity (chapter 2.1), particularly in response to temperature changes, suggest that the ability of different accessions to acclimate to dynamic temperature regimes may be rooted in their differential capacities for hexose phosphorylation. This enzymatic variation could thus influence respiratory and photosynthetic acclimation, ultimately affecting plant fitness in fluctuating environmental conditions (Kelly et al., 2017).

While the correlation between the maximal ETR and subcellular sugars was striking, the correlation between sugars and the residuals showed a more complicated pattern. For instance, vacuolar sucrose was positively correlated with the residuals in eastern accessions acclimated to 34°C and measured at 4°C, suggesting that sucrose remobilization from the vacuole helps stabilize photosynthesis at low temperatures. This was further supported by a negative correlation between cytosolic sucrose and residuals. However, in western accessions acclimated and measured at 34°C, vacuolar sucrose showed a negative correlation with residuals, likely due to significant enzymatic rate changes between 4°C and 34°C.

These findings suggest that conditions stabilizing photosynthesis depend on specific stress factors and metabolite concentrations, making it difficult to generalize. Previously, it was discussed that metabolic regulation differs dramatically between 22°C and 4°C (Nägele, 2022). To fully understand these stabilizing effects, temperature-specific analysis of the Jacobian matrix, possibly using an SKM approach and Arrhenius equation scaling, may be useful.

Interestingly, plants previously exposed to low temperatures exhibited a more stable ETR curve at high temperatures compared to those exposed to 22°C, indicating that some physiological changes are conserved, enhancing photosynthetic stability across varying conditions. A key factor in this stability seems to be sucrose remobilization from the vacuole to the cytosol, along with an increased sucrose-to-starch ratio, which was observed in plants acclimated to both low and high temperatures. These changes likely influence photosynthetic stability, as carbon partitioning is critical for maintaining metabolic homeostasis during cold acclimation (Herrmann et al., 2019).

These findings, together with the observed correlation with the maximal ETR, highlight the importance of understanding metabolic regulation on a subcellular level. Particularly, the subcellular distribution of sucrose was found to play a vital role in adapting the cellular homeostasis to a change in temperature.

3.2 Stabilization of carbon assimilation by photorespiration

In the scope of the second project, the role of photorespiration in stabilizing carbon assimilation was analyzed. The project set out to answer two key questions. The first being whether the location and structure of the photorespiratory pathways promotes or decreases the stability of the CBBC. The second question set out to unravel the role of 2-PG in the regulation of the CBBC. Here, a SKM approach was applied which used normalized saturation parameters for modeling instead of explicit enzymatic parameters such as the V_{max} and K_m. The stability of a metabolic steady state was then analyzed. In order to analyze the distribution of spectral abscissa (maximal real part of eigenvalues of the Jacobian matrix, which are indicative of the systems stability) of a given network, parameters were repeatedly randomly sampled and the corresponding eigenvalues were determined in a monte-carlo experiment.

The analysis revealed, that indeed the oxygenation of RuPB had a stabilizing effect on the function of the CBBC by itself. Here, the presence of the photorespiratory pathway, which reintroduces carbon back to the CBBC, was of secondary importance to the stability. This results from the observation, that auto-catalytic cycles, such as the CBBC, are not stable (Reznik & Segrè, 2010). A perturbation will be passed throughout the cycle and lead to an exponential deviation of a steady state. As such, the CBBC is inherently unstable when operating in a linear-range (Hahn, 1991). Without photorespiration, the stabilization of the cycle can be achieved by strongly regulating cyclic reactions downstream of export branches or by having these operate close to saturation. This was reflected in the analysis of the CBBC without photorespiration where stability was only observed with (i) a high export of TPs for sucrose synthesis, and (ii) with TPI operating close at saturation, thus forcing perturbations to be buffered by the export.

The oxygenation of RuBP, however, allows perturbations to be buffered by exporting 2 carbon atoms from the CBBC in the form of 2-PG, while not requiring a high sucrose synthesis rate. It is situated at a key position in the cycle where it influences all downstream fluxes, thus permitting perturbations to be

buffered more easily than at a later stage, making the stabilizing effect of an export reaction more efficient. These effects are demonstrated in Fig. 8 for model simulations of a substantially simplified CBBC considering linear mass-action kinetics. The observations of Fig. 8 can be generalized to a full model considering nonlinear dynamics with physiological metabolite concentrations and fluxes, as was shown in chapter 2.2. A pure export of RuBP would also promote an increase in the stability of the CBBC (Fig. 8 C). However, the flux through a RuBP export, needed to completely stabilize the system, would be higher than the RuBP regeneration rate, thus being impossible, highlighting the unique role of the oxygenation reaction of RuBP in stabilizing the CBBC.

These findings suggested, that photorespiration represents a trade-off function between the carbon assimilation rate and the stability of metabolism. In addition, these stabilizing effects allow for less stringent regulation of TP allocation towards reactions of the CBBC and export for sucrose synthesis, allowing a higher flux of carbon going towards F6P. As such, it was shown that photorespiration is necessary for maintaining a physiological rate of starch synthesis which would otherwise not be possible.

Besides the influence of the oxygenation reaction, photorespiration exhibits control over the CBBC via the inhibition of TPI and SBPase by 2-PG. It is thus capable of controlling fluxes of GAP utilization and regulates Starch accumulation (Flügel et al., 2017). As mentioned previously, autocatalytic cycles can be stabilized by regulating the downstream reactions of the export. It is thus tempting to consider stabilizing effects of the CBBC via the regulation of TPI and SBPase. When analyzing the impact of these interactions without the context of other regulatory effects, it was observed that both inhibition of TPI and SBPase decreased the stability of the CBBC. The interaction of 2-PG with these reactions does, however, not exist in a vacuum, with many reactions of the CBBC being regulated (Kadereit et al., 2014). As such, the regulatory context of a metabolic network is important when gaging inhibitory interactions, as they can profoundly change the dynamics of a system.
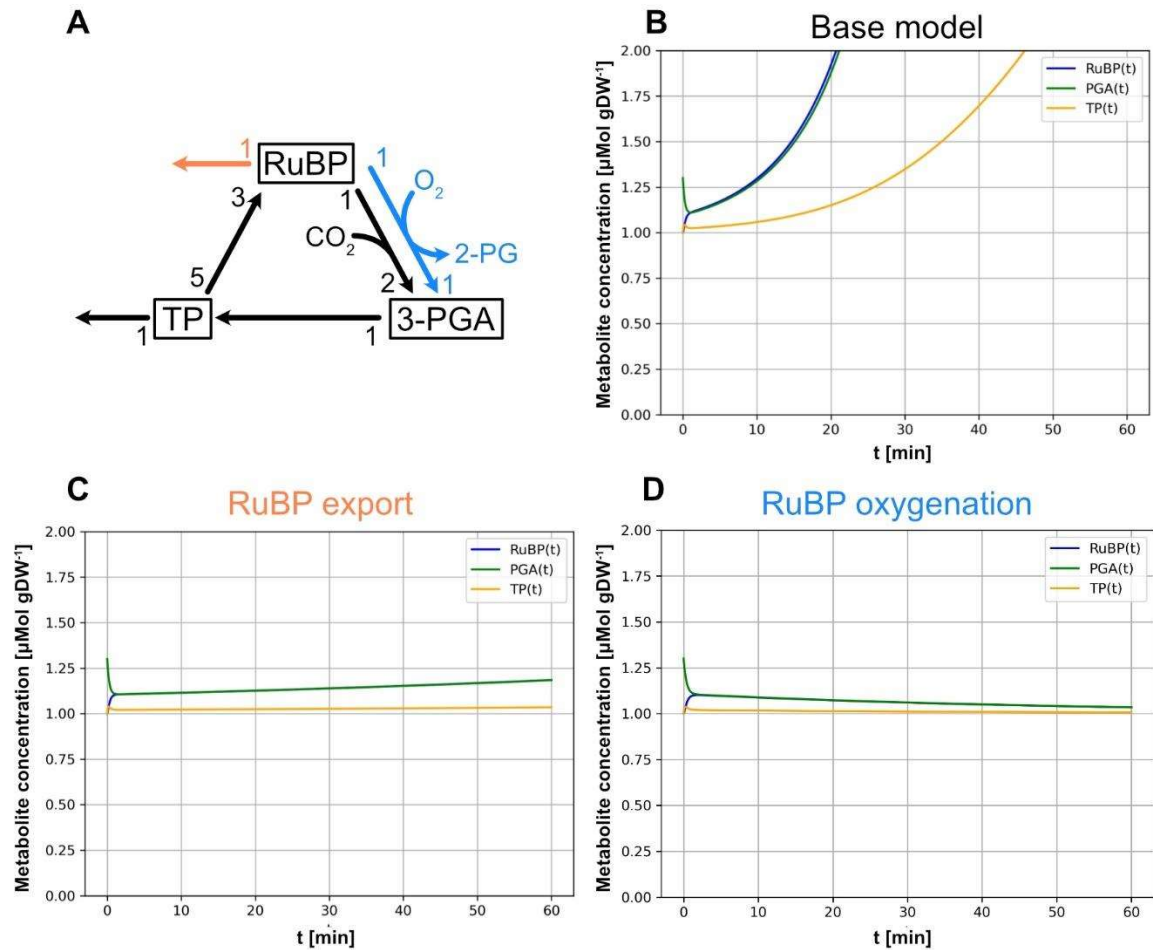
Fig. 8: Stabilization of an autocatalytic cycle by Rubisco. Demonstration of how the oxygenation reaction of RuBP stabilizes the CBBC on toy data. Stoichiometry is indicated by numbers next to reaction arrows. The model was simulated assuming a toy steady state of 1mM for all metabolites to allow for easier model formulation. Stabilization occurs via the location and high flux capacity of the oxygenation reaction. A) Schematic of model structure used. Black induced the base model, orange a model with an added toy export of RuBP, and blue a model with RuBP oxygenation. B) Simulation results for the base model using starting concentrations of RuBP(0) = 1 mM, PGA(0) = 1.3 mM, and TP(0) = 1 mM. C) Simulation results with an added RuBP export. 85% of carbon was simulated to be exported via RuBP and 15% via TPs. Starting concentration was the same as for B. If all carbon is exported via RuBP, the highest eigenvalue becomes 0. The model demonstrates less instability, compared to when carbon is exported at the level of TPs. This is a consequence of complicated stoichiometry of the CBBC. D) Simulation results of a model containing RuBP oxygenation. Oxygenation reaction rate was set to 40% of RuBP consumption. Starting concentration was the same as B. The high flux though the oxygenation reaction acts as an export capable of stabilizing the system, which is not possible with a pure RuBP export. Higher oxygenation fluxes decrease eigenvalues and result in a more responsive system.

The analysis of the regulatory context is, however, complicated by a host of challenges. Although much effort has been put into finding regulatory interactions of the CBBC, the picture is not complete with new interactions still being discovered (Flügel et al., 2017). In addition, the exact kinetic properties of enzymatic regulation is not trivial to incorporate into a model as they rely on the knowledge of the regulatory mechanism and inhibitory constants (Klipp et al., 2016). The SKM approach used within this project partially negates such a problem, as inhibitory parameters are normalized. As such, one way of analyze stabilizing effects, is to treat possible metabolite-reaction interactions as parameters which are

optimized to boost the stability of the system. For such an approach, possible interactions can be found in literature and incorporated into the model. The optimized value of the normalized regulation term thus reflects the regulatory strength in the most stable model, which can then be compared to physiological data in literature.

The project thus proposed a novel analysis approach focused on discrete parameter. In this approach the normalized regulation term is fixed to one of four values, corresponding to either activation, no regulation, weak inhibition, or strong inhibition. An algorithm based on a Branch-and-Bound approach then finds combinations of discrete parameters which result in the most stable system and any solution which is not significantly worse, based on a z-test.

In brief, a Branch-and-Bound algorithm can be envisioned as forming a tree in which one parameter is fixed to a discrete value in each layer. The breaches represent all discrete possibilities available, with low performing branches being pruned based on a heuristic solution. This greatly simplifies the combinatory problem posed by the possible parameter space. In the project, 21 parameters were considered which results in $4^{21} = 4 * 10^{12}$ possible combinations. If all combinations would be considered, this would result in an approximate computation time of 26 years (MATLAB® R2021a, Intel® Core™ i7-10700 @ 2.90 GHz). This could be greatly reduced to a computation time of less than 700 h, by pruning combinations which were significantly worse than a heuristic solution. The pruning of branches results from the fact, that fixing a parameter to a discrete value will result in a less optimized system compared to a continuous parameter which can take any value. As such, if a branch is not fully developed (i.e. not all parameters are fixed to a discrete value) and performs worse than the current best discrete solution, it can be pruned. As the proportion of stable solutions of each solution depends on a monte-carlo simulation, the pruning of solutions was performed via a one-sided z-test using a critical value of p < 0.01. A schematic overview of the modified BnB algorithm used in this study is presented in Fig. 9. Detailed information of the Particle Swarm Algorithm (PSO) used to optimize continuous parameters can be viewed in the material and methods section in chapter 2.2.
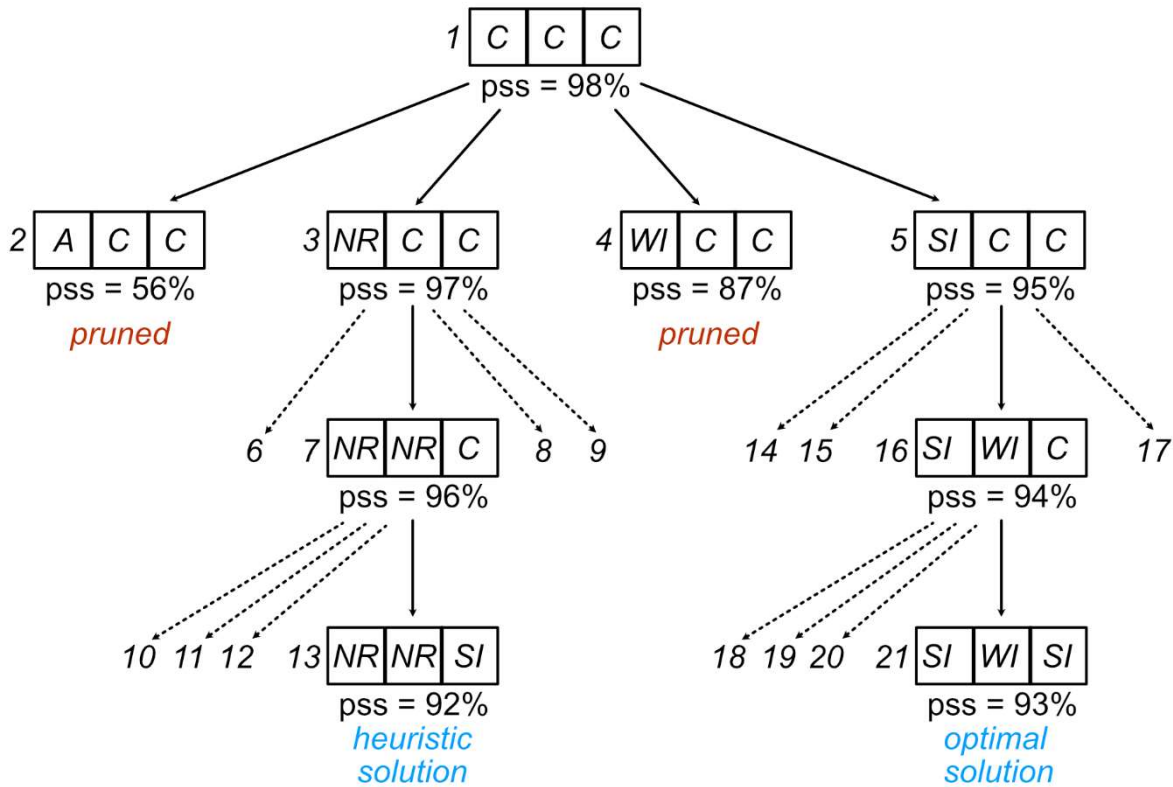
Fig. 9: Schematic overview of the BnB algorithm used in this study with 3 parameters. C: continuous parameter. A: activation (fixed to 1). NR: no regulation (fixed to 0). WI: weak inhibition (fixed to -0.1). SI: strong inhibition (fixed to -0.99). pss: proportion of stable solutions. Each node not in the final layer is optimized using a particle swarm (PSO) approach. The dotted lines indicate nodes which are less stable than the current best node and are not explicitly shown in this overview for the sake of space. The number indicates the order of computation. First, all parameters are left continuous and the pss is obtained after PSO. In a second step the first parameter is fixed leading to 4 nodes (2-5). Node 3 possesses the highest pss and is developed next by fixing the second parameter, leading to nodes 6-9. Again, the best node (7) is developed next, leading to first fully developed nodes (10 − 13). The best of these developed nodes (13) represents the heuristic solution, which is used to filter out low performing nodes which are significantly worse than the heuristic solution based on a one-sided z-test using a critical value of p < 0.01. The best node which was not pruned (5) is then further developed, continuing this process until the next fully developed solutions. The heuristic can then be updated, if a more optimal solution is found, leading to more nodes being pruned. This process is repeated until all nodes are either fully developed or pruned. The best solution found, thus represents the optimal solution. In a final step, all fully developed solutions which are significantly worse than the most optimal solution, are again pruned based on a z-test. The fully developed solutions which remain thus represent the parameter space capable of optimally stabilizing the system. As obtaining the pss relies on a monte-carlo simulation, some randomness is inherent to this algorithm, especially considering the multitude of z-test which are performed. As such the reported parameter space of the most optimal solutions in and of itself is a heuristic.

When analyzing the parameter space of the most stable solutions, it was observed that strong inhibition of SBPase by 2-PG was favored, while no inhibition to weak inhibition of TPI was favored. This indicates that indeed 2-PG possesses an important regulatory function in a full context of enzyme inhibition. In *A. thaliana* it was reported that the K_i of 2-PG was approximately 10 μM for SBPase and 36 μM for TPI (Flügel et al., 2017). This suggests that indeed, the inhibitory effect is stronger for SBPases as compared to TPI, matching the simulation results found for optimal regulation. As such stabilizing effects were only

uncovered in the full regulatory context. This highlights the importance of the BnB approach when considering the impact of inhibition. The analysis of enzyme inhibition without such context can thus lead to misleading results.

In conclusion, this project suggests that photorespiration represents a trade-off function between the carbon assimilation rate and metabolic stability. In addition, it was shown that photorespiration is needed in order to maintain physiological starch synthesis rates. A shift in carbon portioning towards sucrose synthesis is, however, capable of boosting the stability of the full model with photorespiration. Such a scenario may be beneficial under increased levels of plant stress. Indeed, such a change of carbon allocation was observed in *A. thaliana* when subjected to low temperatures (Strand et al., 1997; Strand et al., 1999). Finally, this study supports and expands on the suggested regulatory function of 2-PG (Flügel et al., 2017). It was shown that 2-PG can stabilize the CBBC by strongly inhibiting SBPase and weakly inhibiting TPI. These observations were matched in the reported K_i values for the two enzymes.

3.3 Interaction of photorespiration with metabolic pathways

The final project presented in this dissertation aimed to unravel the response of metabolism of the *A. thaliana* under elevated atmospheric CO_2 concentrations. For this, mutants affected in the photorespiratory pathway were analyzed together with wild type plants. In brief, *hpr1-1* plants lacked the enzyme Hydroxypyruvate reductase 1 (HPR1), which is directly involved in the photorespiratory pathway. The heterozygous knockout line *h-bou* was affected in A BOUT DE SOUFFLE (BOU), which is hypothesized to be a mitochondrial glutamate transporter needed to synthesis of THF (Eisenhut et al., 2013). A heterozygous knockout of BOU was chosen in this study, as the homozygous *bou* mutant had a strong stunted phenotype under aCO_2. Finally, *hxk1* was deficient in HXK1, which functions both as a sugar sensor involved in signaling and as a kinase that phosphorylates glucose and fructose. Recent reports have implicated HXK1 in the regulation of photorespiration, providing a rationale for its inclusion in this project (Küstner et al., 2019).

Plants were initially grown under aCO_2 (approx. 400 ppm) before they were transferred to eCO_2 (1000 ppm), where the proportion of Rubisco catalyzed oxygenation of RuBP was significantly reduced. Transcriptomes were analyzed together with proteomes and subcellular metabolomes at ambient CO_2 and after 1, 3, 5, and 7 days at elevated CO_2. This multi-omics approach was designed to provide detailed insights into regulation of photorespiration and primary metabolism, revealing potential regulatory interactions within the carbon assimilation process.

The multi-omics data obtained in such an approach represents a highly dimensional tensor, making analysis and interpretation challenging. A common method used to analyze such data is to project the variables to a set of components, which are made up of linear combinations of the original variables. This allows for reduction of the dimension of the tensor which supports the identification and understanding of correlated structures within the data set. Such an analysis can be, for example,

completed with the R package mixOmics, which additionally offers sparse multivariate models, thus allowing key variables to be identified (Rohart et al., 2017). While such an approach can provide a comprehensive statistical view on the data, it hardly provides information about biological pathway regulations. As such, an SQLite Database was developed for this project in conjunction with a Python Application Programming Interface (API), which enabled the available multi-omics data to be queried based on biological function (Fig. 10). When uploading the data to the SQLite DB, the API pulled additional relevant biological information such as the GO-Terms from Uniprot, Kegg, and the PantherDB (Kanehisa, 2019; Kanehisa et al., 2023; Kanehisa & Goto, 2000; The UniProt, 2023; Thomas et al., 2022). The data obtained in such a way was then passed on to a python class which handles the projection to components, following a principle component analysis (PCA) or a partial least-squares regression (PLS), both of which can also be performed in a sparse manner to promote variable selection. This approach allowed for formulation of a novel hypothesis, focused on relevant biological terms such as "Photorespiration" or "Chloroplast".

In the *hpr1-1* mutant, glycerate was observed to accumulate in a pattern similar to glycine and serine. All three metabolites accumulated under aCO_2 in the mutant compared to the wild type, but their levels dropped to match the wild type when shifted to eCO_2. This pattern is expected for glycine and serine since the disrupted photorespiratory pathway in *hpr1-1* creates a bottleneck under the high photorespiratory flux of $aCO2$. This bottleneck eases when the flux through the pathway is reduced under $eCO2$.

However, it's unclear why glycerate behaves similarly. Since HPR1 reduces hydroxypyruvate to glycerate in the photorespiratory cycle, knocking out this enzyme should theoretically lead to the opposite effect. An artifact can be ruled out, as glycerate accumulation in *hpr1-1* has been previously reported, but no clear explanation has been provided for this observation (Timm et al., 2008).

The data analysis approach developed for this project proved instrumental, for shedding light on such complex phenotypes. The data suggested, that cysteine was being synthesized from the accumulating serine. Cysteine was then desulfurated via L-CYSTEINE DESULFHYDRASE 1 (DES1) in order to from pyruvate plus ammonia and sulfide. The pyruvate generated in this way, along with other sources, was then seemingly utilized in the gluconeogenic pathway to generate 3P-glycerate. These observations, however, do not answer the question as to how glycerate is produced in the cytosol of hpr-1. One possible explanation could be in relation to a cytosolic phosphoglycerate phosphatase which was previously reported to exist in plants (Randall & Tolbert, 1971). However, this enzyme remains to be further analyzed. Taken together, the data suggested, that the regulation of cysteine synthesis and degradation is significantly influenced by photorespiration. Consequently, it is conceivable that photorespiration represents a key player in modulating sulfide and cysteine signalling, which in turn, impacts stomatal movement, photosynthesis, and resistance to biotic stress (Romero et al., 2014).
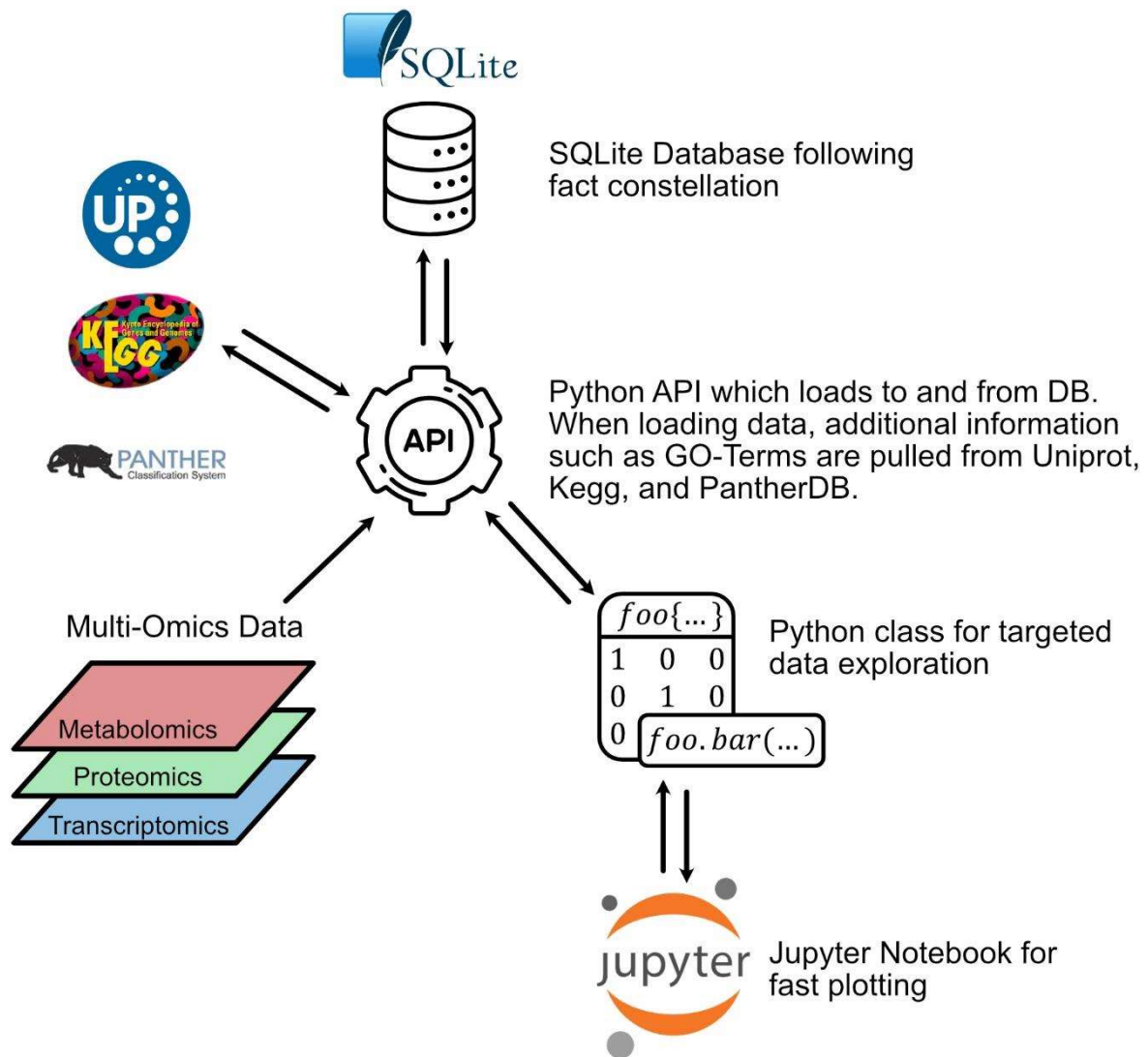
Fig. 10: Overview of multi-omics tech-stack. During the process of loading multi-omics data into the SQLite database, additional information regarding the genes and metabolites is pulled and uploaded into a dimension table. This additional data can then be used via the API to query the database based on biological go-terms such as "photorespiration" or "chloroplast". Such go-terms can be chained for an even more granular view of data. The data retrieved in such a manner is then used to populate an object from a data exploration class. This object possesses several methods capable of performing multivariate data modeling such as PCA or PLS, with associated plots being easily viewable in a jupyter notebook.

The data pipeline presented in this project was, however, not only useful in characterizing the response *hpr1*-1 to eCO$_2$. Such an approach also proved useful when analyzing the other genotypes included in this study. In *hxk1* querying based on biological functions, such as redox homeostasis, fatty acid biosynthesis, and hormone signaling proved crucial for understanding complex interactions and for comprehending the broader impact of HXK1 on plant metabolism and stress responses.

On the surface level, *hxk1* demonstrated a significant increase in soluble sugars under eCO$_2$. Specifically, hexoses accumulated in the cytosol, while sucrose was stored in the vacuole, suggesting

a slow-down in sucrose cycling due to reduced HXK1 activity. A deeper analysis of the subcellular metabolomes of both Col-0 and *hxk1* revealed contrasting patterns in pyruvate allocation between chloroplasts and mitochondria, suggesting differential activity of plastidial glycolysis. Under aCO$_2$, *hxk1* accumulated pyruvate in the plastid as compared to Col-0. This in turn could indicate that HXK1 deficiency might impair glycolytic flux and affect the redox status of the NAD pool. When analyzing this further, it was found that proteins associated with go-terms "cell redox homeostasis" and "TCA cycle" showed a delayed response in *hxk1* when transferred to eCO2 as compared to the other genotypes analyzed in this study. This effect was particularly evident for catalase 2 (CAT2), an enzyme responsible for dissipating hydrogen peroxide in photorespiration. Together with other evidence (see chapter 2.3), this suggested that HXK1 might influence oxylipin metabolism through its impact on glycolysis, potentially affecting the biosynthesis of polyunsaturated fatty acids (PUFAs) and phytohormones like jasmonic acid (JA). It was additionally found, that *hxk1* may impact fatty acid biosynthesis in chloroplasts, as the proteome of this biosynthetic pathway revealed opposite trends for *hxk1* and the wild type. Taken together, this suggests a complex role of HXK1 extending beyond carbohydrate metabolism with this enzyme being involved in redox balancing, fatty acid and lipid metabolism and integrate ROS with phytohormonal signaling.

With the help of such a biological function-driven data approach, the proposed role of BOU as a mitochondrial glutamate transporter was revisited (see chapter 2.3). Strikingly, it was shown that glutamate tended to accumulate in the mitochondria of *h-bou*, calling into question if BOU does indeed function as a glutamate transporter *in vivo* and not just as reported *in vitro* (Eisenhut et al., 2013). This suggested that BOU might act as a carnitine /acylcarnitine transporter, as was initially suggested (Lawand et al., 2002). As such, it was proposed, that BOU transports fatty acid carnitine esters into the mitochondrial matrix, where they participate in the lipoylation of decarboxylase enzymes. Indeed, an increase in transcript levels of Lipoyl synthase 1 (LIP1) involved in lipoic acid *de novo* synthesis was observed in *h-bou* under aCO$_2$ which return to wild type levels upon transfer to eCO$_2$. This suggested, that mitochondrial decarboxylases featuring E2 subunits would be directly affect by the reduced availability of lipoate in the mitochondria of *h-bou*. At aCO$_2$, elevated mitochondrial pyruvate levels indicated reduced turnover, despite increased expression of three PDH subunits, including the lipoate-dependent E2 subunit. After transitioning to eCO2, the expression of these subunits decreased along with pyruvate levels, suggesting more efficient turnover, likely due to reduced competition for lipoic acid between the glycine cleavage system and PDH as photorespiration declined.

Overall, the study's omics approach, along with a biological function-driven data pipeline provided new insights into the complex effects of mutations and helped to characterize non-intuitive phenotypes as observed in *hpr1-1* and *h-bou*. Furthermore, this project highlighted the limitations of whole-cell metabolome analysis for understanding highly compartmentalized processes like photorespiration. This project underscored the intricate regulatory interactions between photorespiration and the broader carbon assimilation process.

3.4 Conclusion

In an era of increasing environmental fluctuations, sessile organisms like plants face unique challenges in adapting to rapidly changing conditions. Plants must rely on their internal physiological mechanisms to cope with stressors such as temperature shifts, elevated CO_2 levels, and altered precipitation patterns. Understanding how plants respond to these environmental changes is crucial for developing strategies to enhance crop resilience and ensure ecosystem stability. As climate change increases both the frequency and magnitude of environmental fluctuation (Masson-Delmotte et al., 2021), gaining deeper insights into plant acclimation processes becomes ever more essential for safeguarding food security and maintaining the balance of natural ecosystems.

This dissertation highlights the critical role of advanced experimental strategies and computational algorithms in advancing our understanding of plant responses to environmental fluctuations, particularly in the context of climate variability. By leveraging these innovative approaches, the research has revealed key insights into plant metabolism and carbon assimilation. The stabilizing effect of specific subcellular carbohydrate distributions, particularly in plastids, emphasized the importance of metabolic regulation at the subcellular level. In addition, the metabolic plasticity provided by the oxygenation reaction catalyzed by Rubisco, provided compelling evidence for a trade-off function between the carbon assimilation rate and buffering fluctuations away from the CBBC. It was further found, that metabolic stability could be increased by allocating more carbon towards sucrose synthesis in times of stress. Taken together, these findings deepen the current understanding of, how plants sustain their physiological balance under fluctuating environmental conditions, but also how they adapt at the metabolic level to preserve functionality. Finally, novel interactions between metabolic pathways and photorespiration where uncovered, which illustrate the complexity and adaptability of plant metabolic networks in coping with environmental perturbations. As such, photorespiration, though previously seen as a futile process, emerges here as a vital adaptive mechanism that interacts with various metabolic pathways to aid plants in coping with environmental stressors and in stabilizing carbon assimilation.

4. References

Aguilera-Alvarado, G. P., & Sánchez-Nieto, S. (2017). Plant hexokinases are multifaceted proteins. *Plant and Cell Physiology*, *58*(7), 1151-1160. https://doi.org/10.1093/pcp/pcx062

Anderson, L. E. (1971). Chloroplast and cytoplasmic enzymes II. Pea leaf triose phosphate isomerases. *Biochimica et Biophysica Acta - Enzymology*, *235*(1), 237-244. https://doi.org/10.1016/0005-2744(71)90051-9

Atanasov, V., Fürtauer, L., & Nägele, T. (2020). Indications for a central role of hexokinase activity in natural variation of heat acclimation in *Arabidopsis thaliana*. *Plants*, *9*(7). https://doi.org/10.3390/plants9070819

Athanasiou, K., Dyson, B. C., Webster, R. E., & Johnson, G. N. (2010). Dynamic acclimation of photosynthesis increases plant fitness in changing environments. *Plant Physiology*, *152*(1), 366-373. https://doi.org/10.1104/pp.109.149351

Bar-On, Y. M., Phillips, R., & Milo, R. (2018). The biomass distribution on Earth. *Proceedings of the National Academy of Sciences*, *115*(25), 6506-6511. https://doi.org/10.1073/pnas.1711842115

Bassham, J. A., Benson, A. A., Kay, L. D., Harris, A. Z., Wilson, A. T., & Calvin, M. (1954). The path of carbon in photosynthesis. XXI. The cyclic Regeneration of carbon dioxide acceptor1. *Journal of the American Chemical Society*, *76*(7), 1760-1770. https://doi.org/10.1021/ja01636a012

Bisswanger, H. (2017). pH and temperature dependence of enzymes. *Wiley–VCH Verlag, Berlin, Germany*, 145-147. https://doi.org/10.1002/9783527806461.ch6

Bowes, G., Ogren, W. L., & Hageman, R. H. (1971). Phosphoglycolate production catalyzed by ribulose diphosphate carboxylase. *Biochemical and Biophysical Research Communications*, *45*(3), 716-722. https://doi.org/10.1016/0006-291X(71)90475-X

Breazeale, V. D., Buchanan, B. B., & Wolosiuk, R. A. (1978). Chloroplast sedoheptulose 1,7-bisphosphatase: Evidence for regulation by the ferredoxin/thioredoxin system. *Zeitschrift für Naturforschung C*, *33*(7-8), 521-528. https://doi.org/doi:10.1515/znc-1978-7-812

Busch, F. A. (2020). Photorespiration in the context of Rubisco biochemistry, CO_2 diffusion and metabolism. *The Plant Journal*, *101*(4), 919-939. https://doi.org/10.1111/tpj.14674

Cano-Ramirez, D. L., Carmona-Salazar, L., Morales-Cedillo, F., Ramírez-Salcedo, J., Cahoon, E. B., & Gavilanes-Ruíz, M. (2021). Plasma membrane fluidity: An environment thermal detector in plants. *Cells*, *10*(10). https://doi.org/10.3390/cells10102778

Carrera, D. Á., George, G. M., Fischer-Stettler, M., Galbier, F., Eicke, S., Truernit, E., Streb, S., & Zeeman, S. C. (2021). Distinct plastid fructose bisphosphate aldolases function in photosynthetic and non-photosynthetic metabolism in *Arabidopsis*. *Journal of Experimental Botany*, *72*(10), 3739-3755. https://doi.org/10.1093/jxb/erab099

Choudhury, F. K., Rivero, R. M., Blumwald, E., & Mittler, R. (2017). Reactive oxygen species, abiotic stress and stress combination. *The Plant Journal*, *90*(5), 856-867. https://doi.org/10.1111/tpj.13299

Dodd, A. N., Borland, A. M., Haslam, R. P., Griffiths, H., & Maxwell, K. (2002). Crassulacean acid metabolism: plastic, fantastic. *Journal of Experimental Botany*, *53*(369), 569-580. https://doi.org/10.1093/jexbot/53.369.569

Eisenhut, M., Planchais, S., Cabassa, C., Guivarc'h, A., Justin, A. M., Taconnat, L., Renou, J. P., Linka, M., Gagneul, D., Timm, S., Bauwe, H., Carol, P., & Weber, A. P. (2013). *Arabidopsis* A BOUT DE SOUFFLE is a putative mitochondrial transporter involved in photorespiratory metabolism and is required for meristem growth at ambient CO_2 levels. *The Plant Journal*, *73*(5), 836-849. https://doi.org/10.1111/tpj.12082

Elias, M., Wieczorek, G., Rosenne, S., & Tawfik, D. S. (2014). The universality of enzymatic rate–temperature dependency. *Trends in Biochemical Sciences*, *39*(1), 1-7. https://doi.org/10.1016/j.tibs.2013.11.001

Erb, T. J., & Zarzycki, J. (2018). A short history of RubisCO: the rise and fall (?) of nature's predominant CO_2 fixing enzyme. *Current Opinion in Biotechnology*, *49*, 100-107. https://doi.org/10.1016/j.copbio.2017.07.017

Farquhar, G. D., von Caemmerer, S., & Berry, J. A. (1980). A biochemical model of photosynthetic CO_2 assimilation in leaves of C3 species. *Planta*, *149*(1), 78-90. https://doi.org/10.1007/BF00386231

Flügel, F., Timm, S., Arrivault, S., Florian, A., Stitt, M., Fernie, A. R., & Bauwe, H. (2017). The photorespiratory metabolite 2-phosphoglycolate regulates photosynthesis and starch accumulation in *Arabidopsis*. *The Plant Cell*, *29*(10), 2537-2551. https://doi.org/10.1105/tpc.17.00256

Foyer, C. H., Bloom, A. J., Queval, G., & Noctor, G. (2009). Photorespiratory metabolism: genes, mutants, energetics, and redox signaling. *Annual Review Plant Biology*, *60*, 455-484. https://doi.org/10.1146/annurev.arplant.043008.091948

Fürtauer, L., Küstner, L., Weckwerth, W., Heyer, A. G., & Nägele, T. (2019). Resolving subcellular plant metabolism. *The Plant Journal*, *100*(3), 438-455. https://doi.org/10.1111/tpj.14472

Fürtauer, L., & Nägele, T. (2016). Approximating the stabilization of cellular metabolism by compartmentalization. *Theory in Biosciences*, *135*(1), 73-87. https://doi.org/10.1007/s12064-016-0225-y

Fürtauer, L., Weckwerth, W., & Nägele, T. (2016). A benchtop fractionation procedure for subcellular analysis of the plant metabolome. *Frontiers in Plant Science*, *7*, 1912. https://doi.org/10.3389/fpls.2016.01912

Gan, P., Liu, F., Li, R., Wang, S., & Luo, J. (2019). Chloroplasts— Beyond energy capture and carbon fixation: Tuning of photosynthesis in response to chilling stress. *International Journal of Molecular Sciences*, *20*(20). https://doi.org/10.3390/ijms20205046

Gilmour, S. J., Hajela, R. K., & Thomashow, M. F. (1988). Cold acclimation in *Arabidopsis thaliana*. *Plant Physiology*, *87*(3), 745-750. https://doi.org/10.1104/pp.87.3.745

Granot, D., & Kelly, G. (2019). Evolution of guard-cell theories: The story of sugars. *Trends in Plant Science*, *24*(6), 507-518. https://doi.org/10.1016/j.tplants.2019.02.009

Grimbs, S., Selbig, J., Bulik, S., Holzhütter, H.-G., & Steuer, R. (2007). The stability and robustness of metabolic states: identifying stabilizing sites in metabolic networks. *Molecular Systems Biology*, *3*(1), 146. https://doi.org/10.1038/msb4100186

Hahn, A., Vonck, J., Mills, D. J., Meier, T., & Kühlbrandt, W. (2018). Structure, mechanism, and regulation of the chloroplast ATP synthase. *Science*, *360*(6389), eaat4318. https://doi.org/10.1126/science.aat4318

Hahn, B. D. (1991). Photosynthesis and photorespiration: Modelling the essentials. *Journal of theoretical biology*, *151*(1), 123-139. https://doi.org/10.1016/S0022-5193(05)80147-X

Hannah, M. A., Heyer, A. G., & Hincha, D. K. (2005). A global survey of gene regulation during cold acclimation in *Arabidopsis thaliana*. *PLOS Genetics*, *1*(2), e26. https://doi.org/10.1371/journal.pgen.0010026

Herrmann, H. A., Schwartz, J.-M., & Johnson, G. N. (2019). Metabolic acclimation—a key to enhancing photosynthesis in changing environments? *Journal of Experimental Botany*, *70*(12), 3043-3056. https://doi.org/10.1093/jxb/erz157

Hincha, D. K., Zuther, E., & Heyer, A. G. (2003). The preservation of liposomes by raffinose family oligosaccharides during drying is mediated by effects on fusion and lipid phase transitions. *Biochimica et Biophysica Acta - Biomembranes*, *1612*(2), 172-177. https://doi.org/10.1016/S0005-2736(03)00116-0

Hodges, M., Dellero, Y., Keech, O., Betti, M., Raghavendra, A. S., Sage, R., Zhu, X.-G., Allen, D. K., & Weber, A. P. M. (2016). Perspectives for a better understanding of the metabolic integration of photorespiration within a complex plant primary metabolism network. *Journal of Experimental Botany*, *67*(10), 3015-3026. https://doi.org/10.1093/jxb/erw145

Hoermiller, I. I., Naegele, T., Augustin, H., Stutz, S., Weckwerth, W., & Heyer, A. G. (2017). Subcellular reprogramming of metabolism during cold acclimation in *Arabidopsis thaliana*. *Plant, Cell & Environment*, *40*(5), 602-610. https://doi.org/10.1111/pce.12836

Hurry, V. (2017). Metabolic reprogramming in response to cold stress is like real estate, it's all about location. *Plant, Cell & Environment*, *40*(5), 599-601. https://doi.org/10.1111/pce.12923

Islam, M. M., Schroeder, W. L., & Saha, R. (2021). Kinetic modeling of metabolism: Present and future. *Current Opinion in Systems Biology*, *26*, 72-78. https://doi.org/10.1016/j.coisb.2021.04.003

Järvi, S., Gollan, P. J., & Aro, E.-M. (2013). Understanding the roles of the thylakoid lumen in photosynthesis regulation. *Frontiers in Plant Science*, *4*. https://doi.org/10.3389/fpls.2013.00434

Kadereit, J. W., Körner, C., Kost, B., & Sonnewald, U. (2014). *Strasburger– Lehrbuch der Pflanzenwissenschaften*. Springer-Verlag. ISBN: 978-3-662-61942-1.

Kaiser, E., Morales, A., Harbinson, J., Kromdijk, J., Heuvelink, E., & Marcelis, L. F. M. (2015). Dynamic photosynthesis in different environmental conditions. *Journal of Experimental Botany*, *66*(9), 2415-2426. https://doi.org/10.1093/jxb/eru406

Kanehisa, M. (2019). Toward understanding the origin and evolution of cellular organisms. *Protein Science*, *28*(11), 1947-1951. https://doi.org/10.1002/pro.3715

Kanehisa, M., Furumichi, M., Sato, Y., Kawashima, M., & Ishiguro-Watanabe, M. (2023). KEGG for taxonomy-based analysis of pathways and genomes. *Nucleic Acids Research*, *51*(D1), D587-d592. https://doi.org/10.1093/nar/gkac963

Kanehisa, M., & Goto, S. (2000). KEGG: Kyoto encyclopedia of genes and genomes. *Nucleic Acids Research*, *28*(1), 27-30. https://doi.org/10.1093/nar/28.1.27

Kelly, G., Sade, N., Doron-Faigenboim, A., Lerner, S., Shatil-Cohen, A., Yeselson, Y., Egbaria, A., Kottapalli, J., Schaffer, A. A., Moshelion, M., & Granot, D. (2017). Sugar and hexokinase suppress expression of PIP aquaporins and reduce leaf hydraulics that preserves leaf water potential. *The Plant Journal, 91*(2), 325-339. https://doi.org/10.1111/tpj.13568

Kelly, G. J., & Latzko, E. (1976). Inhibition of spinach-leaf phosphofructokinase by 2-phosphoglycollate. *FEBS Letters*, *68*(1), 55-58. https://doi.org/10.1016/0014-5793(76)80403-6

Klipp, E., Liebermeister, W., Wierling, C., & Kowald, A. (2016). *Systems biology: a textbook*. John Wiley & Sons. ISBN: 978-3-527-31874-2

Klughammer, C., & Schreiber, U. (2008). Complementary PS II quantum yields calculated from simple fluorescence parameters measured by PAM fluorometry and the Saturation Pulse method. *PAM application notes*, *1*(2), 201-247.

Knaupp, M., Mishra, K. B., Nedbal, L., & Heyer, A. G. (2011). Evidence for a role of raffinose in stabilizing photosystem II during freeze-thaw cycles. *Planta*, *234*(3), 477-486. https://doi.org/10.1007/s00425-011-1413-0

Koch, K. (2004). Sucrose metabolism: regulatory mechanisms and pivotal roles in sugar sensing and plant development. *Current Opinion in Plant Biology*, *7*(3), 235-246. https://doi.org/10.1016/j.pbi.2004.03.014

Kölling, K., Thalmann, M., Müller, A., Jenny, C., & Zeeman, S. C. (2015). Carbon partitioning in rabidopsis thaliana is a dynamic process controlled by the plants metabolic status and its circadian clock. *Plant, Cell & Environment*, *38*(10), 1965-1979. https://doi.org/10.1111/pce.12512

Kuhnert, F., Schlüter, U., Linka, N., & Eisenhut, M. (2021). Transport proteins enabling plant photorespiratory metabolism. *Plants*, *10*(5). https://doi.org/10.3390/plants10050880

Küstner, L., Fürtauer, L., Weckwerth, W., Nägele, T., & Heyer, A. G. (2019). Subcellular dynamics of proteins and metabolites under abiotic stress reveal deferred response of the Arabidopsis thaliana hexokinase-1 mutant gin2-1 to high light. *The Plant Journal*, *100*(3), 456-472. https://doi.org/10.1111/tpj.14491

Land, A., & Doig, A. (1960). An automatic method of solving discrete programming problems. *Econometrica*, *28*(3), 497-520.

Lavergne, D., Bismuth, E., & Champigny, M. L. (1974). Further studies of phosphoglycerate kinase and ribulose-5-phosphate kinase of the photosynthetic carbon reduction cycle: Regulation of the enzymes by the adenine nucleotides. *Plant Science Letters*, *3*(6), 391-397. https://doi.org/10.1016/0304-4211(74)90021-2

Lawand, S., Dorne, A.-J., Long, D., Coupland, G., Mache, R. g., & Carol, P. (2002). *Arabidopsis* A BOUT DE SOUFFLE, Which Is homologous with mammalian carnitine acyl carrier, is required for

postembryonic growth in the Light. *The Plant Cell*, *14*(9), 2161-2173. https://doi.org/10.1105/tpc.002485

Lehretz, G. G., Sonnewald, S., Lugassi, N., Granot, D., & Sonnewald, U. (2021). Future-proofing potato for drought and heat tolerance by overexpression of hexokinase and SP6A. *Frontiers in Plant Science*, *11*, 614534. https://doi.org/10.3389/fpls.2020.614534

Lorimer, G. H., & Andrews, T. J. (1973). Plant photorespiration—an inevitable consequence of the existence of atmospheric oxygen. *Nature*, *243*(5406), 359-360. https://doi.org/10.1038/243359a0

Lundmark, M., Cavaco, A. M., Trevanion, S., & Hurry, V. (2006). Carbon partitioning and export in transgenic Arabidopsis thaliana with altered capacity for sucrose synthesis grown at low temperature: a role for metabolite transporters. *Plant, Cell & Environment*, *29*(9), 1703-1714. https://doi.org/10.1111/j.1365-3040.2006.01543.x

Lunn, J. E. (2016). Sucrose metabolism. In *eLS* (pp. 1-9). https://doi.org/10.1002/9780470015902.a0021259.pub2

Masson-Delmotte, V., Zhai, P., Pirani, A., Connors, S. L., Péan, C., Berger, S., Caud, N., Chen, Y., Goldfarb, L., & Gomis, M. (2021). Climate change 2021: the physical science basis. *Contribution of working group I to the sixth assessment report of the intergovernmental panel on climate change*, *2*(1), 2391. ISBN 978-92-9169-158-6

Michelet, L., Zaffagnini, M., Morisse, S., Sparla, F., Pérez-Pérez, M. E., Francia, F., Danon, A., Marchand, C., Fermani, S., Trost, P., & Lemaire, S. D. (2013). Redox regulation of the Calvin–Benson cycle: something old, something new. *Frontiers in Plant Science*, *4*. https://doi.org/10.3389/fpls.2013.00470

Mirkovic, T., Ostroumov, E. E., Anna, J. M., van Grondelle, R., Govindjee, & Scholes, G. D. (2017). Light absorption and energy transfer in the antenna complexes of photosynthetic organisms. *Chemical Reviews*, *117*(2), 249-293. https://doi.org/10.1021/acs.chemrev.6b00002

Moore, B., Zhou, L., Rolland, F., Hall, Q., Cheng, W.-H., Liu, Y.-X., Hwang, I., Jones, T., & Sheen, J. (2003). Role of the *Arabidopsis* glucose sensor HXK1 in nutrient, light, and hormonal signaling. *Science*, *300*(5617), 332-336. https://doi.org/10.1126/science.1080585

Müller, P., Li, X.-P., & Niyogi, K. K. (2001). Non-photochemical quenching. A response to excess light energy. *Plant Physiology*, *125*(4), 1558-1566. https://doi.org/10.1104/pp.125.4.1558

Murphy, D. J., & Walker, D. A. (1982). The properties of transketolase from photosynthetic tissue. *Planta*, *155*(4), 316-320. https://doi.org/10.1007/BF00429458

Nägele, T. (2022). Metabolic regulation of subcellular sucrose cleavage inferred from quantitative analysis of metabolic functions. *Quantitative Plant Biology*, *3*, e10, Article e10. https://doi.org/10.1017/qpb.2022.5

Nägele, T., Stutz, S., Hörmiller, I. I., & Heyer, A. G. (2012). Identification of a metabolic bottleneck for cold acclimation in *Arabidopsis thaliana*. *The Plant Journal*, *72*(1), 102-114. https://doi.org/10.1111/j.1365-313X.2012.05064.x

Niittylä, T., Messerli, G., Trevisan, M., Chen, J., Smith, A. M., & Zeeman, S. C. (2004). A previously unknown maltose transporter essential for starch degradation in leaves. *Science*, *303*(5654), 87-89. https://doi.org/10.1126/science.1091811

Niyogi, K. K., Grossman, A. R., & Björkman, O. (1998). *Arabidopsis* mutants define a central role for the xanthophyll cycle in the regulation of photosynthetic energy conversion. *Plant Cell*, *10*(7), 1121-1134. https://doi.org/10.1105/tpc.10.7.1121

Patzke, K., Prananingrum, P., Klemens, P. A. W., Trentmann, O., Rodrigues, C. M., Keller, I., Fernie, A. R., Geigenberger, P., Bölter, B., Lehmann, M., Schmitz-Esser, S., Pommerrenig, B., Haferkamp, I., & Neuhaus, H. E. (2019). The plastidic sugar transporter pSuT influences flowering and affects cold responses. *Plant Physiology*, *179*(2), 569-587. https://doi.org/10.1104/pp.18.01036

Pfister, B., & Zeeman, S. C. (2016). Formation of starch in plant cells. *Cellular and Molecular Life Sciences*, *73*(14), 2781-2807. https://doi.org/10.1007/s00018-016-2250-x

Pichersky, E., & Gottlieb, L. D. (1984). Plant triose phosphate isomerase isozymes 1: Purification, immunological and structural characterization, and partial amino acid sequences. *Plant Physiology*, *74*(2), 340-347. https://doi.org/10.1104/pp.74.2.340

Poudel, S., Pike, D. H., Raanan, H., Mancini, J. A., Nanda, V., Rickaby, R. E. M., & Falkowski, P. G. (2020). Biophysical analysis of the structural evolution of substrate specificity in RuBisCO. *Proceedings of the National Academy of Sciences*, *117*(48), 30451. https://doi.org/10.1073/pnas.2018939117

Randall, D. D., & Tolbert, N. E. (1971). 3-Phosphoglycerate phosphatase in plants. I. Isolation and characterization from sugarcane leaves. *Journal of Biological Chemistry*, *246*(17), 5510-5517. https://doi.org/10.1016/S0021-9258(18)61935-0

Reznik, E., & Segrè, D. (2010). On the stability of metabolic cycles. *Journal of theoretical biology*, *266*(4), 536-549. https://doi.org/10.1016/j.jtbi.2010.07.023

Rohart, F., Gautier, B., Singh, A., & Lê Cao, K.-A. (2017). mixOmics: an R package for 'omics feature selection and multiple data integration. *bioRxiv*, 108597. https://doi.org/10.1101/108597

Romero, L. C., Aroca, M. Á., Laureano-Marín, A. M., Moreno, I., García, I., & Gotor, C. (2014). Cysteine and cysteine-related signaling pathways in *Arabidopsis thaliana*. *Molecular plant*, *7*(2), 264-276. https://doi.org/10.1093/mp/sst168

Sage, R. F. (2004). The evolution of C4 photosynthesis. *New Phytologist*, *161*(2), 341-370. https://doi.org/10.1111/j.1469-8137.2004.00974.x

Schulman, M. D., & Gibbs, M. (1968). d-glyceraldehyde 3-phosphate dehydrogenases of higher lants 12. *Plant Physiology*, *43*(11), 1805-1812. https://doi.org/10.1104/pp.43.11.1805

Seydel, C., Kitashova, A., Fürtauer, L., & Nägele, T. (2022). Temperature-induced dynamics of plant carbohydrate metabolism. *Physiologia Plantarum*, *174*(1), e13602. https://doi.org/10.1111/ppl.13602

Shi, Q., Sun, H., Timm, S., Zhang, S., & Huang, W. (2022). Photorespiration alleviates photoinhibition of photosystem I under fluctuating light in tomato. *Plants*, *11*(2). https://doi.org/10.3390/plants11020195

Somerville, C. R., & Ogren, W. L. (1979). A phosphoglycolate phosphatase-deficient mutant of Arabidopsis. *Nature*, *280*(5725), 833-836. https://doi.org/10.1038/280833a0

Somerville, C. R., & Ogren, W. L. (1982). Mutants of the cruciferous plant *Arabidopsis thaliana* lacking glycine decarboxylase activity. *Biochemical Journal*, *202*(2), 373-380. https://doi.org/10.1042/bj2020373

Steuer, R., Gross, T., Selbig, J., & Blasius, B. (2006). Structural kinetic modeling of metabolic networks. *Proceedings of the National Academy of Sciences*, *103*(32), 11868. https://doi.org/10.1073/pnas.0600013103

Stitt, M., Lunn, J., & Usadel, B. (2010). *Arabidopsis* and primary photosynthetic metabolism - more than the icing on the cake. *The Plant Journal*, *61*(6), 1067-1091. https://doi.org/10.1111/j.1365-313X.2010.04142.x

Stitt, M., & Zeeman, S. C. (2012). Starch turnover: pathways, regulation and role in growth. *Current Opinion in Plant Biology*, *15*(3), 282-292. https://doi.org/10.1016/j.pbi.2012.03.016

Strand, Å., Foyer, C. H., Gustafsson, P., GardestRÖM, P., & Hurry, V. (2003). Altering flux through the sucrose biosynthesis pathway in transgenic *Arabidopsis thaliana* modifies photosynthetic acclimation at low temperatures and the development of freezing tolerance. *Plant, Cell & Environment*, *26*(4), 523-535. https://doi.org/10.1046/j.1365-3040.2003.00983.x

Strand, Å., Hurry, V., Gustafsson, P., & Gardeström, P. (1997). Development of *Arabidopsis thaliana* leaves at low temperatures releases the suppression of photosynthesis and photosynthetic gene expression despite the accumulation of soluble carbohydrates. *The Plant Journal*, *12*(3), 605-614. https://doi.org/10.1046/j.1365-313X.1997.00583.x

Strand, A., Hurry, V., Henkes, S., Huner, N., Gustafsson, P., Gardeström, P., & Stitt, M. (1999). Acclimation of *Arabidopsis* leaves developing at low temperatures. Increasing cytoplasmic volume accompanies increased activities of enzymes in the Calvin cycle and in the sucrose-biosynthesis pathway. *Plant Physiology*, *119*(4), 1387-1398. https://doi.org/10.1104/pp.119.4.1387

Surek, B., Heilbronn, A., Austen, A., & Latzko, E. (1985). Purification and characterization of phosphoribulokinase from wheat leaves. *Planta*, *165*(4), 507-512. https://doi.org/10.1007/BF00398096

Suzuki, N., Rivero, R. M., Shulaev, V., Blumwald, E., & Mittler, R. (2014). Abiotic and biotic stress combinations. *New Phytologist*, *203*(1), 32-43. https://doi.org/10.1111/nph.12797

Takahashi, S., Bauwe, H., & Badger, M. (2007). Impairment of the photorespiratory pathway accelerates photoinhibition of photosystem II by suppression of repair but not acceleration of damage processes in *Arabidopsis*. *Plant Physiology*, *144*(1), 487-494. https://doi.org/10.1104/pp.107.097253

Tcherkez, G. (2016). The mechanism of Rubisco-catalysed oxygenation. *Plant, Cell & Environment*, *39*(5), 983-997. https://doi.org/10.1111/pce.12629

The UniProt, C. (2023). UniProt: the universal protein knowledgebase in 2023. *Nucleic Acids Research*, *51*(D1), D523-D531. https://doi.org/10.1093/nar/gkac1052

Thomas, P. D., Ebert, D., Muruganujan, A., Mushayahama, T., Albou, L.-P., & Mi, H. (2022). PANTHER: Making genome-scale phylogenetics accessible to all. *Protein Science*, *31*(1), 8-22. https://doi.org/10.1002/pro.4218

Timm, S., Nunes-Nesi, A., Pärnik, T., Morgenthal, K., Wienkoop, S., Keerberg, O., Weckwerth, W., Kleczkowski, L. A., Fernie, A. R., & Bauwe, H. (2008). A cytosolic pathway for the conversion of hydroxypyruvate to glycerate during photorespiration in *Arabidopsis*. *The Plant Cell*, *20*(10), 2848-2859. https://doi.org/10.1105/tpc.108.062265

Tripathy, B. C., & Oelmüller, R. (2012). Reactive oxygen species generation and signaling in plants. *Plant signaling & behavior*, *7*(12), 1621-1633. https://doi.org/10.4161/psb.22455

Tzin, V., Galili, G., & Aharoni, A. (2012). Shikimate pathway and aromatic amino acid biosynthesis. In *eLS*. https://doi.org/10.1002/9780470015902.a0001315.pub2

Vinyard, D. J., Ananyev, G. M., & Charles Dismukes, G. (2013). Photosystem II: The Reaction Center of Oxygenic Photosynthesis*. *Annual Review of Biochemistry*, *82*(Volume 82, 2013), 577-606. https://doi.org/https://doi.org/10.1146/annurev-biochem-070511-100425

Wada, M. (2013). Chloroplast movement. *Plant Science*, *210*, 177-182. https://doi.org/https://doi.org/10.1016/j.plantsci.2013.05.016

Wang, Q. L., Chen, J. H., He, N. Y., & Guo, F. Q. (2018). Metabolic reprogramming in chloroplasts under heat stress in plants. *International Journal of Molecular Sciences*, *19*(3). https://doi.org/10.3390/ijms19030849

Warburg, O. (1920). Uber die Gesehwindigkeit der photochemichen. *Biochemische Zeitschrift*, *103*, 188-217.

Weaver, L. M., & Herrmann, K. M. (1997). Dynamics of the shikimate pathway in plants. *Trends in Plant Science*, *2*(9), 346-351. https://doi.org/10.1016/S1360-1385(97)84622-5

Weiszmann, J., Fürtauer, L., Weckwerth, W., & Nägele, T. (2018). Vacuolar sucrose cleavage prevents limitation of cytosolic carbohydrate metabolism and stabilizes photosynthesis under abiotic stress. *The FEBS Journal*, *285*(21), 4082-4098. https://doi.org/10.1111/febs.14656

Wind, J., Smeekens, S., & Hanson, J. (2010). Sucrose: Metabolite and signaling molecule. *Phytochemistry*, *71*(14), 1610-1614. https://doi.org/10.1016/j.phytochem.2010.07.007

Wittig, U., Rey, M., Kania, R., Bittkowski, M., Shi, L., Golebiewski, M., Weidemann, A., Müller, W., & Rojas, I. (2014). Challenges for an enzymatic reaction kinetics database. *The FEBS Journal*, *281*(2), 572-582. https://doi.org/10.1111/febs.12562

VII Acknowledgments

I would like to thank Prof. Thomas Nägele for being a great mentor in my studies and for supervising this dissertation. I would additionally like to thank all members of Plant Evolutionary Cell Biology at the Faculty of Biology, LMU Munich, for many fruitful discussions and the amazing times. Special thanks goes out to Vladimir Brodsky for having to share an office with me. Further, I thank the Graduate School Life Science Munich for all the opportunities they provided.

I would also like to thank my wonderful girlfriend Lisa for the continued support, assistance, and patience in writing this dissertation. Without her continuous support and words of encouragement, this thesis would not have been possible.

JAKOB SEBASTIAN HERNANDEZ

· ·

EDUCATION

Ludwig-Maximilians-Universität: Doctoral candidate

2021 – Present   Munich, Bavaria, Germany

Ludwig-Maximilians-Universität: Bachelor's Studies Biology

2016 – 2021   Munich, Bavaria, Germany

Helmholtz-Gymnasium Heidelberg

2010 – 2015, 2007 – 2008   Heidelberg, Baden-Württemberg, Germany

Martin Luther King Jr. Middle School

2009   Berkeley, California, USA